# COMPOSITES OF MULTI-WALLED CARBON NANOTUBES WITH POLYPROPYLENE AND THERMOPLASTIC OLEFIN BLENDS PREPARED BY MELT COMPOUNDING

by

Kyle G. Petrie

A thesis submitted to the Department of Chemical Engineering

In conformity with the requirements for

the degree of Master's of Applied Science

Queen’s University

Kingston, Ontario, Canada

(September, 2013)

# Abstract

Composites of multi-walled carbon nanotubes (MWCNTs) with polypropylene (PP) and thermoplastic olefins (TPOs) were prepared by melt compounding. Two non-covalent functionalization methods were employed to improve nanotube dispersion and the resulting composite properties are reported.

The first functionalization approach involved partial coating of the surface of the nanotubes with a hyperbranched polyethylene (HBPE). MWCNT functionalization with HBPE was only moderately successful in breaking up the large aggregates that formed upon melt mixing with PP. In spite of the formation of large aggregates, the samples were conductive above a percolation threshold of 7.3 wt%. MWCNT functionalization did not disrupt the electrical conductivity of the nanotubes. The composite strength was improved with addition of nanotubes, but ductility was severely compromised because of the existence of aggregates.

The second method involved PP matrix functionalization with aromatic moieties capable of π-π interaction with MWCNT sidewalls. Various microscopy techniques revealed the addition of only 25 wt% of PP-g-pyridine (Py) to the neat PP was capable of drastically reducing nanotube aggregate size and amount. Raman spectroscopy confirmed improved polymer/nanotube interaction with the PP-g-Py matrix. Electrical percolation threshold was obtained at a MWCNT loading of approximately 1.2 wt%. Electrical conductivity on the order of $10^{-2}$ S/m was achieved, suggesting possible use in semi-conducting applications. Composite strength was improved upon addition of MWCNTs. The matrix functionalization with Py resulted in a significant improvement in composite ductility when filled with MWCNTs in comparison to its maleic anhydride (MA) counterpart. Preliminary investigations suggest that the use of alternating current (AC) electric fields may be effective in aligning nanotubes in PP to reduce the filler loading required for electrical percolation.

Composites containing MWCNT within PP/ethylene-octene copolymer (EOC) blends were prepared. Microscopy revealed that MWCNTs localized preferentially in the EOC phase. This was explained by the tendency of the system to minimize interfacial energy when the MWCNTs reside in the thermodynamically preferential phase. A kinetic approach, which involved pre-mixing the MWCNTs with PP and adding the EOC phase subsequently was attempted to monitor the migration of MWCNTs. MWCNTs began to migrate after two minutes of melt mixing with the EOC. The PP-g-Py matrix functionalization appears to slightly delay the migration. A reduction in electrical percolation threshold to 0.5 wt% MWCNTs was achieved with a co-continuous blend morphology, consisting of a 50/50 by weight ratio of PP and EOC.

# Co-Authorship

This thesis contains one chapter that presents results that have been published in the form of an original journal article. The complete citation for this paper and the chapters in which they appear are provided below:

Chapter 3: O. Osazuwa, K. Petrie, M. Kontopoulou, P. Xiang, Z. Ye, A. Docoslis *Compos. Sci. Technol.* 2012; 72:27.

This article was co-authored and reviewed prior to submission by O. Osazuwa, Dr. M. Kontopoulou and Dr. A. Docoslis. This paper was also co-authored by P. Xiang and Dr. Z. Ye, who were responsible for the synthesis of the hyperbranched polyethylene used in the work. The author of this thesis conducted the adsorption experiments from the specified article. All other experiments and writing contained within the following document have been prepared by the author with revisions from Dr. M. Kontopoulou and Dr. A. Docoslis.

# Acknowledgements

This dissertation is lovingly dedicated to my father who left me too soon and to my mother who was strong enough to keep me moving forward.

I would like to express extreme gratitude to everyone in the Department of Chemical Engineering at Queen's University. Special thanks to my primary supervisor Dr. Marianna Kontopoulou. Your positive, understanding and enthusiastic approach to learning throughout my time at Queen's will not be forgotten. The support, guidance and humor provided by Dr. Aris Docoslis were also integral to the completion of my research.

# Table of Contents

# List of Figures

# List of Tables

# Nomenclature

*Abbreviations*

| | |
|---|---|
| PP | Polypropylene |
| TPO | Thermoplastic olefin |
| EPDM | Ethylene propylene diene monomer |
| EPR | Ethylene propylene rubber |
| EC | Ethylene/α-olefin copolymer |
| EOC | Ethylene-octene copolymer |
| PC | Polycarbonate |
| PE | Polyethylene |
| PS | Polystyrene |
| MA | Maleic anhydride |
| Py | Amino-pyridine |
| AMP | 4-aminomethylpyridine |
| PMMA | polymethyl methacrylate |
| PP-g-MA | Polypropylene-graft-maleic anhydride |
| PP-g-Py | Polypropylene-graft-amino-pyridine |
| HBPE | Hyperbranched polyethylene |
| CNTs | Carbon nanotubes |
| MWCNTs | Multi-walled carbon nanotubes |
| SWCNTs | Single-walled carbon nanotubes |
| THF | Tetrahydrofuran |
| CVD | Chemical vapor decomposition |
| TEM | Transmission electron microscopy |

| | |
|---|---|
| SEM | Scanning electron microscopy |
| AC | Alternating current |
| DC | Direct current |
| DEP | Dielectrophoresis |
| SSA | Specific surface area |
| DLS | Dynamic light scattering |
| MFR | Melt flow rate |
| TGA | Thermogravimetric analysis |
| FTIR | Fourier transform infrared |
| LVE | Linear viscoelastic |

*Symbols*

| | |
|---|---|
| wt% | weight percent |
| $M_w$ | Weight-average molecular weight (kg/mol) |
| $\omega_a$ | Wetting coefficient ($mJ/m^2$) |
| $\sigma_{i/j}$ | Interfactial tension between blend components *i* and *j* ($mJ/m^2$) |
| $\sigma_i$ | Surface tension of component *i* ($mJ/m^2$) |
| $T_c$ | Crystallization temperature ($^oC$) |
| $T_m$ | Melting temperature ($^oC$) |
| $\Delta H_m$ | Heat of fusion (J/g) |
| $X_m$ | Crystallinity |
| $\rho$ | Volume resistivity ($\Omega$.m) |
| $\varphi$ | MWCNT volume fraction |
| $\varphi_c$ | Critical MWCNT volume fraction at electrical percolation |
| S | Siemens, SI unit of electrical conductance (reciprocal ohm) |
| $\sigma$ | Electrical conductivity (S/m) |

| | |
|---|---|
| $\sigma_{matrix}$ | Electrical conductivity of base matrix (S/m) |
| R | Resistance (Ω) |
| $V_{pp}$ | Voltage peak to peak (V) |
| \|Z\| | Magnitude of impedance |
| I | Current through the system (A) |
| $\theta_z$ | Phase angle of voltage to current in capacitive system ($^o$) |
| $\eta_i$ | Complex viscosity of polymer *i* (Pa.s) |
| $\varphi_i$ | Volume fraction of polymer *i* |

# Chapter 1

# Introduction

## 1.1 Background

Isotactic polypropylene (PP) is a highly crystalline, commercially relevant polymer, comprising over 20% of all thermoplastic polyolefins produced globally [1]. It is used in many applications such as films, packaging, automotive parts, containers and in countless other areas of modern life. PP is utilized because of its low production cost, easy processability, strength, stiffness, thermal resistance, corrosion resistance and recyclability. One major drawback of PP is that it exhibits brittle material performance at low temperatures. The addition of a dispersed rubbery phase within a PP matrix, to produce thermoplastic olefin (TPO) compounds, has been commonly used when impact resistance at low temperatures is important.

TPOs are industrially important PP based materials that have a dispersed rubbery phase, usually ethylene propylene diene monomer (EPDM), ethylene propylene rubber (EPR) or more recently metallocene-catalyzed ethylene/α-olefin copolymers (ECs). These materials act as impact modifiers in PP. ECs offer benefits compared to other elastomeric polyolefins such as improved processability and controlled chain branching. Due to relatively low viscosities, ECs can be easily dispersed within PP matrices by standard melt compounding techniques [2]. Depending upon their composition TPOs can be used as soft, interior components for automobiles, and as rigid exterior panels. These are important developments for reducing vehicle weight for improved fuel economy.

Inorganic nano-fillers are being increasingly used to enhance the mechanical properties of PP and TPO blends. Nanoparticles offer the potential for imparting novel material properties, such as electrical conductivity, for value-added applications for commodity plastics [3]. Nano-sized fillers such as carbon black, silica and clay have been used to reinforce polymer composites

and to improve electrical and thermal properties. TPOs are commonly reinforced with nanofillers such as silica and clay [4, 5]. It has also been shown with carbon black that electrical conductivity can be achieved at low filler loadings [6].

Since their identification in 1991 by Iijima [7], carbon nanotubes (CNTs) have presented a new class of filler material with intriguing properties. CNTs have a cylindrical nanostructure, which has been theoretically and experimentally demonstrated to be stronger than steel, lighter than aluminum and more conductive than copper [8]. These impressive properties can be attributed to their structural arrangement and extremely high length to width (aspect) ratio [3, 8]. CNTs have received attention from industry and academia on a scale unlike any other emerging technology. Figure 1.1 below shows the number of reported publications from a Web of Science search result with a topic of "carbon nanotubes" over the last decade. There have been over 3800 international patents filed over that time period according to the World Intellectual Property Organization.

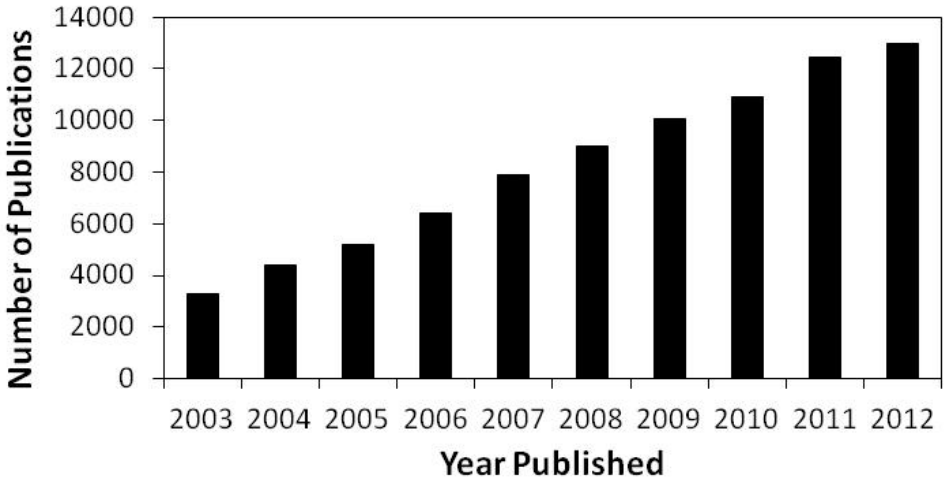


**Figure 1.1: Web of Science search results for publications having a keyword of carbon nanotubes.**

Despite the obvious potential to produce polymeric materials that are lightweight, highly conductive and less expensive alternatives to metals, commercialization of nanotube/polymer

composites remains scarce. The primary reasons for this are the variation of dimensions and surface defects between production batches and the inherent difficulty of translating nanotube properties to their polymer composites [3, 9].

Nanotube dispersion within a polymer matrix has been shown to be an important factor for achieving mechanical reinforcement and formation of an interconnected three-dimensional network capable of electrical conductivity [10]. This has been difficult to achieve by conventional mixing techniques. While various production methods have been developed to achieve isotropic dispersion of nanotubes, melt compounding represents the most industrially scalable and important route of fabrication [11]. However, CNTs tend to form large aggregates when mixed in non-polar polyolefin matrices, due to strong van der Waals interactions between nanotubes [1]. This results in poor transfer of the nanotube properties to the polymer in melt compounded composites.

Given the industrial importance of PP and TPO blends as outlined above, their melt compounded composites with CNTs hold significant promise for applications where improved mechanical strength and electrical conductivity are required. It is therefore of great importance industrially to develop methods that will enable good dispersion of nanotubes in these commodity plastics. Investigation of chemical modification techniques that can break up the interactions between the nanotubes and improve interfacial adhesion with PP matrices are required to fulfill this technology's potential.

## 1.2 Objective and Outline

The objective of this dissertation is to develop methods for improved dispersion of multi-walled carbon nanotubes (MWCNTs) in PP and TPO blends. Two non-covalent functionalization approaches are employed; the first involves modification of the surface of the MWCNTs, whereas the second involves matrix functionalization. The effect of the functionalization approaches on the resulting mechanical and electrical properties of the composites is investigated.

Following this introductory chapter, a literature review is presented in Chapter 2. This review outlines the current state of knowledge of MWCNTs and their composites with PP and TPOs, with common preparation and functionalization methods outlined. Chapter 3 investigates the adsorption of a hyperbranched polyethylene (HBPE) compatibilizing agent to the surface of MWCNTs and evaluates its effectiveness in breaking up filler/filler interactions when melt mixed with a PP homopolymer. Dispersion is characterized using various microscopy techniques. The effect of this non-covalent functionalization on mechanical and electrical performance is reported.

Chapter 4 describes a PP matrix functionalization procedure with aromatic moieties prepared by a reactive melt compounding procedure. The effectiveness of grafting aromatic groups to PP chains on the dispersion of the MWCNTs is investigated by various microscopy techniques. The electrical and mechanical properties of the resulting composites are reported.

In Chapter 5, TPO blends containing MWCNTs are investigated as a means to reduce filler loadings required to achieve electrical percolation. The mechanisms of partitioning of the MWCNTs within the two phases of the blend are investigated. The morphology development of the ternary composite blends is monitored at various compounding times. Chapter 6 summarizes conclusions and proposes recommendations for future work.

## 1.3 References


[1] D. Bikiaris, "Microstructure and Properties of Polypropylene/Carbon Nanotube Nanocomposites," *Materials 3*, pp. 2884-2946. 2010.

[2] M. Kontopoulou, W. Wang, T. G. Gopakumar and C. Cheung, "Effect of composition and comonomer type on the rheology, morphology and properties of ethylene-alpha-olefin copolymer/polypropylene blends," *Polymer 44(24)*, pp. 7495-7504. 2003.

[3] R. Baughman, A. Zakhidov and W. de Heer, "Carbon nanotubes - the route toward applications," *Science 297(5582)*, pp. 787-792. 2002.

[4] C. Li, Q. Zhao, H. Deng, C. Chen, K. Wang, Q. Zhang, F. Chen and Q. Fu, "Preparation, structure and properties of thermoplastic olefin nanocomposites containing functionalized carbon nanotubes," *Polym. Int. 60(11)*, pp. 1629-1637. 2011.

[5] M. Bailly and M. Kontopoulou, "Preparation and characterization of thermoplastic olefin/nanosilica composites using a silane-grafted polypropylene matrix," *Polymer 50(11)*, pp. 2472-2480. 2009.

[6] M. Sumita, K. Sakata, S. Asai, K. Miyasaka and H. Nakagawa, "Dispersion of fillers and the electrical-conductivity of polymer blends filled with carbon-black," *Polymer Bulletin 25(2)*, pp. 265-271. 1991.

[7] S. Iijima, "Helical microtubules of graphitic carbon," *Nature 354(6348)*, pp. 56-58. 1991.

[8] M. Moniruzzaman and K. I. Winey, "Polymer nanocomposites containing carbon nanotubes," *Macromolecules 39(16)*, pp. 5194-5205. 2006.

[9] M. Rahmat and P. Hubert, "Carbon nanotube-polymer interactions in nanocomposites: A review," *Composites Sci. Technol. 72*, pp. 72-84. 2011.

[10] I. Alig, P. Poetschke, D. Lellinger, T. Skipa, S. Pegel, G. R. Kasaliwal and T. Villmow, "Establishment, morphology and properties of carbon nanotube networks in polymer melts," *Polymer 53*, pp. 4-28. 2012.

[11] T. McNally and P. Potschke, *Polymer-Carbon Nanotube Composites - Preparation, Properties and Applications*, Philadelphia: Woodhead Publishing Limited, 2011.

# Chapter 2

# Literature Review

## 2.1 Carbon Nanotubes

Graphene is the precursor to carbon nanotubes (CNTs). Graphene is composed of a monolayer of $sp^2$-bonded carbon atoms. These atoms form a hexagonal lattice [1]. CNTs are seamlessly 'rolled' sheets of graphene. These cylinders of covalently bonded carbon have large aspect ratios; they are long in length and narrow in diameter (diameters as small as 1 nm with lengths many thousand times longer) [2]. They can be categorized into two main types: single-walled carbon nanotubes (SWCNTs) or multi-walled carbon nanotubes (MWCNTs). SWCNTs can be visualized as an individual sheet of seamlessly 'rolled' graphene. MWCNTs are simply made up of concentric graphene cylinders [1]. A representation can be seen in Figure 2.1.

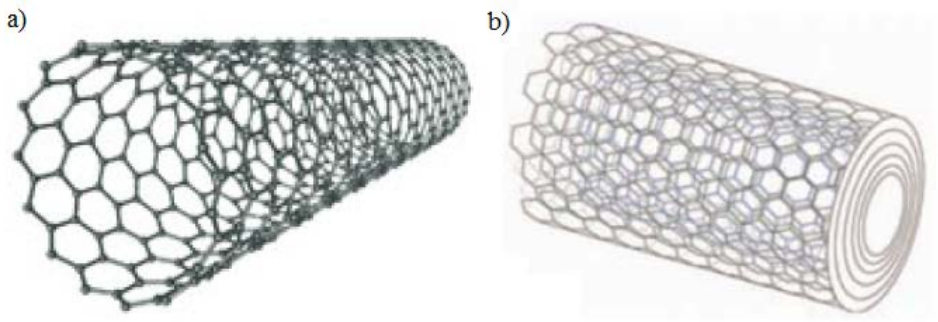


**Figure 2.1: Representation of an individual a) SWCNT and b) MWCNT** [3]**.**

The chirality or helicity with which the sheet of graphene is 'rolled' can be defined by a circumferential vector ($\overrightarrow{C_h}$) made up of the sum of $n\vec{a}_1$ and $m\vec{a}_2$, where n and m are the number of steps along the unit vectors $\vec{a}_1$ and $\vec{a}_2$ (visualized in Figure 2.2) [4]. There are three types of orientations which impact the transport properties of the resulting nanotube; the 'armchair' configuration (when n=m), 'zig-zag' (when n or m = 0) or 'chiral' (any other n, m combination).

All armchair rolling configurations result in SWCNTs that are metallic since the band gap is essentially 0 eV. When the values of n-m = 3*i* (where *i* is a non-zero integer), the resulting nanotubes are semiconductors with a small band gap. All other configurations result in semiconductive nanotubes with a band gap that inversely depends on the nanotube diameter [5, 6]. It has been reported that the non-linear mechanical stability of nanotubes is only slightly dependent on the chirality [7]. While these configurations dictate transport properties of SWCNTs, MWCNTs are made up of rolled sheets with multiple configurations, increasing the complexity of determining their resulting electrical properties [8].

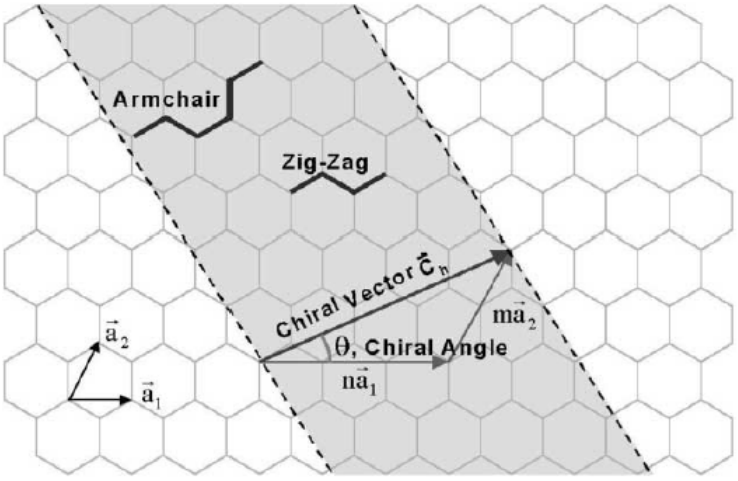


**Figure 2.2: Representation of potential nanotube chiralities upon 'rolling' a sheet of graphene** [4]**.**

CNTs exhibit remarkable mechanical and electrical properties. They have a lower specific density (approximately 1.6 compared to 7.8), higher Young's modulus (approximately 1 compared to 0.2 TPa) and higher tensile strength (approximately 10-60 compared to 4 GPa) when compared to stainless steel [9]. Extended π conjugation occurs from the bond structure between carbon atoms of the CNTs and facilitates electrical conductivity [10]. Electrical conductivities of over $10^7$ S/m have been reported for CNTs (comparable to copper at approximately $6x10^7$ S/m) [9]. Another important aspect of CNTs is the tendency to form bundles or aggregates when dispersed in solvents and polymers. This is attributed to their long length and more importantly

because of high attraction between nanotubes through van der Waals interactions. The $sp^2$ structure of the graphene results in strong π-π interaction between tubes [11-13].

### 2.1.1 Production Methods

The various technologies and techniques used to produce CNTs can play an important role on their resulting properties. The distribution of tube length, dimensions and chirality are impacted by production method. Impurities such as residual catalyst and surface defects introduced during purification are important considerations that determine their properties. Following is an outline of the most prominent methods for the production of CNTs.

#### 2.1.1.1 Arc-discharge

Iijima [14] and Iijima el al. [15] first identified and produced what are now known as MWCNTs and SWCNTs in 1991 and 1993, respectively. The 'helical microtubes of graphitic carbon' were produced using an arc-discharge evaporation method, which had been previously used to produce fullerenes. Arc-discharge evaporation occurs when passing a current between two carbon electrodes in the presence of a cobalt catalyst within an inert atmosphere at low pressure. The discharge between electrodes vaporizes the carbon, depositing small rod shaped carbon deposits on the negative electrode [16]. Commercial production of CNTs using this method is not practical for multiple reasons. The process has low yield due to the difficulties of separating the mixture of products and is only capable of producing gram quantities of purified CNTs [16, 17]. This leads to inefficient use of input materials and energies on separation processes [17]. It has been estimated that over 30% of the CNT yield is lost through purifications processes. This value is high since impure product is formed that hinders nanotube performance in end-use applications [18]. Intensive purification of CNTs can lead to oxidative shortening and reduced material performance in end use application [17]. Nanotube entanglement occurs from this production method, which creates dispersion and performance issues when used as fillers in polymer composites. Also, CNT agglomerates produced using this method often require

ultrasonication to break them up [18]. Sonication requires long time periods, high energy inputs and can lead to shortening of CNTs. Sonication is near impossible to scale up. Therefore sonication is not a practical step for commercialization for both economic and environmental perspectives. Low yield, rigorous purification and potentially inferior products reduce the economic outlook of large scale production of CNTs by arc-discharge evaporation.

#### 2.1.1.2 Chemical Vapor Decomposition

Chemical vapor decomposition (CVD) is the most widely used method of CNT production owing to its low cost and ability to produce bulk quantities of high purity product. CVD for CNT production is done in an inert gas system ranging from 500-1000$^{o}$C at low pressure. Production rates have been reported to be as high as 1.5 g CNT $m^{-2}$ $min^{-1}$ when operating around 800$^{o}$C (higher throughput than for arc-discharge) [17]. Metal catalysts (usually cobalt or iron) are entrained in the system, followed by hydrocarbon gas. The hydrocarbon decomposition occurs and begins to deposit onto the vessel walls and substrates in the form of well aligned CNT [17]. Figure 2.3 shows alignment of deposited CNTs by CVD, normal to the growing surface. The performance of polymer composites is improved by the better dispersed CNTs, which would otherwise act as defects in base polymer matrices if not properly dispersed. This suggests that CVD is a favorable method of production for producing CNTs that are suitable as additives in polymer composites.

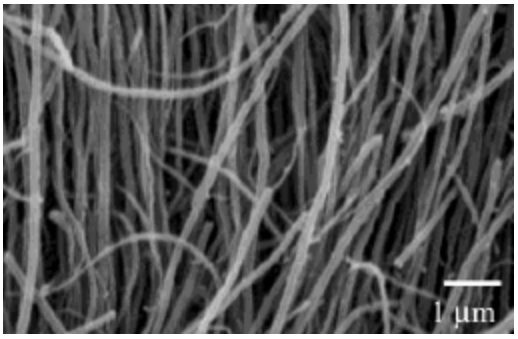


**Figure 2.3: CNTs formed by CVD aligned normal to the growing surface** [17]**.**

Current catalyst mechanisms for CVD are not well understood, but are believed to play an integral role in higher synthesis yields, higher purity, CNT dimensions and surface defects of resulting CNTs [12, 19]. Defining catalyst mechanisms will reduce material and energy inputs for CNT production, while making the technology more economically viable.

Many hydrocarbons which are decomposed and deposited during CVD generally come from accessible sources, and in the future could potentially be designed to extract carbon from any organic source. Therefore abundant input material is available for CNT production. Through producing highly pure CNTs that are well aligned with no side products, purification steps can almost be removed. No sonication is required to break up agglomerates of CNTs, thus avoiding the drawbacks discussed for arc-discharge production methods. Trace amounts of metal catalyst in the nanotubes can be removed, but through increased catalyst performance, this purification step is also minimized as smaller amount of catalyst are required [17, 19]. One purification step that has been reported is the annealing of produced CNTs to better define graphene structure. Since CVD operates at lower temperatures than other methods, heating to temperatures above 1800$^{o}$C in an inert atmosphere corrects for structural defects, but also has been shown to be effective in removing residual catalyst [17]. The nanotubes used in the experiments for this dissertation were prepared using a CVD production method having a purity of > 95%.

## 2.2 Carbon Nanotube/Polymer Composites

A primary area of industrial potential is the use of CNTs as nanofillers in polymer composites [3, 6, 8, 12, 20]. Polymer matrices such as polycarbonate (PC) [21, 22], polyethylene (PE) [23], polystyrene (PS) [24] and many others filled with CNTs have been explored [20], this thesis will focus exclusively on thermoplastic technologies. The potential exists to use CNTs to create thermally and electrically conductive plastics that are mechanically reinforced. Creating CNT/polymer composites with novel properties depends on many factors. In particular the CNT impurities, surface properties and aspect ratios are important considerations. The major obstacle

facing mass application of this class of material is achieving good dispersion of CNTs. Physical chain entanglements and van der Waals interactions exist, resulting in the formation of large aggregates of nanotubes and poor interfacial adhesion at the filler/polymer interface [25]. Upon initial addition into a polymer, nanotubes form what are referred to as 'primary aggregates' and various processing methods are employed in an attempt to break up these aggregates and distribute the nanotubes. 'Secondary aggregates' are formed by thermal and/or shear induced attraction during the processing procedure.

In order to achieve conductivity, the formation of an interconnected, three-dimensional network of nanotubes spanning the entire sample is considered necessary. According to percolation theory, nanotubes that are evenly distributed will form such a network of nanotubes at a particular loading. This loading is referred to as a 'percolation threshold'. It can be determined by a sharp increase in electrical conductivity [1, 26]. The formation of a nanotube network can also be identified by rheological means; a transition of viscoelastic liquid to solid-like behavior due to long-range restriction of polymer chains becomes apparent at the percolation threshold [27]. Electrical and rheological percolation is observed even in polymer composites with poor nanotube dispersion; this is attributed to residual primary aggregates and interconnected secondary aggregates [28-30]. This negatively affects mechanical properties of the composites, even though they do have conductive properties. Generally, limited secondary aggregation is considered beneficial for electrical performance because it facilitates transition from insulating to conductive materials at very low filler loadings [30, 31].

This is particularly true for non-polar polyolefins. It has been shown in the literature that CNT dispersion in matrices such as PE and polypropylene (PP) is poor, and large aggregates tend to form. This occurs due to poor polymer wetting and infiltration of strongly interacting nanotubes [23, 28, 32, 33]. Poor interfacial adhesion and the formation of large aggregates (inability to break up primary aggregates) results in poor stress transfer during mechanical testing,

diminishing ductility and composite strength [23, 34]. On the contrary polymers containing polar functionalities such as PC have been extensively confirmed to have isotropic dispersion [21, 31].

Furthermore, the addition of CNTs to polymer composites induces polymer crystallization through heterogeneous nucleation [35-37]. Higher degrees of crystallinity will improve polymer strength. At high concentrations the formation of a carbon nanotube network restricts PP chain mobility and hinders further improvements in crystallization [36].

### 2.2.1 Composite Preparation

The importance of dispersing CNTs to achieve mechanical reinforcement and electrically conductive composites has been outlined above. Various processing methods can be used to distribute nanotubes, but all involve similar mechanisms which occur simultaneously; wetting of primary aggregates by the polymer, infiltration of polymer chains into these aggregates, dispersion of these aggregates by rupture and erosion and distributing individual nanotubes [30]. The following section will outline the methods commonly used to break-up primary aggregates and disperse CNTs in polymer composites.

#### 2.2.1.1 Solution Blending

Solution blending involves dispersing polymer in a suitable solvent and adding CNTs. Nanotubes can also be dispersed in solvent (colloidal suspension) or added directly to the dissolved polymer solution [38, 39]. In order to achieve stable CNT suspensions, functionalization and/or sonication is required [40]. Elevated temperatures and mixing are needed [39, 41]. The use of solvents and sonication has been shown to disrupt nanotube surface properties and degrade the mixing polymer in comparison to dry mixing [39]. This method for the production of CNT/polymer composites is capable of providing reasonable dispersion and requires no formal processing equipment. Scale-up is a concern with solution blending because residual solvent must be recovered. The surface properties of nanotubes can be impacted negatively by solution blending [20].

2.2.1.2 *In-situ* Polymerization

Another method for fabricating CNT/polymer composites is the use of a polymerizing monomer in the presence of nanotubes. For in-situ polymerization, the catalyst required for polymerization can be covalently pre-anchored to the nanotubes [42, 43] or nanotubes simply added to a system prior to polymerization [44]. Funck et al. [42] covalently bonded co-catalyst to the surface of oxidized MWCNTs in a coating technique prior to polymerization to form composites with PP. In contrast, Zhao et al. [45] did not attach catalyst to the CNTs. They used ultrasonication in an attempt to disperse MWCNTs in a master solution containing elements for polymerization of polyamide 6. Both are effective in producing composites with reasonable nanotube dispersion

The benefits of in-situ polymerization are the ability to form composites with polymers that are not easily solution blended or melt compounded. Also, grafting polymer to the surface of the nanotubes can be used in dispersing CNTs in compliment to other processing methods for better dispersion [46]. It is speculated that the covalent functionalization of catalyst to the surface of nanotubes impacts the electrical properties of the nanotubes (extended $\pi$ conjugation) [10]. There is an added complication with excess catalyst and solvent removal.

2.2.1.3 Melt Compounding

Melt compounding is the most commonly used method for producing CNT/polymer composites. Although it requires specialized equipment, it is industrially relevant because it is simple, fast and capable of producing large volumes of sample [46]. The polymer is heated to above its melting temperature and CNTs are added to the melt. High shear mixing is then performed with the use of various extruder set-ups [21, 47, 48]. The shear force generated in the compounder is responsible for breaking up primary aggregates and dispersing nanotubes into the polymer. Therefore the viscosity of the matrix (partially controllable by temperature) plays an integral role in CNT dispersion [29, 30, 34, 49]. The primary disadvantage with this method is the

suspected decrease of nanotubes aspect ratio upon application of high shear rates [30, 49, 50]. This is a problem because as CNTs decrease in length, the amount of filler required for the formation of a conductive network is increased.

### 2.2.2 Compatibilization

Many compatibilization techniques have been developed and employed to facilitate the dispersion of CNTs in polymers. These methods modify either the surface of the CNTs, or the polymer matrix. Both strategies aim at disrupting the strong van der Waals interactions between nanotubes and/or improve polymer wetting of the nanotubes surface for better interfacial adhesion [25, 51]. The following section will highlight the two major types of interactions used in compatibilization; covalent and non-covalent.

#### 2.2.2.1 Covalent Functionalization

Covalent functionalizations establish chemical bonds between functional molecules (often polymers) and the surfaces of the CNTs. Oxidative reactions with oxygen or various acid treatments can add -COOH and -OH functionalities to the surface of the CNTS [37, 52]. These treatments hinder the aspect ratio and surface properties of the nanotubes but also introduce functional groups to the surface of the nanotubes. The attachment of polymer to the surface of CNTs has been proven to be effective in dispersing CNTs and improving composite strength. [25, 37, 53]. This is done using either a 'grafting-from' or 'grafting-to' technique.

Grafting-from involves the chemical functionalization of a CNT surface to act as a macro initiator for polymerization. The main advantage of this method is that the grafting density can be controlled by the amount of surface functionalization of the CNTs. Li et al. [54] used a free radical polymerization method to produce CNTs with grafted PE. They first chemically attached α-alkenes to nanotubes and then with the use of a metallocene catalyst grew PE chains from their surface. These nanotubes were dispersed in PE and the composites resulted in improved Young's modulus, elongation at break and thermal behavior because of the enhanced nanotube dispersion

versus the non-functionalized counterparts. Multiple groups [55-57] have functionalized the surface of CNTs with atom transfer radical polymerization initiators, allowing for controlled polymerization from the surface of nanotubes.

Grafting-to involves the chemical attachment of functional polymers to the surface of CNTs. CNTs can be pristine, oxidized or pre-functionalized depending on the functionality of the polymer to be grafted [20]. Yang et al. [58, 59] have used this technique to improve interfacial adhesion in CNT composites with PP and PE. CNTs were surface functionalized with -COOH through acid treatment and ultrasonication. Reactions were then carried out with ethyldiamine and then the respective polyolefin-grafted-maleic anhydride (MA) to form CNT-grafted-PP and PE respectively. Composites with these grafted CNTs had improved mechanical performance. However, there is no mention of the impact of the functionalization procedure on electrical performance of the composites. Various hyperbranched polymers have been synthesized with aromatic functional end-groups to be grafted to the surface of CNTs [60].

#### 2.2.2.2 Non-Covalent Functionalization

While covalent functionalization approaches have been shown to improve nanotube dispersion, the chemical modification introduces surface defects, which can negatively affect mechanical and transports properties. The use of non-covalent functionalization approaches is thus favorable since it does not impact the structure or extended π conjugation of the nanotubes in polymer composites. Non-covalent functionalization involves wrapping or adsorption of macromolecules to the surface of nanotubes through carbon-hydrogen group (CH)-π interactions, π-π stacking, or various other electrostatic and hydrophobic interactions [20, 61].

Physically adsorbed polymers to the surface of CNTs have been shown to improve dispersion in various organic solvents and polyolefin matrices. Baskaran et al. [61] used a wide variety of small and macro molecules to investigate the impact of non-covalent/non-specific functionalizations on nanotube dispersion in solvents and polymers. They found that the weak

CH-π intermolecular interaction occurs generally between polymers and CNTs and is capable of improving nanotube solubility and dispersion.

Ye et al. [62] have developed dendritic-like structures of hyperbranched polyethylenes (HBPE) using a 'chain walking' palladium-diimine catalysts. They are capable of synthesizing this complex, branch on branch structure polymers without having any end functionalities. HBPE is capable of non-covalent CH-π interaction with the surface of CNTs and has been shown to improve nanotube solubility in chloroform, tetrahydrofuran [40] and improved dispersion upon solution blending with a polyolefin elastomer [48].

The use of matrix functionalizations capable of non-covalent interactions with nanotubes offers another possible route for compatibilization. Maleic anhydride (MA) and various block copolymers have been employed as matrix functionalizations in attempts to improve wetting and adhesion of nanotubes with polyolefins [63-65]. Thomassin et al. [66] developed a matrix functionalization approach by grafting aromatic moieties to PP. Aromatic moieties are believed to non-covalently interact with CNTs through π-π stacking, improving interfacial adhesion and disrupting van der Waals interactions between nanotubes. Similar procedures have been followed for linear low density PE [49] and polymethyl methacrylate (PMMA) [67] confirming that the addition of aromatic moieties as an effective compatibilizer for various polymers.

## 2.3 Polymer Blends containing Carbon Nanotubes

A polymer blend is a mixture of at least two polymeric materials that can be used to develop materials with tailored properties. Given the range of properties that can be accomplished using this approach, polymer blends are industrially significant materials. Thermodynamically there are two classifications of blends; miscible or immiscible. Miscible blends are completely homogeneous. Immiscible blends are characterized by limited solubility between the polymers and results in the formation of two distinct phases. Most polymer blends are immiscible, and display a separated phase morphology, with the capability of retaining important material

properties from both phases [68]. Thermoplastic polyolefin (TPO) blends contain PP mixed with an elastomeric component, to achieve improved low temperature impact resistance.

Inorganic nanofillers are commonly used to form ternary blends with TPOs for increased stiffness, compatibilization and improved phase stability [69, 70]. Filler localization in ternary polymer blends is important for both mechanical and electrical properties. Figure 2.4 below shows 5 wt% of nanosilica localized in the dispersed phase (a) and in the matrix phase (b) in various immiscible blends. It has been shown in blends with droplet/matrix morphology that nanofillers such as clay and silica must localize exclusively in the matrix phase for reinforcement [70-72].

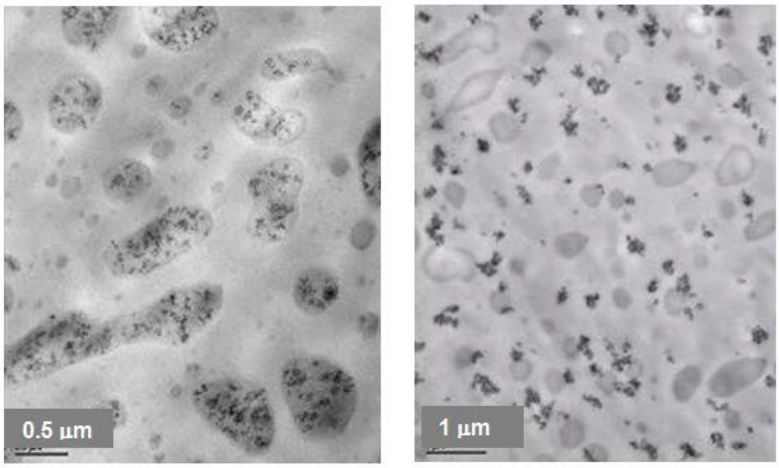


**Figure 2.4: Transmission Electron Microscopy (TEM) images of TPO blends containing 5 wt% nanosilica. a) PP/ethylene-propylene rubber-grafted-MA (80/20 wt %/wt %) with filler residing in the droplet phase and b) PP/ethylene-octene copolymer (80/20 wt %/ wt %) where the filler resides in the matrix phase. Adapted from** [73]**.**

Fillers such as carbon black and more recently CNTs have been added to produce electrically conductive blends [74-76]. For electrical percolation to occur, the filler must reside within the matrix phase or at the interface between the two immiscible phases. Co-continuous blend morphologies are considered especially beneficial, given that they facilitate the formation

of a sample spanning network. The importance of filler dispersion as discussed throughout section 2.2 remains, and similar methods of compatibilization are beneficial for blends.

### 2.3.1 Immiscible Blend Morphology

The morphology of immiscible polymer blends is integral to the resulting properties [77-79]. Blends can display a phase dispersed in a continuous matrix (droplet/matrix morphology) or a co-continuous morphology [80]. While mechanical performance is greatly hindered with co-continuous morphology, mechanical performance of droplet/matrix blends has been found to improve with finer dispersed droplet formation [81]. Droplet size of the dispersed phase is partially dictated by droplet break-up and coalescence [82]. It is known that droplet break-up is facilitated by energy of the mixing process (shear rate), viscosity ratio of the components, component viscoelasticity and interfacial tension. Coalescence involves joining of multiple dispersed droplets through collision. Therefore, as the composition of the dispersed phase increases, the size of the dispersed phase should increase [83, 84].

It has been shown that addition of nanofillers such as clay, silica and CNTs results in a narrowing of dispersed droplet phase distribution and decrease in droplet diameter for immiscible polymer blends (represented in Figure 2.5 below) [22, 69, 71, 75, 85-87]. The proposed mechanisms for this vary based on the location of the filler within the matrix phase, the dispersed phase or at the interface. If the filler resides at the interface it has been suggested that a decrease in the interfacial tension results in the change in morphology [88, 89]. If the particles reside in the matrix phase, it has been suggested that coalescence is hindered with addition of the nanoparticles [69, 90]. Changes in polymer viscosity upon filler addition may play a role, resulting in better droplet break-up.

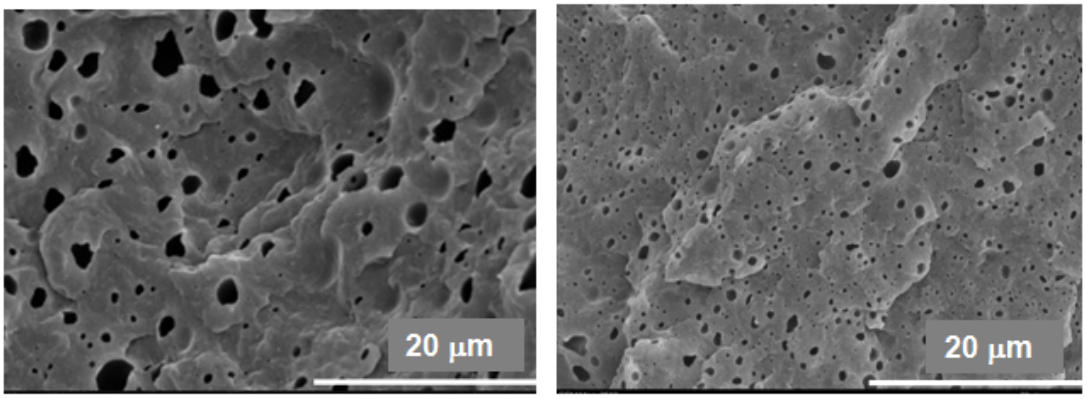


**Figure 2.5: Scanning Electron Microscopy (SEM) images of a) unfilled and b) 7 wt% nanosilica filled 80/20 wt%/wt% blends of PP/ethylene-octene copolymer, demonstrating a decrease in etched droplet phase (dark) diameter upon addition of nanofiller. Adapted from** [73]**.**

Sumita et al. [74] wrote the seminal paper on the impact of blend morphology on the electrical conductivity. Carbon black was used as electrically conductive filler in various immiscible polymer blends. It was concluded that the electrical conductivity was dependent on two things; the concentration of filler within a phase and the continuity of that phase. This has been referred to as "double percolation". The main conclusion is that if filler localization can be controlled, electrical percolation can be reduced by increasing the blend component, where a co-continuous morphology would result in the highest conductivity. Groups studying various ternary blend systems have reported similar results since then [22, 91, 92].

### 2.3.2 Filler Localization

As mentioned above, upon addition to a polymer blend, fillers will reside in either the matrix phase, the droplet phase or at the interface between the two. There are two main factors that determine the localization of the filler; thermodynamic and kinetic effects.

#### 2.3.2.1 Thermodynamic Effects

The thermodynamic affinity for the filler to locate within a particular component of a polymer blend system is important in filler localization. Sumita et al. [74] used a 'wetting

coefficient' derived from Young's equation to predict where the filler will localize. The wetting coefficient ($\omega_a$) can be estimated using Equation 2.1 based on interfacial tensions between the various ternary blend components ($\sigma_{i/j}$) from surface tension values ($\sigma_i$) of the individual components involved.

$$\omega_a = \frac{\sigma_{\text{Filler/Polymer1}} - \sigma_{\text{Filler/Polymer2}}}{\sigma_{\text{Polymer2/Polymer1}}} \qquad (2.1)$$

Filler partitioning criteria are as follows [74]:

If $\omega_a > 1$, filler will distribute within polymer 2

If $-1 < \omega_a < 1$, filler will reside at interface between phases

If $\omega_a < -1$, filler will distribute within polymer 1

The interfacial tension between components can be estimated using two approaches: the harmonic and geometric mean equations. Equation 2.2 is the harmonic mean equation which can be used to estimate interfacial energy between low energy materials and Equation 2.3 is the geometric mean equation which can be used to estimate interfacial energy between high and low energy materials. Experimental determinations of the dispersive (d) and polar (p) components of the surface tension for various materials are temperature dependent and difficult to perform [77].

Harmonic Mean

$$\sigma_{1/2} = \sigma_1 + \sigma_2 - 4\left(\frac{\sigma_1^{\mathrm{d}}\sigma_2^{\mathrm{d}}}{\sigma_1^{\mathrm{d}}+\sigma_2^{\mathrm{d}}} + \frac{\sigma_1^{\mathrm{p}}\sigma_2^{\mathrm{p}}}{\sigma_1^{\mathrm{p}}+\sigma_2^{\mathrm{p}}}\right) \qquad (2.2)$$

Geometric Mean

$$\sigma_{1/2} = \sigma_1 + \sigma_2 - 2\left(\sqrt{\sigma_1^d \sigma_2^d} + \sqrt{\sigma_1^p \sigma_2^p}\right) \qquad (2.3)$$

Based on this approach filler localization has been predicted successfully in polymer blends with similar melt viscosities. Many other groups have used the same prediction criterion to successfully predict localization for fillers of various shape and surface chemistries [74, 93, 94].

Modifications allow for improved affinity between a particular polymer and filler. Compatibilizers, filler modifications and matrix functionalization approaches have commonly been attempted to localize filler within a particular phase [32, 69, 71, 94]. One difficulty associated with this method is the accurate measurement of surface energy and prediction of interfacial tensions between phases for modified CNTs and chemically modified polymers. These measurements are difficult to complete and do not exist in the literature.

#### 2.3.2.2 Kinetic Effects

Other factors than thermodynamics can influence filler localization. These include polymer properties, compounding sequence and mixing time. These factors are referred to as 'kinetic' effects.

It has been shown that if there is a large discrepancy in polymer phase viscosities or melting temperatures, the filler will tend to the polymer that has the lower viscosity or melting point [95]. The order with which the filler is added to the various phases can dictate localization. If the filler is first premixed within the thermodynamically less desirable phase, it is possible to maintain in that phase by controlling the time of mixing [96].

In the limited studies conducted of TPO blends filled with CNTs, localizing within a PP rich matrix phase or at the interface remains elusive [32, 75, 86, 97]. The transfer between polymer phases for spherical fillers has been shown to be slower than that of high aspect ratio fillers [85, 98]. Goeldel et al. [99] compared the impact of filler shape on kinetic transfer between immiscible blend phases. They proposed a 'Slim-Fast Mechanism', where low interfacial stability and fast transfer times between phases occur in fillers with high aspect ratios.

## 2.4 Use of AC Electric Fields for Reduced Percolation Thresholds in CNT/Polymer Composites

Percolation thresholds for thermoplastics filled with CNTs range from loadings lower than 0.5 wt% and as high as 8 wt% [20]. Composite ductility is less affected at lower filler

loadings and material cost can be reduced. Therefore, achieving electrical percolation in CNT/polymer composites at low filler loadings is of interest. A proposed method for realizing this is through the alignment of CNTs within polymers [100]. Alternating current (AC) electric fields have been shown to be effective in aligning CNTs suspended between electrodes [101, 102]. The following section will investigate the phenomena responsible for the motion of polarizable particles subjected to an AC electric field.

The main phenomenon responsible for particle motion in an electric field is dielectrophoresis (DEP). DEP is defined as the force that is exerted on a polarizable particle in the presence of a non-uniform electric field [103]. The difference of the Coulomb forces caused by the induced dipoles of a polarizable particle in the presence of a non-uniform electric-field results in a net force being exerted on the particle. The movement of the particle by this force is DEP. Assuming carbon nanotube bundles can be modeled as a prolate ellipsoid, the dielectrophoretic force is directly proportional to the volume of the particle, the permittivity of the suspending medium and the gradient of the electric field squared. DEP is also impacted by field frequency. The speed of motion of the particle is related to the viscosity of the suspending medium [101].

Particles in an electric field attract one another as they locally distort field lines, resulting in 'pearl-chaining' (linear alignment of particles) [104]. This is known as mutual DEP and it is a dipole-dipole interaction between particles in the presence of an external non-uniform electric field. Electro-orientation occurs along the longest axis of a polarized particle, and will result in alignment of particles along the electric field as the particles align with high and low potentials [105].

DEP, mutual DEP and electro-orientation facilitate the formation of aligned structures of CNTs in the presence of AC electric fields. Figure 2.6 shows a schematic of the mechanisms involved in these phenomena. Opposing the alignment of CNTs by AC electric fields is random

particle motion due to thermal energy in the system. This can be described as Brownian motion. The impact of Brownian motion increases as the size of the particle decreases [101].

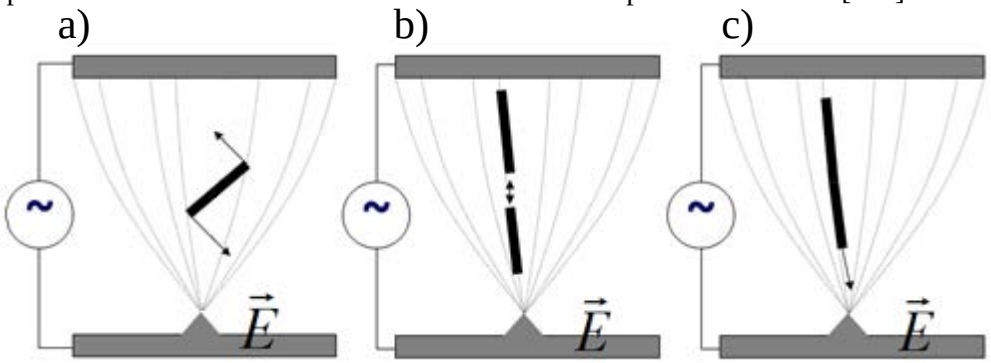


**Figure 2.6: CNTs in the presence of an AC electric field ($\vec{E}$) showing a) electro-orientation b) mutual DEP and c) DEP. Adapted from** [106]**.**

The use of AC electric fields to align CNTs in polyolefins has not often been reported in the literature, but is currently under investigation in our group with promising preliminary results [107].

## 2.5 References


[1] M. Moniruzzaman and K. I. Winey, "Polymer nanocomposites containing carbon nanotubes," *Macromolecules 39(16),* pp. 5194-5205. 2006.

[2] L. Zheng, M. O'Connell, S. Doorn, X. Liao, Y. Zhao, E. Akhadov, M. Hoffbauer, B. Roop, Q. Jia, R. Dye, D. Peterson, S. Huang, J. Liu and Y. Zhu, "Ultralong single-wall carbon nanotubes," *Nat. Mater. 3(10),* pp. 673-676. 2004.

[3] D. Bikiaris, "Microstructure and Properties of Polypropylene/Carbon Nanotube Nanocomposites," *Materials 3,* pp. 2884-2946. 2010.

[4] E. Thostenson, Z. Ren and T. Chou, "Advances in the science and technology of carbon nanotubes and their composites: A review," *Composites Sci. Technol. 61(13),* pp. 1899-1912. 2001.

[5] S. Louie, "Electronic properties, junctions, and defects of carbon nanotubes," in *Carbon Nanotubes,* pp. 113-145. 2001.

[6] M. Dresselhaus, G. Dresselhaus and P. Eklund, *Science of Fullerenes and Carbon Nanotubes: Their Properties and Applications.* San Deigo: Academic Press, 1996.

[7] B. Yakobson, C. Brabec and J. Bernholc, "Nanomechanics of carbon tubes: Instabilities beyond linear response," *Phys. Rev. Lett. 76(14),* pp. 2511-2514. 1996.

[8] R. Baughman, A. Zakhidov and W. de Heer, "Carbon nanotubes - the route toward applications," *Science 297(5582),* pp. 787-792. 2002.

[9] Nanocyl, "Nanocyl: The Carbon Nanotube Specialist - Carbon Nanotubes," 2013 .

[10] M. O'Connell, S. Bachilo, C. Huffman, V. Moore, M. Strano, E. Haroz, K. Rialon, P. Boul, W. Noon, C. Kittrell, J. Ma, R. Hauge, R. Weisman and R. Smalley, "Band gap fluorescence from individual single-walled carbon nanotubes," *Science 297(5581),* pp. 593-596. 2002.

[11] H. Dai, "Carbon nanotubes: Synthesis, integration, and properties," *Acc. Chem. Res. 35(12),* pp. 1035-1044. 2002.

[12] P. Ajayan, "Nanotubes from carbon," *Chem. Rev. 99(7),* pp. 1787-1799. 1999.

[13] T. Hertel, R. Walkup and P. Avouris, "Deformation of carbon nanotubes by surface van der waals forces," *Phys. Rev. B 58(20),* pp. 13870-13873. 1998.

[14] S. Iijima, "Helical microtubules of graphitic carbon," *Nature 354(6348),* pp. 56-58. 1991.

[15] S. Iijima and T. Ichihashi, "Single-shell carbon nanotubes of 1-nm diameter," *Nature 363(6430),* pp. 603-605. 1993.

[16] M. Wilson, "The carbon age," in *Nanotechnology: Basic Science and Emerging Technology* CRC Press, 2002.

[17] R. Andrews, D. Jacques, D. Qian and T. Rantell, "Multiwall carbon nanotubes: Synthesis and application," *Acc. Chem. Res. 35(12),* pp. 1008-1017. 2002.

[18] M. L. Healy, L. J. Dahlben and J. A. Isaacs, "Environmental assessment of single-walled carbon nanotube processes," *J. Ind. Ecol. 12(3),* pp. 376-393. 2008.

[19] A. Dupuis, "The catalyst in the CCVD of carbon nanotubes - a review," *Prog. Mater. Sci. 50(8),* pp. 929-961. 2005.

[20] T. McNally and P. Potschke, *Polymer-Carbon Nanotube Composites - Preparation, Properties and Applications.* Philadelphia: Woodhead Publishing Limited, 2011.

[21] P. Potschke, A. Bhattacharyya and A. Janke, "Melt mixing of polycarbonate with multiwalled carbon nanotubes: Microscopic studies on the state of dispersion," *Eur. Polym. J. 40(1),* pp. 137-148. 2004.

[22] P. Potschke, A. Bhattacharyya and A. Janke, "Carbon nanotube-filled polycarbonate composites produced by melt mixing and their use in blends with polyethylene," *Carbon 42(5-6),* pp. 965-969. 2004.

[23] T. McNally, P. Potschke, P. Halley, M. Murphy, D. Martin, S. Bell, G. Brennan, D. Bein, P. Lemoine and J. Quinn, "Polyethylene multiwalled carbon nanotube composites," *Polymer 46(19),* pp. 8222-8232. 2005.

[24] D. Qian, E. Dickey, R. Andrews and T. Rantell, "Load transfer and deformation mechanisms in carbon nanotube-polystyrene composites," *Appl. Phys. Lett. 76(20),* pp. 2868-2870. 2000.

[25] N. G. Sahoo, S. Rana, J. W. Cho, L. Li and S. H. Chan, "Polymer nanocomposites based on functionalized carbon nanotubes," *Progress in Polymer Science 35(7),* pp. 837-867. 2010.

[26] W. Bauhofer and J. Z. Kovacs, "A review and analysis of electrical percolation in carbon nanotube polymer composites," *Composites Sci. Technol. 69(10),* pp. 1486-1498. 2009.

[27] S. Abbasi, P. J. Carreau, A. Derdouri and M. Moan, "Rheological properties and percolation in suspensions of multiwalled carbon nanotubes in polycarbonate," *Rheol. Acta 48(9),* pp. 943-959. 2009.

[28] K. Menzer, B. Krause, R. Boldt, B. Kretzschmar, R. Weidisch and P. Poetschke, "Percolation behaviour of multiwalled carbon nanotubes of altered length and primary agglomerate morphology in melt mixed isotactic polypropylene-based composites," *Composites Sci. Technol.71,* pp. 1936-1943. 2011.

[29] R. Socher, B. Krause, M. T. Mueller, R. Boldt and P. Poetschke, "The influence of matrix viscosity on MWCNT dispersion and electrical properties in different thermoplastic nanocomposites," *Polymer 53,* pp. 495-504. 2012.

[30] I. Alig, P. Poetschke, D. Lellinger, T. Skipa, S. Pegel, G. R. Kasaliwal and T. Villmow, "Establishment, morphology and properties of carbon nanotube networks in polymer melts," *Polymer,* 53, pp. 4-28. 2012.

[31] S. Pegel, P. Poetschke, G. Petzold, I. Alig, S. M. Dudkin and D. Lellinger, "Dispersion, agglomeration, and network formation of multiwalled carbon nanotubes in polycarbonate melts," *Polymer 49(4),* pp. 974-984. 2008.

[32] F. Ciardelli, S. Coiai, E. Passaglia, A. Pucci and G. Ruggeri, "Nanocomposites based on polyolefins and functional thermoplastic materials," *Polym. Int. 57(6),* pp. 805-836. 2008.

[33] P. Poetschke, S. Pegel, M. Claes and D. Bonduel, "A novel strategy to incorporate carbon nanotubes into thermoplastic matrices," *Macromol. Rapid Commun. 29(3),* pp. 244-251. 2008.

[34] M. Rahmat and P. Hubert, "Carbon nanotube-polymer interactions in nanocomposites: A review," *Composites Sci. Technol. 72*, pp. 72-84. 2011.

[35] E. Assouline, A. Lustiger, A. Barber, C. Cooper, E. Klein, E. Wachtel and H. Wagner, "Nucleation ability of multiwall carbon nanotubes in polypropylene composites," *Journal of Polymer Science Part B-Polymer Physics 41(5),* pp. 520-527. 2003.

[36] D. Xu and Z. Wang, "Role of multi-wall carbon nanotube network in composites to crystallization of isotactic polypropylene matrix," *Polymer 49(1),* pp. 330-338. 2008.

[37] D. Bikiaris, A. Vassiliou, K. Chrissafis, K. M. Paraskevopoulos, A. Jannakoudakis and A. Docoslis, "Effect of acid treated multi-walled carbon nanotubes on the mechanical, permeability, thermal properties and thermo-oxidative stability of isotactic polypropylene," *Polym. Degrad. Stab. 93(5),* pp. 952-967. 2008.

[38] B. Grady, F. Pompeo, R. Shambaugh and D. Resasco, "Nucleation of polypropylene crystallization by single-walled carbon nanotubes,"*J. Phys. Chem. B 106(23),* pp. 5852-5858. 2002.

[39] A. M. K. Esawi, H. G. Salem, H. M. Hussein and A. R. Ramadan, "Effect of processing technique on the dispersion of carbon nanotubes within polypropylene carbon nanotube-composites and its effect on their mechanical properties," *Polym. Compos. 31(5),* pp. 772-780. 2010.

[40] L. Xu, Z. Ye, Q. Cui and Z. Gu, "Noncovalent nonspecific functionalization and solubilization of multi-walled carbon nanotubes at high concentrations with a hyperbranched polyethylene," *Macromolecular Chemistry and Physics 210(24),* pp. 2194-2202. 2009.

[41] Y. Xi, A. Yamanaka, Y. Bin and M. Matsuo, "Electrical properties of segreated ultrahigh molecular weight polyethylene/multiwalled carbon nanotube composites.," *J. Appl. Polym. Sci. 105(5),* pp. 2868-2876. 2007.

[42] A. Funck and W. Kaminsky, "Polypropylene carbon nanotube composites by in situ polymerization," *Composites Sci. Technol. 67(5),* pp. 906-915. 2007.

[43] W. Kaminsky, A. Funck and K. Wiemann, "Nanocomposites by in situ polymerization of olefins with metallocene catalysts," *Macromol. Symp. 239,* pp. 1-6. 2006.

[44] D. Bonduel, M. Mainil, M. Alexandre, F. Monteverde and P. Dubois, "Supported coordination polymerization: A unique way to potent polyolefin carbon nanotube nanocomposites," *Chem. Commun. (6),* pp. 781-783. 2005.

[45] C. Zhao, G. Hu, R. Justice, D. Schaefer, S. Zhang, M. Yang and C. Han, "Synthesis and characterization of multi-walled carbon nanotubes reinforced polyamide 6 via in situ polymerization," *Polymer 46(14),* pp. 5125-5132. 2005.

[46] J. N. Coleman, U. Khan, W. J. Blau and Y. K. Gun'ko, "Small but strong: A review of the mechanical properties of carbon nanotube-polymer composites," *Carbon 44(9),* pp. 1624-1652. 2006.

[47] K. Prashantha, J. Soulestin, M. F. Lacrampe, P. Krawczak, G. Dupin and M. Claes, "Masterbatch-based multi-walled carbon nanotube filled polypropylene nanocomposites: Assessment of rheological and mechanical properties," *Compos. Sci. Technol. 69(11-12),* pp. 1756-1763. 2009.

[48] K. Petrie, A. Docoslis, S. Vasic, M. Kontopoulou, S. Morgan and Z. Ye, "Non-covalent/non-specific functionalization of multi-walled carbon nanotubes with a hyperbranched polyethylene and characterization of their dispersion in a polyolefin matrix," *Carbon 49,* pp. 3378-3382. 2011.

[49] A. Vasileiou, A. Docoslis and M. Kontopoulou, "The role of non-covalent functionalization and matrix viscosity on the dispersion and properties of LLDPE/MWCNT nanocomposites," *Polymer (accepted).* 2013.

[50] B. Krause, M. Mende, G. Petzold, R. Boldt and P. Poetschke, "Methods to Characterize the Dispersability of Carbon Nanotubes and Their Length Distribution," *Chemie Ingenieur Technik 84,* pp. 263-271. 2012.

[51] Y. Sun, K. Fu, Y. Lin and W. Huang, "Functionalized carbon nanotubes: Properties and applications," *Acc. Chem. Res. 35(12),* pp. 1096-1104. 2002.

[52] V. Georgakilas, K. Kordatos, M. Prato, D. Guldi, M. Holzinger and A. Hirsch, "Organic functionalization of carbon nanotubes," *J. Am. Chem. Soc. 124(5),* pp. 760-761. 2002.

[53] S. A. Girei, S. P. Thomas, M. A. Atieh, K. Mezghani, S. K. De, S. Bandyopadhyay and A. Al-Juhani, "Effect of -COOH Functionalized Carbon Nanotubes on Mechanical, Dynamic Mechanical and Thermal Properties of Polypropylene Nanocomposites," *J. Thermoplast. Compos. Mater. 25,* pp. 333-350. 2012.

[54] S. Li, H. Chen, W. Bi, J. Zhou, Y. Wang, J. Li, W. Cheng, M. Li, L. Li and T. Tang, "Synthesis and characterization of polyethylene chains grafted onto the sidewalls of single-walled carbon nanotubes via copolymerization," *J. Polym. Sci. Pol. Chem. 45(23),* pp. 5459-5469. 2007.

[55] S. Qin, D. Oin, W. Ford, D. Resasco and J. Herrera, "Polymer brushes on single-walled carbon nanotubes by atom transfer radical polymerization of n-butyl methacrylate," *J. Am. Chem. Soc. 126(1),* pp. 170-176. 2004.

[56] D. Baskaran, J. Mays and M. Bratcher, "Polymer-grafted multiwalled carbon nanotubes through surface-initiated polymerization," *Angew. Chem. -Int. Edit. 43(16),* pp. 2138-2142. 2004.

[57] Z. Yao, N. Braidy, G. Botton and A. Adronov, "Polymerization from the surface of single-walled carbon nanotubes - preparation and characterization of nanocomposites," *J. Am. Chem. Soc. 125(51),* pp. 16015-16024. 2003.

[58] B. Yang, J. Shi, K. P. Pramoda and S. H. Goh, "Enhancement of the mechanical properties of polypropylene using polypropylene-grafted multiwalled carbon nanotubes," *Composites Sci. Technol. 68(12),* pp. 2490-2497. 2008.

[59] B. Yang, K. P. Pramoda, G. Q. Xu and S. H. Goh, "Mechanical reinforcement of polyethylene using polyethylene-grafted multiwalled carbon nanotubes," *Adv. Funct. Mater. 17(13),* pp. 2062-2069. 2007.

[60] Q. Feng, X. Xie, Y. Liu, W. Zhao and Y. Gao, "Synthesis of hyperbranched aromatic polyamide-imide and its grafting onto multiwalled carbon nanotubes," *J. Appl. Polym. Sci. 106(4),* pp. 2413-2421. 2007.

[61] D. Baskaran, J. Mays and M. Bratcher, "Noncovalent and nonspecific molecular interactions of polymers with multiwalled carbon nanotubes," *Chemistry of Materials 17(13),* pp. 3389-3397. 2005.

[62] Z. Ye and S. Li, "Hyperbranched polyethylenes and functionalized polymers by chain walking polymerization with pd-diimine catalysis," *Macromolecular Reaction Engineering 4(5),* pp. 319-332. 2010.

[63] K. Prashantha, J. Soulestin, M. F. Lacrampe, M. Claes, G. Dupin and P. Krawczak, "Multi-walled carbon nanotube filled polypropylene nanocomposites based on masterbatch route: Improvement of dispersion and mechanical properties through PP-g-MA addition," *Express Polym. Lett. 2(10),* pp. 735-745. 2008.

[64] M. Pollanen, S. Pirinen, M. Suvanto and T. T. Pakkanen, "Influence of carbon nanotube-polymeric compatibilizer masterbatches on morphological, thermal, mechanical, and tribological properties of polyethylene," *Composites Sci. Technol. 71(10),* pp. 1353-1360. 2011.

[65] S. H. Lee, E. Cho, S. H. Jeon and J. R. Youn, "Rheological and electrical properties of polypropylene composites containing functionalized multi-walled carbon nanotubes and compatibilizers," *Carbon 45(14),* pp. 2810-2822. 2007.

[66] J. Thomassin, I. Huynen, R. Jerome and C. Detrembleur, "Functionalized polypropylenes as efficient dispersing agents for carbon nanotubes in a polypropylene matrix; application to electromagnetic interference (EMI) absorber materials," *Polymer 51(1),* pp. 115-121. 2010.

[67] E. Cohen, H. Dodiuk, A. Ophir, S. Kenig, C. Barry and J. Mead, "Evidences for pi-interactions between pyridine modified copolymer and carbon nanotubes and its role as a compatibilizer in poly(methyl methacrylate) composites," *Composites Sci. Technol. 79*pp. 133-139. 2013.

[68] M. Kontopoulou, "Polymer blends," in *CHEE 901: Principles and Applications of Polymer Rheology*. 2012.

[69] M. Bailly and M. Kontopoulou, "Preparation and characterization of thermoplastic olefin/nanosilica composites using a silane-grafted polypropylene matrix," *Polymer 50(11),* pp. 2472-2480. 2009.

[70] Y. Liu and M. Kontopoulou, "The structure and physical properties of polypropylene and thermoplastic olefin nanocomposites containing nanosilica," *Polymer 47(22),* pp. 7731-7739. 2006.

[71] J. R. Austin and M. Kontopoulou, "Effect of organoclay content on the rheology, morphology, and physical properties of polyolefin elastomers and their blends with polypropylene," *Polym. Eng. Sci. 46(11),* pp. 1491-1501. 2006.

[72] Y. Liu and M. Kontopoulou, "Effect of filler partitioning on the mechanical properties of TPO/nanosilica composites," *Journal of Vinyl & Additive Technology 13(3),* pp. 147-150. 2007.

[73] M. Bailly and M. Kontopoulou, "Nanocomposite blends containing polyolefins," in *Advances in Polyolefin Nanocomposites*, V. Mittal, Ed. CRC Press, 2011.

[74] M. Sumita, K. Sakata, S. Asai, K. Miyasaka and H. Nakagawa. "Dispersion of fillers and the electrical-conductivity of polymer blends filled with carbon-black," *Polymer Bulletin 25(2),* pp. 265-271. 1991.

[75] S. Hom, A. R. Bhattacharyya, R. A. Khare, A. R. Kulkarni, M. Saroop and A. Biswas, "Blends of polypropylene and ethylene octene comonomer with conducting fillers: Influence of state of dispersion of conducting fillers on electrical conductivity," *Polym. Eng. Sci. 49(8),* pp. 1502-1510. 2009.

[76] C. Li, Q. Zhao, H. Deng, C. Chen, K. Wang, Q. Zhang, F. Chen and Q. Fu, "Preparation, structure and properties of thermoplastic olefin nanocomposites containing functionalized carbon nanotubes," *Polym. Int. 60(11),* pp. 1629-1637. 2011.

[77] S. Wu, *Polymer Interface and Adhesion.* New York: Macel Dekker, 1982.

[78] S. Wu, "A generalized criterion for rubber toughening - the critical matrix ligament thickness," *J. Appl. Polym. Sci. 35(2),* pp. 549-561. 1988.

[79] S. Wu, "Phase-structure and adhesion in polymer blends - a criterion for rubber toughening," *Polymer 26(12),* pp. 1855-1863. 1985.

[80] D. Paul and J. Barlow, "Polymer blends (or alloys)," *J. Macromol. Sci. -Rev. Macromol. Chem. Phys. C18(1),* pp. 109-168. 1980.

[81] M. Kontopoulou, W. Wang, T. G. Gopakumar and C. Cheung, "Effect of composition and comonomer type on the rheology, morphology and properties of ethylene-alpha-olefin copolymer/polypropylene blends," *Polymer 44(24),* pp. 7495-7504. 2003.

[82] P. Martin, P. Carreau, B. Favis and R. Jerome, "Investigating the morphology/rheology interrelationships in immiscible polymer blends," *J. Rheol. 44(3),* pp. 569-583. 2000.

[83] N. Kukaleva, M. Jollands, F. Cser and E. Kosior, "Influence of phase structure on impact toughening of isotactic polypropylene by metallocene-catalyzed linear low-density polyethylene," *J. Appl. Polym. Sci. 76(7),* pp. 1011-1018. 2000.

[84] B. Favis and D. Therrien, "Factors influencing structure formation and phase size in an immiscible polymer blend of polycarbonate and polypropylene prepared by twin-screw extrusion," *Polymer 32(8),* pp. 1474-1481. 1991.

[85] M. Kontopoulou, Y. Liu, J. R. Austin and J. S. Parent, "The dynamics of montmorillonite clay dispersion and morphology development in immiscible ethylene-propylene rubber/polypropylene blends," *Polymer 48(15),* pp. 4520-4528. 2007.

[86] C. Li, H. Deng, K. Wang, Q. Zhang, F. Chen and Q. Fu, "Strengthening and toughening of thermoplastic polyolefin elastomer using polypropylene-grafted multiwalled carbon nanotubes," *J. Appl. Polym. Sci. 121(4),* pp. 2104-2112. 2011.

[87] L. Liu, Y. Wang, Y. Li, J. Wu, Z. Zhou and C. Jiang, "Improved fracture toughness of immiscible polypropylene/ethylene-co-vinyl acetate blends with multiwalled carbon nanotubes," *Polymer 50(14),* pp. 3072-3078. 2009.

[88] S. Ray, S. Pouliot, M. Bousmina and L. Utracki, "Role of organically modified layered silicate as an active interfacial modifier in immiscible polystyrene/polypropylene blends," *Polymer 45(25),* pp. 8403-8413. 2004.

[89] D. Voulgaris and D. Petridis, "Emulsifying effect of dimethyldioctadecylammonium-hectorite in polystyrene/poly(ethyl methacrylate) blends," *Polymer 43(8),* pp. 2213-2218. 2002.

[90] B. Khatua, D. Lee, H. Kim and J. Kim, "Effect of organoclay platelets on morphology of nylon-6 and poly(ethylene-ran-propylene) rubber blends," *Macromolecules 37(7),* pp. 2454-2459. 2004.

[91] J. Huang, "Carbon black filled conducting polymers and polymer blends," *Adv. Polym. Technol. 21(4),* pp. 299-313. 2002.

[92] F. Gubbels, S. Blacher, E. Vanlathem, R. Jerome, R. Deltour, F. Brouers and P. Teyssie, "Design of electrical conductive composites - key role of the morphology on the electrical-properties of carbon-black filled polymer blends," *Macromolecules 28(5),* pp. 1559-1566. 1995.

[93] F. Fenouillot, P. Cassagnau and J. Majeste, "Uneven distribution of nanoparticles in immiscible fluids: Morphology development in polymer blends," *Polymer 50(6),* pp. 1333-1350. 2009.

[94] T. Y. Hwang, Y. Yoo and J. W. Lee, "Electrical conductivity, phase behavior, and rheology of polypropylene/polystyrene blends with multi-walled carbon nanotube," *Rheol. Acta 51(7),* pp. 623-636. 2012.

[95] P. Zhou, W. Yu, C. Zhou, F. Liu, L. Hou and J. Wang, "Morphology and electrical properties of carbon black filled LLDPE/EMA composites," *J. Appl. Polym. Sci. 103(1),* pp. 487-492. 2007.

[96] A. Dasari, Z. Yu and Y. Mai, "Effect of blending sequence on microstructure of ternary nanocomposites," *Polymer 46(16),* pp. 5986-5991. 2005.

[97] L. Valentini, J. Biagiotti, J. Kenny and M. Manchado, "Physical and mechanical behavior of single-walled carbon nanotube/polypropylene/ethylene-propylene-diene rubber nanocomposites," *J. Appl. Polym. Sci. 89(10),* pp. 2657-2663. 2003.

[98] A. Goeldel, G. R. Kasaliwal, P. Poetschke and G. Heinrich, "The kinetics of CNT transfer between immiscible blend phases during melt mixing," *Polymer 53*, pp. 411-421. 2012.

[99] A. Goeldel, A. Marmur, G. R. Kasaliwal, P. Poetschke and G. Heinrich, "Shape-dependent localization of carbon nanotubes and carbon black in an immiscible polymer blend during melt mixing," *Macromolecules 44(15),* pp. 6094-6102. 2011.

[100] O. Osazuwa, M. Kontopoulou, P. Xian, Z. Ye and A. Docoslis, "Polymer composites containing non-covalently functionalized carbon nanotubes: A study of their dispersion characteristics and response to AC electric field," in *20th International Congress of Chemical and Process Engineering CHISA 2012,* 25-29 August 2012, Prague, Czech Republic, 2012 .

[101] Y. Lu, C. Chen, L. Yang and Y. Zhang, "Theoretical simulation on the assembly of carbon nanotubes between electrodes by AC dielectrophoresis," *Nanoscale Res. Lett. 4(2),* pp. 157-164. 2009.

[102] X. Chen, T. Saito, H. Yamada and K. Matsushige, "Aligning single-wall carbon nanotubes with an alternating-current electric field," *Appl. Phys. Lett. 78(23),* pp. 3714-3716. 2001.

[103] H. Morgan and N. Green, *AC Electrokinetics: Colloids and Nanoparticles.* Research Studies Press Ltd., 2002.

[104] B. C. Gierhart, D. G. Howitt, S. J. Chen, R. L. Smith and S. D. Collins, "Frequency dependence of gold nanoparticle superassembly by dielectrophoresis," *Langmuir 23(24),* pp. 12450-12456. 2007.

[105] M. Hughes, *Nanoelectromechanics in Engineering and Biology.* New York: CRC Press, 2003.

[106] O. Osazuwa, "Synthesis and characterization of electrically conductive polyolefin/carbon nanotube composites," Student Seminar Presentation, Queen's University, 2013.

[107] O. Osazuwa, M. Kontopoulou, P. Xiang, Z. Ye and A. Docoslis, "Electrically conducting polyolefin composites containing electric field-aligned multiwalled carbon nanotube structures: the effect of process parameters and filler loading," *Manuscript in Preparation*, 2013.

# Chapter 3[1]

# Non-Covalently Functionalized MWCNTs with a Hyperbranched Polyethylene and their Composites with Polypropylene

## 3.1 Introduction

The realization of multi-walled carbon nanotube (MWCNT)/polyolefin composites as valuable engineering materials is hindered by the tendency of MWCNTs to extensively aggregate when melt compounded with non polar polymers. This aggregation is thermodynamically driven by van der Waals and π-π interactions between MWCNTs [1]. Numerous covalent and non-covalent MWCNT functionalization approaches have been employed in an attempt to break-up these interactions and improve dispersion in polyolefin composites. These approaches aim to improve mechanical and electrical performance. Covalent functionalizations can efficiently disperse nanotubes, but have been shown to disrupt the extended π conjugation, thus negatively impacting the electrical properties of the nanotubes [1-5]. Non-covalent functionalization approaches are based on carbon-hydrogen group-π (CH-π) and/or π-π interactions. They have been shown to improve MWCNT solubility in various solvents, break-up filler/filler interactions and enhance interfacial adhesion between a polyolefin matrix and the sidewalls of the MWCNTs, without hindering electrical performance [6-9].

It has recently been shown that hyperbranched polymers that have a dendritic structure are capable of non-covalent interactions with the surface of MWCNTs and can thus be used to functionalize them [6, 10]. Dendrimers have a highly ordered, branched and globular structure with valuable properties, but are intensive to synthesize. The industrially practical alternative is hyperbranched polymers that have more irregular three-dimensional structures, but similar resultant properties [11, 12]. Hyperbranched polyethylene (HBPE) has a complex and irregular

[1] Portions of the work contained within this chapter have been published in Osazuwa O, Petrie K, Kontopoulou M, Xiang P, Ye Z, Docoslis A. *Compos. Sci. Technol.* 2012; 72:27.

dendritic structure containing many branches (methyl to hexyl and higher) and also branch on branch structures. The complex structure can be controlled by ethylene pressure using a 'chain walking' palladium-diimine catalyst. The resulting polymer can have extremely high molecular weight ($M_w \approx 150$ kg/mol) while maintaining a low viscosity, due to its conformation [13].

Recent work in our laboratory has shown that this non-covalent non-specific functionalization of MWCNTs using HBPE is effective in improving the MWCNT dispersion within polyethylene (PE) matrices [14]. In the present chapter, this procedure is employed in an attempt to improve MWCNT dispersion by melt mixing within a polypropylene (PP) matrix. The surface properties at various functionalization concentrations of HBPE with nanotubes are investigated through adsorption experiments. The effectiveness of the HBPE functionalization on MWCNT dispersion is characterized using optical microscopy and TEM imaging. The resulting mechanical and electrical properties are reported.

## 3.2 Experimental

### 3.2.1 Materials

MWCNTs were used as supplied from Nanolab Inc. (purity: >95%, diameter: 30±15nm and length: 1-5 μm). The specific surface area (SSA) of the MWCNTs was 300 $m^2/g$ based on Brunauer-Emmett-Teller characterization. The average pore size of the MWCNTs as determined by $N_2$ sorption experiments is approximately 2.3 nm.

The HBPE used in this work was polymerized using a chain walking palladium-diimine catalyst as outlined by Ye and Li [13]. Samples were supplied by Dr. Ye from Laurentian University. The diameter of the HBPE molecules was determined by Dynamic Light Scattering (DLS) to be 9.5±1.4 and 12.2±0.5 nm in tetrahydrofuran (THF) and toluene, respectively [10].

A PP homopolymer, PP 1042, by ExxonMobil was used as the matrix. Properties of this material can be seen in Table 3.1. Irganox B225 is a hindered phenol antioxidant that was added to each composite at 0.2 wt% for improved thermal stability.

**Table 3.1: Properties of polypropylene matrix.**

| *Material* | *PP* |
|---|---|
| Trade Name | Escorene® PP 1042 |
| MFR (g/10min.) | 1.9 @ 230°C |
| Density (kg/m$^3$) | 900 |
| Melting Point (°C) | 163 |

### 3.2.2 HBPE Functionalization Procedure and Characterization

Mixtures of HBPE and MWCNTs in THF with mass ratio between 0.0 and 3.0 were prepared by adding HBPE into dispersions containing 2.0 mg MWCNT/ml of THF. The resulting mixtures were sonicated for 1 hour, and then stirred overnight. The supernatant solutions were vacuum filtered drop-wise through Teflon membrane with pore size of 0.22 μm. After being washed twice with equal volumes of THF (6 ml) the filters were dried in a vacuum oven overnight at room temperature.

Thermo gravimetric analysis (TGA) was carried out on dried samples using a Q500 TGA by TA Instruments. Data from TGA analysis was used in order to determine the amount of HBPE adsorbed onto the MWCNTs and to construct an adsorption isotherm.

### 3.2.3 Melt Compounding

Pristine and HBPE functionalized MWCNTs were melt mixed with PP in a DSM Research 5ml co-rotating twin-screw micro-compounder at 190°C, 120 RPM and a mixing time of 10 minutes under nitrogen purge. MWCNTs were first pre-mixed with the PP in a Carver hot press at 200°C for 1 minute, by folding and hot-pressing 3 times. The resulting mixtures were subsequently added in the twin-screw micro-compounder to produce composites containing 0.1 to 10 wt% (0.05 to 5.7 vol.% converted using densities of 0.9 and 1.65 g/cm$^3$ for PP and MWCNTs respectively). In the case of HBPE functionalized MWCNT, TGA analysis was employed to specify the amount of bound HBPE onto the MWCNT, so as to ensure that the amount of actual

MWCNT in the composites remained consistent. Neat PP was subjected to a similar processing history, to provide a basis for comparison. It was determined from preliminary investigations that the high temperature and mixing rate during compounding did not significantly impact the complex viscosity of the PP. These preliminary frequency sweep experiments were performed on a Reologica ViscoTech oscillatory rheometer using 20 mm parallel plate fixture at a 1 mm gap and 190$^{o}$C under a nitrogen purge in dynamic oscillation mode.

### 3.2.4 Composite Properties

#### 3.2.4.1 Morphology

The macro-scale dispersion of MWCNTs in the melt blended composites was investigated using an Olympus BX 51 optical microscope. Composite films were loaded on a Linkam SCC 450 Hot Stage at 180$^{o}$C and pressed to a thickness of 50 μm. Images were recorded using transmitted light. Transmission electron microscopy (TEM) images were taken using a FEI Tecnai 20 instrument to investigate the nanoscale dispersion. Ultra-thin films of the composites were prepared by cryosectioning, using a Leica ultra-microtome.

#### 3.2.4.2 Electrical conductivity

Volume resistivity was measured under direct current (DC) at room temperature using a Keithley 8009 Resistivity Test Fixture connected to a Keithley 6517B Electrometer/High Resistance Meter for an electrification time of 1 minute. Samples dimensions of 6 cm in diameter and 0.5 mm thick were prepared by compression molding into discs of the melt-compounded composites in a Carver press at 200$^{o}$C for 1 minute.

#### 3.2.4.3 Tensile testing

Tensile testing was performed using an Instron 3369 Universal testing apparatus. Tests were performed according to ASTM D638 with a type-V die cut from melt compounded samples

that were compression molded in a Carver press at 200°C for 1 minute (dumbbell shaped specimens with dimensions: 7.62 mm x 3.50 mm x 1.45 mm). A crosshead speed of 10 mm/min was used at room temperature. A minimum of three trials were performed on each sample with the average value with one standard deviation reported.

## 3.3 Results and Discussion

### 3.3.1 HBPE absorption on MWCNTs

The HBPE used in this work does not have any specific functionality. Therefore, the driving force for HBPE to adsorb onto CNT is the extensive amount of CH–π interactions between the hyperbranched structure of HBPE and the MWCNT sidewalls [6]. The globular-shaped HBPE, which has a highly compact spherical chain architecture with "hydrodynamic" diameter in THF of 9.5±1.4 nm (Figure 3.1 (a)) is non-covalently adsorbed on the MWCNT sidewalls (Figure 3.1 (b)) [10].

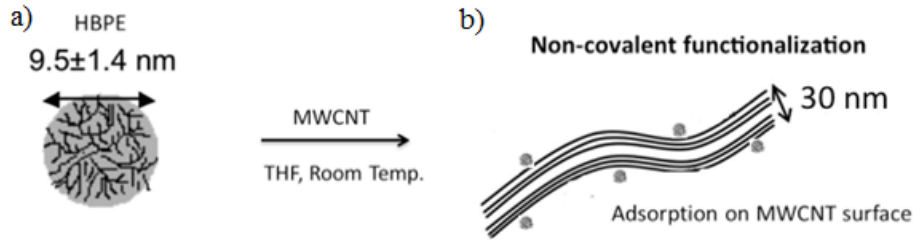


**Figure 3.1: a) Schematic of HBPE molecule with hydrodynamic diameter in THF and b) partial surface coverage of MWCNT with HBPE through non-covalent, non-specific functionalization. Adapted from** [10]**.**

An adsorption isotherm was constructed as follows to characterize the state of adsorption of HBPE on the nanotubes and to obtain an estimate of the degree of surface coverage: Varying amounts of HBPE were added to the MWCNTs, following the procedure described in the experimental section, and were subsequently subjected to non-isothermal TGA experiments. The resulting scans are shown in Figure 3.2. The amount of HBPE that was adsorbed onto the

nanotubes was determined by the wt% loss from 200°C to 500°C for every weight ratio examined. The average weight loss of the pure CNTs was subtracted from the weight loss of the functionalized nanotubes. The differential amount represents the amount of HBPE that remains bound to the MWCNT after functionalization.

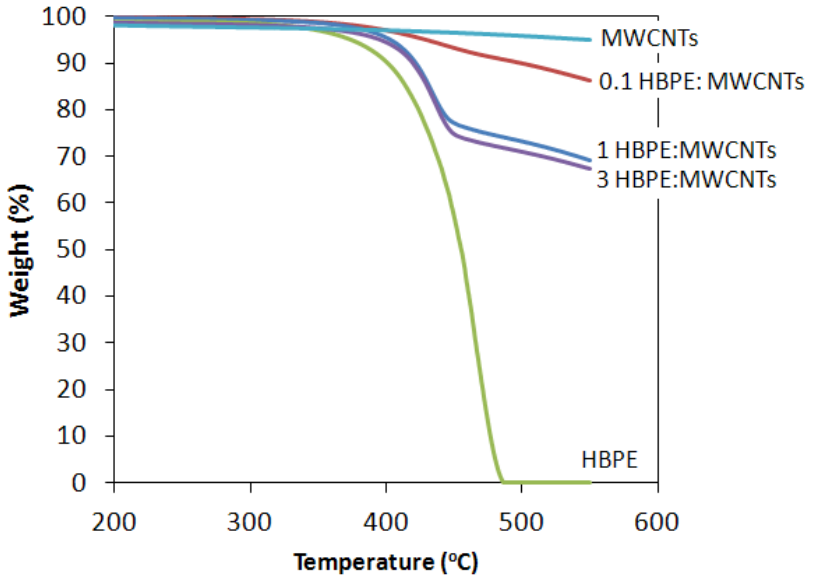


**Figure 3.2: TGA curves for pure MWCNTs, HBPE and MWCNTs coated with HBPE at various weight ratios.**

The resulting data obtained from this procedure were used to build an adsorption isotherm, depicting the actual amount of adsorbed HBPE as a function of the original HBPE:MWCNT ratio used for functionalization (Figure 3.3). The results suggest that after washing with THF to remove all loosely bound polymer, only a fraction of the HBPE remains adsorbed on the MWCNTs. A plateau appears around an applied HBPE:MWCNT mass ratio of 1. This translates into an adsorbed amount of about 0.3-0.34 g of HBPE/g of MWCNT. No increase is observed in the adsorbed HBPE amount beyond this mass ratio. Therefore the ratio of 1.0 is used in the preparation of PP/MWCNT composites.

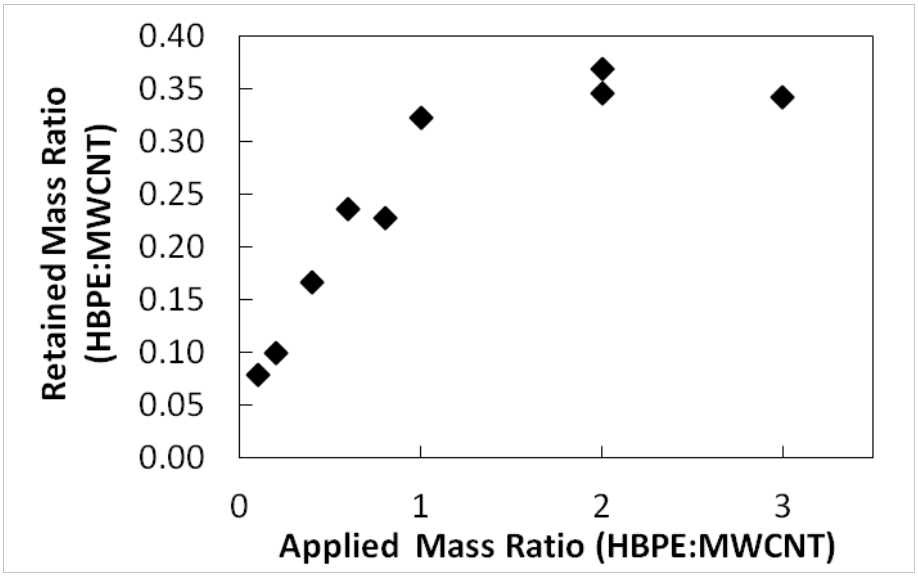


**Figure 3.3: Adsorption isotherm of HBPE on MWCNTs at room temperature in THF with a concentration of 2mg MWCNTs/ml THF.**

Further insight into the surface coverage of HBPE onto the MWCNTs can be obtained by examining the adsorbed amount and molecular dimensions of HBPE along with the pore size of the MWCNTs. The comparable magnitude of the "hydrodynamic" diameter of HBPE in THF (9.5±1.4 nm) to the external dimensions of the MWCNTs (30 nm) along with the pore size of the MWCNTs (1.47 nm) suggests that entrance and diffusion inside of the nanotubes is not likely. Therefore, it is more probable that the HBPE is adsorbed to the sidewalls of the MWCNTs as represented in Figure 3.1 b). Moreover the shape of the adsorption isotherm in Figure 3.3 appears to closely follow a Type 1 or Langmuir isotherm. This indicates that the HBPE exists in a monolayer around the MWCNTs [15, 16]. These results further suggest that HBPE resides on the surface of MWCNTs. Based on the results of Figure 3.3 at the plateau of adsorption approximately 35% of the carbon nanotube surface is covered by HBPE.

### 3.3.2 Composite characterization

3.3.2.1 MWCNT Dispersion

Optical micrographs in Figure 3.4 offer insight into the state of dispersion of the MWCNTs. Extensive MWCNT aggregation can be seen in PP/MWCNT composites containing 3 wt% MWCNTs, with aggregates larger than 100 μm (Figure 3.4 a) and b)). A macrocomposite, rather than a nanocomposite is formed. These images also show areas devoid of filler, indicative of poor distribution. When an equivalent amount of HBPE functionalized MWCNTs are added to PP, it can be seen that the size and number of aggregates decreases, even though many micron-sized aggregates still exist.

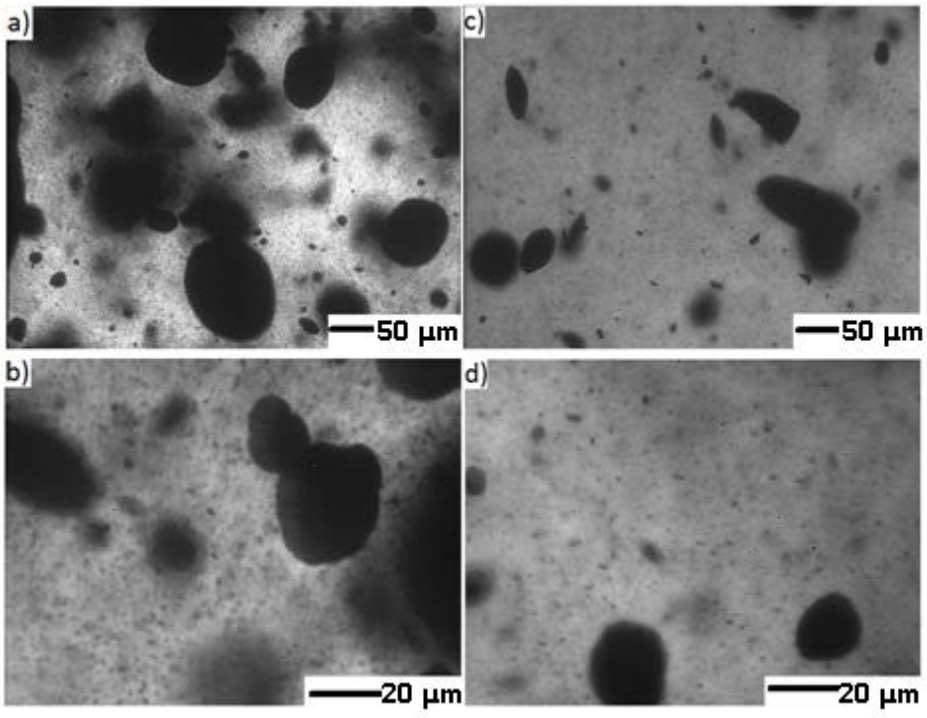


**Figure 3.4: Optical micrographs of PP/3 wt% MWCNTs at 20x (a) and 80x (b) and PP/3 wt% HBPE-MWCNTs at 20x (c) and 80x (d).**

A reduction in MWCNT aggregate size and number with HBPE functionalization is also evident in the TEM images shown in Figure 3.5. Only a few individual nanotubes can be seen within the PP composites, while most of the nanotubes still exist as aggregates. The aggregate size remains similar upon increasing HBPE-MWCNT loading, whereas very large aggregates exist in the composites containing high contents of pristine MWCNTs (Figure 3.5 a) and b)).

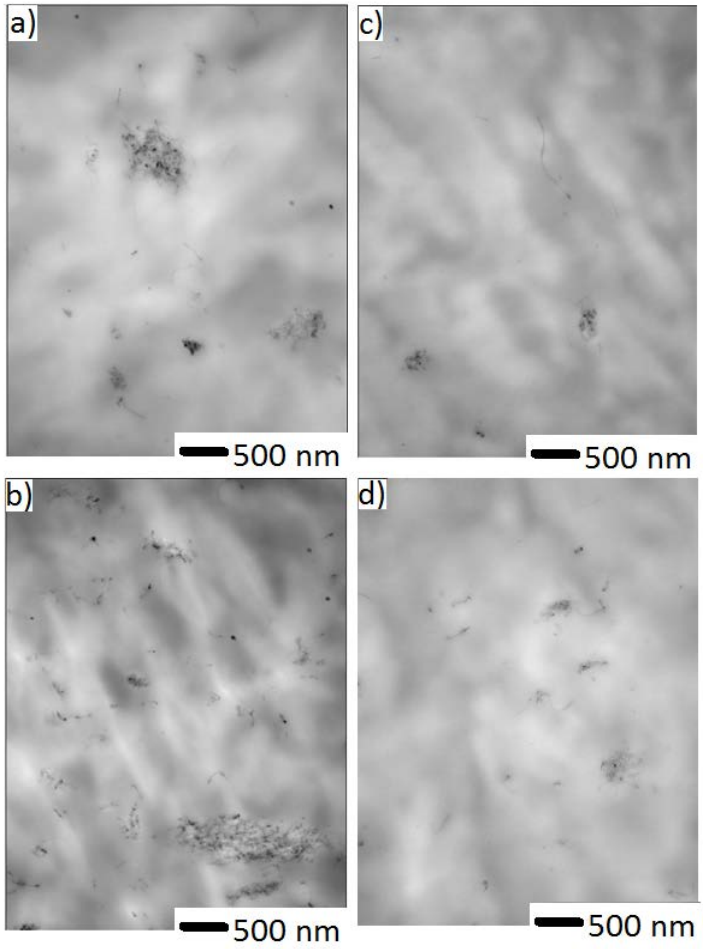


**Figure 3.5: TEM images of pristine (a,b) and HBPE-functionalized (c, d) MWCNTS at 3 (a, c) and 6 wt% (b, d) loadings.**

These findings suggest that the HBPE functionalization reduces filler/filler interactions, by disrupting the van der Waals forces between MWCNTs to a limited extent, thus resulting in smaller aggregates of MWCNTs in the polypropylene matrix. Interfacial interactions are also likely improved with the addition of the HBPE, allowing for better stress transfer to the MWCNTs during compounding. This leads to more efficient aggregate break-up upon melt mixing. However, dispersion and distribution still remain problematic irrespective of MWCNT functionalization, contrary to the findings from previous work on PE based composites [14]. This suggests that HBPE is not as compatible with PP, as with PE, thus limiting the applicability of this functionalization approach.

3.3.2.2 Electrical Properties

MWCNT microstructure within a polymer composite plays an integral part in the electrical performance of the materials. The formation of an interconnected percolating network results in a transition from an insulating to conductive material as conductive pathways through the material are created with the addition of more MWCNTs [17]. The 'percolation threshold' is defined as the concentration of nanotubes above which the conductivity of the material increases exponentially, and can be estimated by fitting the following power-law models above and below the threshold [17, 18]:

$$\sigma = \sigma_{matrix}\left(\frac{\varphi_c-\varphi}{\varphi_c}\right)^{-s}, \ \varphi < \varphi_c \qquad (3.1)$$

$$\sigma = \mathrm{m}\left(\frac{\varphi\text{-}\varphi_c}{1\text{-}\varphi_c}\right)^{t} \approx \mathrm{m}\left(\varphi\text{-}\varphi_c\right)^{t}, \ \varphi > \varphi_c \qquad (3.2)$$

where $\varphi_c$ is the percolation threshold in volume fraction of MWCNTs, $\varphi$ is the volume fraction of MWCNTs, $\sigma$ is the conductivity of the sample, $\sigma_{matrix}$ is the initial matrix conductivity, s and t are the critical exponent factors below and above percolation respectively and m is a constant. Typical values are $s \approx 0.73$ and $t \approx 2$ [19].

Figure 3.6 below shows the electrical conductivities of the composites filled with pristine and HBPE functionalized MWCNTs. The lines represent the model fit of Equations 3.1 and 3.2 to the experimental data, with model parameters summarized in Table 3.2.

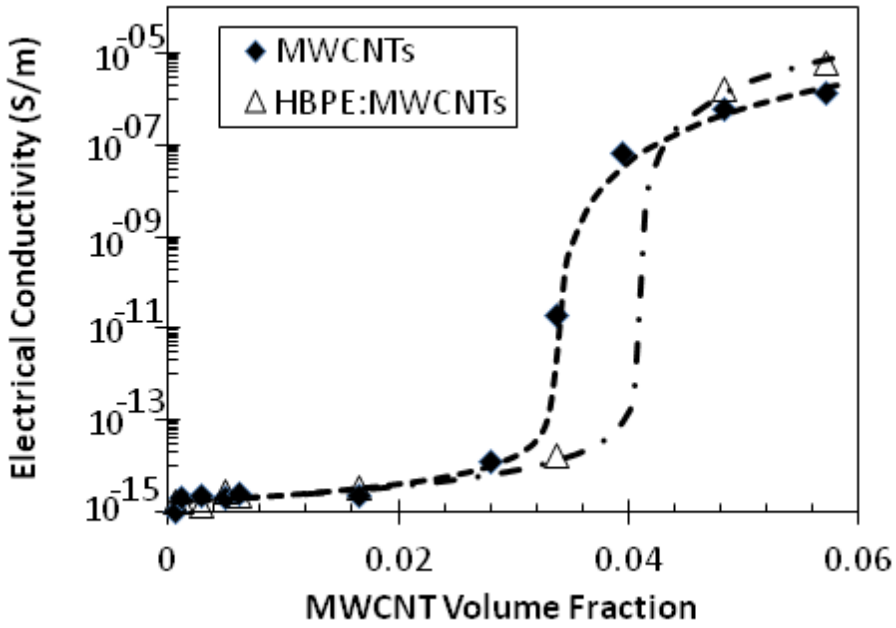


**Figure 3.6: Electrical conductivity of PP/MWCNT composites. Lines represent power-law model fit (Equations 3.1 and 3.2).**

**Table 3.2: Power-law model parameters for electrical conductivities.**

| *Sample* | *s* | *t* | $\varphi_c$ *(vol. %)* | $\varphi_c$ *(wt%)* |
|---|---|---|---|---|
| PP/MWCNTs | 1 | 2.9 | 3.4 | 6.0 |
| PP/ HBPE-MWCNTs | 1.1 | 2.1 | 4.1 | 7.3 |

Based on the model fits the percolation threshold occurs at 6 wt% and 7.3 wt% for the pristine and HBPE functionalized MWCNTs respectively. These percolation threshold values are slightly higher than other reported values for PP based composites [20-25]. It is commonly accepted in the literature that percolation is attributed to the formation of an interconnected, three-dimensional network [17]. It is surprising that the present samples do show a percolation threshold, since all the MWCNTs exist in the form of aggregates. No extensive amount of interconnectivity between nanotubes near the threshold can be seen from the TEM images of Figure 3.5 b) and d).

The transition to a more conductive material is most likely the result of the presence of aggregates, some of which are in the order of hundreds of μm, comparable to the sample thickness (500 μm) during volume resistivity measurements. The pristine MWCNTs in the PP composites form aggregates large enough to span the electrodes measuring resistivity, creating percolation without the formation of an interconnected network. A higher filler loading is required for percolation using the HBPE functionalized MWCNT/PP composites as the size of the aggregates is decreased with functionalization. This is represented in Figure 3.7. Percolation by means of agglomeration in PP is rarely reported in the literature [19], but is likely the cause of conductivity in cases where MWCNT dispersion is poor.

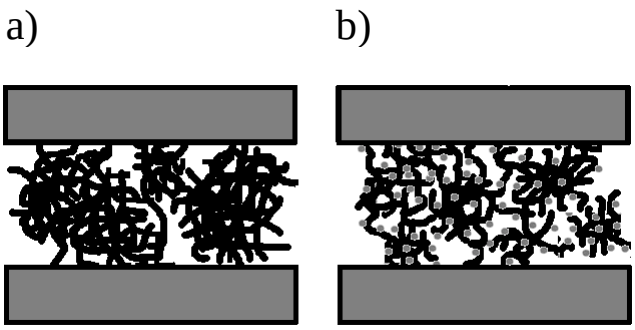


**Figure 3.7: Visual representation of aggregates spanning electrodes (500 μm in gap), thus causing electrical percolation for a) pristine MWCNT aggregates and b) HBPE-MWCNTs (HBPE is represented by grey coverage on nanotubes).**

Upon exceeding the percolation threshold, an increase in conductivity of approximately 10 orders of magnitude with respect to the unfilled matrix is achieved; with maximum conductivity values approaching $10^{-5}$ S/m. These electrical conductivity values are lower than what is expected theoretically for polymer composites with nanotubes [1, 26]. There are several possible reasons for this decrease in electrical conductivity upon incorporation of nanotubes into polymeric systems. Firstly, the synthesis (impurities, surface defects) and preparation method (acid treatment and melt mixing can lead to shortening) of nanotubes prior to being used in polymer composites has been shown to impact resulting conductivity [3, 17, 27, 28]. Inherent

penetration of polymer onto the surface of the nanotubes during any form of processing could also disrupt the extended π conjugation of the nanotubes, and the realization of highly conductive MWCNT/polymer composites [1, 17, 23, 28].

In spite of the increase in the percolation threshold, the composites containing HBPE-MWCNT have slightly higher conductivity. This highlights a potential benefit of this non-covalent functionalization approach as it does not compromise the surface properties of the MWCNTs. The increase in conductivity with functionalization may be attributable to having smaller aggregates, with more active surface area than the larger aggregates seen with pristine MWCNTs.

3.3.2.3 Mechanical Properties

Figure 3.8 below illustrates the impact of HBPE functionalization of MWCNTs on the mechanical properties of the resulting composites. It should be noted that only composites containing 3 wt% are shown because higher nanotube loadings resulted in immediate failure upon testing.

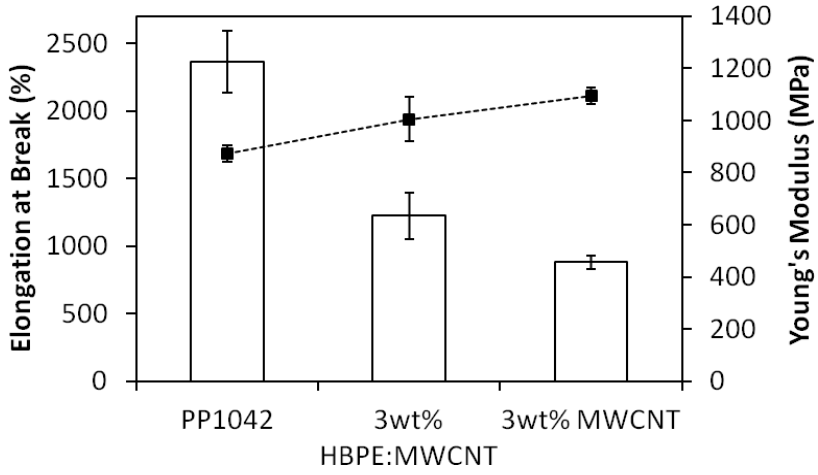


**Figure 3.8: Effect of HBPE functionalization on elongation at break (bars) and Young's modulus (line) for melt mixed composites of MWCNTs with PP1042.**

An increase in Young's modulus of approximately 15 and 25% for functionalized and pristine MWCNT composites, respectively, is seen in comparison to the unfilled polypropylene composite. This increase in stiffness is expected since the reinforcing effect of the addition of nanotubes to polypropylene is well documented [2, 3, 20, 22, 24].

The addition of nanotubes to the base PP matrix resulted in a significant decrease in the ductility of the composite. The elongation at break of the neat PP matrix was reduced by 48 and 62% upon addition of 3wt% of the HBPE functionalized and pristine MWCNTs respectively. This decrease is likely attributable to the micron sized aggregates as observed in the optical microscopy and TEM images, which act as defects in the polymer matrix. Composite ductility was improved with HBPE functionalization of the nanotubes because of the reduction in aggregate size with the addition of HBPE. This provides further support that the functionalization method is capable of breaking-up filler/filler interactions and improving the interfacial interaction between the base polymer and the nanotubes to a limited extent.

Mechanical properties were significantly reduced when filler loadings approached the electrical percolation thresholds due to the formation of extremely large aggregates, making the practical applications of these materials non-existent when ductility is required. This highlights the difficulty in achieving MWCNT/PP composites that are electrically conducting, while maintaining good mechanical properties.

## 3.4 Conclusions

A non-covalent MWCNT functionalization method using HBPE was outlined in this chapter. The functionalization reduced the size of micron-size aggregates moderately. However dispersion was still problematic. The composites had percolation thresholds of 6 wt% and 7.3 wt% for the pristine and HBPE functionalized MWCNTs respectively. It is proposed here that in these composites the method of percolation is not the formation of a three-dimensional network of interconnected, individual nanotubes, but rather the formation of large aggregates spanning the

sample during resistivity measurements. Nanotube functionalization improved the composite ductility in comparison to pristine nanotubes at filler loadings of 3 wt%. Drastic reductions of ductility were noted at higher filler loadings. The following chapter will investigate an alternative functionalization method for the improved electrical and mechanical properties of MWCNT/PP composites.

## 3.5 References


[1] M. Moniruzzaman and K. I. Winey, "Polymer nanocomposites containing carbon nanotubes," *Macromolecules 39(16),* pp. 5194-5205. 2006.

[2] S. A. Girei, S. P. Thomas, M. A. Atieh, K. Mezghani, S. K. De, S. Bandyopadhyay and A. Al-Juhani, "Effect of -COOH Functionalized Carbon Nanotubes on Mechanical, Dynamic Mechanical and Thermal Properties of Polypropylene Nanocomposites," *J. Thermoplast. Compos. Mater.25*, pp. 333-350. 2012.

[3] C. Li, H. Deng, K. Wang, Q. Zhang, F. Chen and Q. Fu, "Strengthening and toughening of thermoplastic polyolefin elastomer using polypropylene-grafted multiwalled carbon nanotubes," *J. Appl. Polym. Sci. 121(4),* pp. 2104-2112. 2011.

[4] C. Dyke and J. Tour, "Covalent functionalization of single-walled carbon nanotubes for materials applications," *Journal of Physical Chemistry a 108(51),* pp. 11151-11159. 2004.

[5] Y. Sun, K. Fu, Y. Lin and W. Huang, "Functionalized carbon nanotubes: Properties and applications," *Acc. Chem. Res. 35(12),* pp. 1096-1104. 2002.

[6] L. Xu, Z. Ye, Q. Cui and Z. Gu, "Noncovalent nonspecific functionalization and solubilization of multi-walled carbon nanotubes at high concentrations with a hyperbranched polyethylene," *Macromolecular Chemistry and Physics 210(24),* pp. 2194-2202. 2009.

[7] J. Thomassin, I. Huynen, R. Jerome and C. Detrembleur, "Functionalized polypropylenes as efficient dispersing agents for carbon nanotubes in a polypropylene matrix; application to electromagnetic interference (EMI) absorber materials," *Polymer 51(1),* pp. 115-121. 2010.

[8] E. Cohen, A. Ophir, S. Kenig, C. Barry and J. Mead, "Pyridine-modified polymer as a non-covalent compatibilizer for multi-walled CNT/Poly[ethylene-co-(methacrylic acid)] composites fabricated by direct melt mixing," *Macromol. Mater. Eng. 298(4),* pp. 419-428. 2013.

[9] N. G. Sahoo, S. Rana, J. W. Cho, L. Li and S. H. Chan, "Polymer nanocomposites based on functionalized carbon nanotubes," *Progress in Polymer Science 35(7),* pp. 837-867. 2010.

[10] K. Petrie, A. Docoslis, S. Vasic, M. Kontopoulou, S. Morgan and Z. Ye, "Non-covalent/non-specific functionalization of multi-walled carbon nanotubes with a hyperbranched polyethylene and characterization of their dispersion in a polyolefin matrix," *Carbon 49,* pp. 3378-3382. 2011.

[11] C. Gao and D. Yan, "Hyperbranched polymers: From synthesis to applications," *Progress in Polymer Science 29(3),* pp. 183-275. 2004.

[12] C. Yates and W. Hayes, "Synthesis and applications of hyperbranched polymers," *European Polymer Journal 40(7),* pp. 1257-1281. 2004.

[13] Z. Ye and S. Li, "Hyperbranched polyethylenes and functionalized polymers by chain walking polymerization with pd-diimine catalysis," *Macromolecular Reaction Engineering 4(5),* pp. 319-332. 2010.

[14] A. Vasileiou, A. Docoslis and M. Kontopoulou, "The role of non-covalent functionalization and matrix viscosity on the dispersion and properties of LLDPE/MWCNT nanocomposites," *Polymer (accepted).* 2013.

[15] S. Brunauer, P. Emmett and E. Teller, "Adsorption of gases in multimolecular layers.," *J. Am. Chem. Soc. 60,* pp. 309-319. 1938.

[16] I. Langmuir, "The constitution and fundamental properties of solids and liquids part I solids," *J. Am. Chem. Soc. 38,* pp. 2221-2295. 1916.

[17] I. Alig, P. Poetschke, D. Lellinger, T. Skipa, S. Pegel, G. R. Kasaliwal and T. Villmow, "Establishment, morphology and properties of carbon nanotube networks in polymer melts," *Polymer 53,* pp. 4-28. 2012.

[18] T. Skipa, D. Lellinger, W. Boehm, M. Saphiannikova and I. Alig, "Influence of shear deformation on carbon nanotube networks in polycarbonate melts: Interplay between build-up and destruction of agglomerates," *Polymer 51(1),* pp. 201-210. 2010.

[19] H. Deng, T. Skipa, R. Zhang, D. Lellinger, E. Bilotti, I. Alig and T. Peijs, "Effect of melting and crystallization on the conductive network in conductive polymer composites," *Polymer 50(15),* pp. 3747-3754. 2009.

[20] H. K. F. Cheng, Y. Pan, N. G. Sahoo, K. Chong, L. Li, S. H. Chan and J. Zhao, "Improvement in properties of multiwalled carbon nanotube/polypropylene nanocomposites through homogeneous dispersion with the aid of surfactants," *J. Appl. Polym. Sci. 124,* pp. 1117-1127. 2012.

[21] G. S. Ezat, A. L. Kelly, S. C. Mitchell, M. Youseffi and P. D. Coates, "Effect of maleic anhydride grafted polypropylene compatibilizer on the morphology and properties of polypropylene/multiwalled carbon nanotube composite," *Polym. Compos. 33,* pp. 1376-1386. 2012.

[22] M. A. Haque, M. F. Mina, A. K. M. M. Alam, M. J. Rahman, M. A. H. Bhuiyan and T. Asano, "Multiwalled carbon nanotubes-reinforced isotactic polypropylene nanocomposites: Enhancement of crystallization and mechanical, thermal, and electrical properties," *Polym. Compos. 33,* pp. 1094-1104. 2012.

[23] K. Menzer, B. Krause, R. Boldt, B. Kretzschmar, R. Weidisch and P. Poetschke, "Percolation behaviour of multiwalled carbon nanotubes of altered length and primary agglomerate morphology in melt mixed isotactic polypropylene-based composites," *Composites Sci. Technol. 71,* pp. 1936-1943. 2011.

[24] D. Bikiaris, "Microstructure and Properties of Polypropylene/Carbon Nanotube Nanocomposites," *Materials 3,* pp. 2884-2946. 2010.

[25] R. Socher, B. Krause, M. T. Mueller, R. Boldt and P. Poetschke, "The influence of matrix viscosity on MWCNT dispersion and electrical properties in different thermoplastic nanocomposites," *Polymer 53,* pp. 495-504. 2012.

[26] E. Thostenson, Z. Ren and T. Chou, "Advances in the science and technology of carbon nanotubes and their composites: A review," *Composites Sci. Technol. 61(13),* pp. 1899-1912. 2001.

[27] P. Liu, K. L. White, H. Sugiyama, J. Xi, T. Higuchi, T. Hoshino, R. Ishige, H. Jinnai, A. Takahara and H. Sue, "Influence of trace amount of well-dispersed carbon nanotubes on structural development and tensile properties of polypropylene," *Macromolecules 46(2),* pp. 463-473. 2013.

[28] K. Miyazaki, N. Okazaki and H. Nakatani, "Improvement of electrical conductivity with phase-separation in polyolefin/multiwall carbon nanotube/polyethylene oxide composites," *J. Appl. Polym. Sci. 128(6),* pp. 3751-3757. 2013.

# Chapter 4

# Functionalized Polypropylene/MWCNT Composites

## 4.1 Introduction

Weak van der Waals and π-π interactions between the sidewalls of nanotubes in non-polar polymer matrices results in aggregation and poor nanotube dispersion [1]. Non-covalent functionalization approaches for improving weak interfacial tension and disrupting filler/filler interactions are preferred over covalent methods because of the preservation of desired electrical properties of the nanotubes [2-8].

The use of hyperbranched polymers that are non-covalently adsorbed to the sidewalls of MWCNTs can improve their dispersion in organic solvents, polyolefin elastomers and polyethylene (PE) [9-12], but resulted in micron-sized aggregates when melt mixed in polypropylene (PP), presumably because of decreased compatibility (refer to Chapter 3). This functionalization approach was only marginally successful in improving mechanical properties in PP composites, reducing the applicability of these materials when ductility is important.

As an alternative to nanotube functionalization, matrix functionalization avoids altogether the complications and costs associated with MWCNT modification. For example PP-grafted-maleic anhydride (PP-g-MA) and various block copolymers, have been tested for their potential to act as coupling agents in formulations containing MWCNTs and PP [13-15]. Thomassin et al. [16] developed a matrix functionalization approach for PP that incorporates the addition of aromatic moieties to the polymer backbone. This procedure resulted in improved nanotube dispersion, attributed to π-π stacking of the aromatic functionalities on the polymer with the surface of the MWCNTs (π orbitals of MWCNTs with the π electrons of conjugated pyridine). This non-covalent interaction improved adhesion of the nanotubes with the PP matrix, without

disrupting the extended π conjugation required for the electrical properties of MWCNTs. However the properties of the resulting composites have not been characterized in detail.

CNT alignment has been demonstrated to improve composite conductivity at a reduced filler loading [17]. Alignment involving the formation of filler networks through the polymer can be achieved by mechanical means, or application of an external magnetic or electric field [18, 19]. The effects of matrix type, frequency and electric potential during the application of external electric fields in carbon black-containing composites have been reported in detail [20-23]. Similar studies using MWCNTs are scarce [17]. Additional research is required to determine if this is a viable option for improved electrical performance of PP/MWCNT composites.

The following chapter employs the grafting of aromatic functionalities to the backbone of a maleated PP, through a reactive melt-compounding approach. The resulting amino-pyridine (Py) grafted derivative is characterized, and its impact on MWCNT dispersion and the resulting mechanical and electrical properties of melt-mixed PP composites is reported. A preliminary study on the response of MWCNTs to an externally applied alternating current (AC) electric field in a melt state PP composite is also reported.

## 4.2 Experimental

### 4.2.1 Materials

MWCNTs were used as supplied from Nanolab Inc. (purity: >95%, diameter: 30±15nm and length: 1-5 μm). The specific surface area (SSA) of the MWCNTs was 300 $m^2/g$ based on Brunauer-Emmett-Teller characterization. The average pore size of the MWCNTs as determined by $N_2$ sorption experiments is about 2.3 nm [10].

A PP homopolymer, Pro-fax® PD 702 by LyondellBasell was used as the matrix. This PP grade was selected to better match the viscosity of the maleated PP. Fusabond® PMD 511D is a PP-g-MA that was used for the grafting reaction with 4-aminomethylpyridine (AMP) (98% purity, supplied by Aldrich). The properties of the polymers used in this work can be seen in

Table 4.1. Irganox B225 is a hindered phenol antioxidant that was added to each composite at 0.2 wt% for improved thermal stability.

**Table 4.1: Properties of polymers.**

| *Material* | *PP* | *PP-g-MA* |
|---|---|---|
| Trade Name | Pro-fax® PD702 | Fusabond® PMD 511D |
| MFR (g/10min.) | 35@230°C | 25 @ 190°C |
| Density (kg/m$^3$) | 900 | 900 |
| Melting Point (°C) | 165 | 159 |
| Graft Content (wt%) | - | 0.25-0.5 |

### 4.2.2 Grafting of aminomethylpyridine to PP-g-MA

PP-g-MA was reacted with an equimolar amount of AMP (assuming 0.5 wt% MA grafts) to form polypropylene-graft-aminomethylpyridine (PP-g-Py). The reaction was carried out in a Haake Rheomix E3000 at 190°C, 45 RPM for 10 minutes. PP-g-MA was mixed in the compounder for 1 minute prior to addition of AMP to allow for dehydration. A Fourier transform infrared (FTIR) spectrometer (Vertex 70 FTIR by Burker Optics) was used to confirm the grafting reaction and conversion. Thin films of the resulting composites were compression molded in a Carver hydraulic press at 200°C for 1 minute under high pressure for use in the FTIR spectrometer. The resolution for each spectrum was 2 cm$^{-1}$ with 24 co-added scans.

### 4.2.3 Melt Compounding Procedure

MWCNTs were melt mixed with mixtures of PP/PP-g-MA or PP-g-Py in a DSM Research 5ml co-rotating twin-screw micro-compounder at 190°C, 120 RPM and a mixing time of 10 minutes under nitrogen purge. MWCNTs were first pre-mixed with the PP in a Carver hot press at 200°C for 1 minute, by folding and hot-pressing 3 times. The resulting mixtures were subsequently added in the twin-screw micro-compounder to produce composites containing 0.5 to 5 wt% (0.3 to 2.8 vol.% converted using densities of 0.9 and 1.65 g/cm$^3$ for PP and MWCNTs

respectively). Neat PP was subjected to a similar processing history, to provide a basis for comparison.

### 4.2.4 Composite Characterization

#### 4.2.4.1 Rheology

Investigation of the linear viscoelastic properties was carried out using an oscillatory rheometer (Anton Paar MCR 301 with CTD 450 oven attached) using a parallel plate measuring system (PP25). The complex viscosity was measured versus frequency at a strain of 2% and 190$^{o}$C.

#### 4.2.4.2 Morphology

The dispersion of MWCNTs in the melt blended composites was investigated using an Olympus BX 51 optical microscope. Molten composite films were compressed to a thickness of 50μm in a Carver hot press at 200$^{o}$C for 1 minute prior to microscopy. Images were recorded using transmitted light. Scanning electron microscopy (SEM) images were taken using a JEOL JMS-840A scanning microscope. Samples were first cold fractured in liquid nitrogen and the fracture surface was gold coated. Transmission electron microscopy (TEM) images were taken using a FEI Tecnai 20 instrument. Ultra-thin films of the composites were prepared by cryosectioning, using a Leica ultra-microtome.

#### 4.2.4.3 Raman Spectroscopy

A Jobin-Yvon/Horiba micro-Raman Spectrometer equipped with a 632 nm He/Ne laser and an Olympus BX41 microscope system was used for Raman studies. Spectra were collected in backscatter mode with a 100x objective lens, 200μm pinhole and slit with a filter in place attenuating the laser power by a tenth to prevent polymer melting during testing. The average of three trials is presented following an exposure time of 15 minutes.

4.2.4.4 Thermal Analysis

Thermal analysis was performed using a TA Instruments Q100 Series differential scanning calorimeter (DSC) calibrated with Indium and Zinc standards. Each sample was weighed to 8.5±0.2 mg and sealed in an aluminum pan. Samples were heated to 200$^{o}$C and held for 5 minutes to eliminate the thermal history, then cooled and reheated using a ramp of 10$^{o}$C/min. to -35 and 200$^{o}$C respectively. The melting temperature ($T_m$), crystallization temperature ($T_c$) and heat of fusion ($\Delta H_m$) were determined from the second heating scan. $\Delta H_m$ was used to determine the composite crystallinity ($X_m$) based on a $\Delta H_m$ value of 177 J/g for fully crystalline PP [24]. Samples were normalized with respect to the actual amount of PP being tested when determining crystallinity.

4.2.4.5 Electrical Conductivity

A Keithley 8009 Resistivity Test Fixture connected to a Keithley 6517B Electrometer/High Resistance Meter was used under DC current at room temperature, for samples having a volume resistivity above $10^6$ Ωcm. The total electrification time was 1 minute. Samples having dimensions 6 cm in diameter and 0.5 mm thick were prepared by compression molding the previously melt compounded composites into discs in a Carver press at 200$^{o}$C for 1 minute.

For samples exhibiting resistivity below $10^6$ Ωcm (limit of high resistance meter), an Agilent 34401A 6 Digit Multimeter was used to measure the resistance. Samples were first gold coated on both sides to create a conductive contact with the surface of the sample, and the measured resistance was converted to volume resistivity using Equation 4.1 below:

$$\rho = \frac{R \times A}{\ell} \qquad (4.1)$$

where ρ is the volume resistivity, R is the resistance from the multimeter, A is the surface area of the sample and ℓ is the thickness. It is important to note that after gold coating the samples all edges were trimmed to ensure only conductive pathway was through the sample.

4.2.4.6 Tensile Testing

Tensile testing was performed using an Instron 3369 Universal testing apparatus. Tests were performed according to ASTM D638 with a type-V die cut from melt compounded samples that were compression molded in a Carver press at 200$^{o}$C for 1 minute (dumbbell shaped specimens with dimensions: 7.62 mm x 3.50 mm x 1.45 mm). A crosshead speed of 10 mm/min was used at room temperature. A minimum of three trials were performed on each sample with the average value with one standard deviation reported.

### 4.2.5 Application of AC Electric Field

Composites were electrified in the presence of an AC electric field inside of a custom electrode cell (Figure 4.1). The cell was preheated to 180$^{o}$C using a hot plate and materials were loaded into the teflon well/electrode spacer (thickness: 600 μm, diameter: 6 cm). Temperature was maintained using a feedback control system and monitored with an external thermocouple. A thin coating of mold release was baked onto the surface of the electrodes for easy removal of the sample. The AC fields were generated with a Hewlett-Packard 33120A function/arbitrary waveform generator. The generated signal was amplified using a Trek 623B high voltage power amplifier. Electrification of composites occurred for 2 hours under a sinusoidal electric potential of 300 $V_{pp}$, 1 KHz and 180$^{o}$C. A schematic of the setup can be seen in Figure 4.2. Tektronix TDS 1002 digital storage oscilloscopes were used to monitor voltage output from the generator and amplifier, as well as potential difference across the cell and current through the system. A physical resistor of 40 kohm was connected in series with the cell to prevent electrical short circuits.

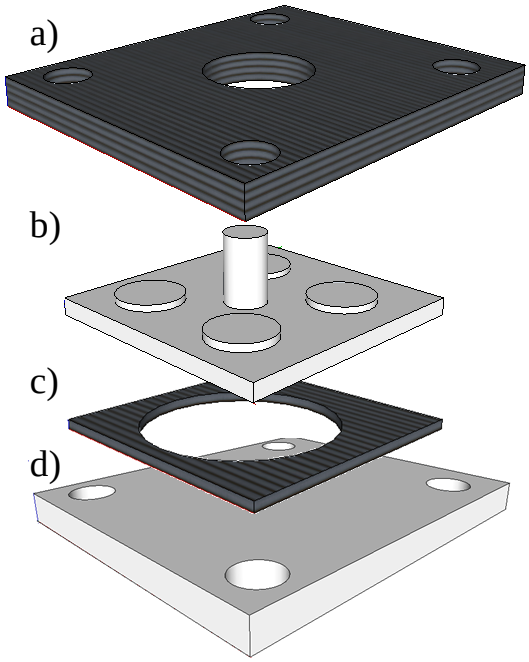


**Figure 4.1: Exploded view of custom electrode cell a) top teflon layer b) top electrode c) teflon sample well d) bottom electrode.**

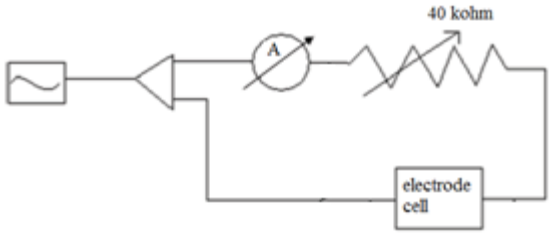


**Figure 4.2: Test circuit used for electrification of composites. Adapted from** [17]**.**

## 4.3 Results and Discussion

### 4.3.1 Synthesis and Characterization of PP-graft-aminomethylpyridine

Scheme 4.1 shows a representation of the reaction of PP-g-MA with AMP to form the amino-pyridine derivative, PP-g-Py. The reaction takes place through nucleophilic attack of the amino group to the anhydride, forming an acid-amide during melt mixing at 190$^{o}$C. This is followed by either reacting further to form a diamide or further condensation to form the desired cyclic imide [11]. Previous work with the melt amination of polymers suggests that due to the

high temperatures and long reaction time used, formation of the cyclic imide is favored and all MA functional groups are converted [11, 25-27].

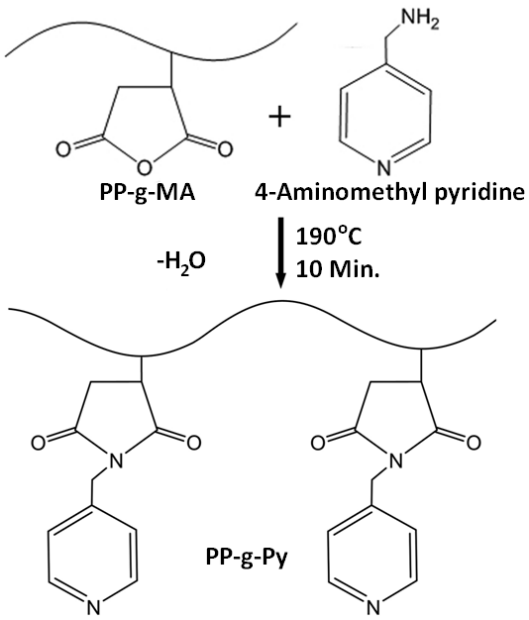


**Scheme 4.1: Schematic of reaction of PP-g-MA with AMP to form PP-g-Py. Adapted from** [11]**.**

Figure 4.3 shows the shift in FTIR absorbance spectra upon the melt-state reaction of PP-g-MA with AMP. The characteristic absorption band of anhydride functionality can be seen at approximately 1783 $cm^{-1}$, corresponding to the symmetrical stretching of the carbonyl of the cyclic anhydride. The slight peak at approximately 1714 $cm^{-1}$ for the PP-g-MA is representative of symmetric stretching of the carbonyl of a carboxylic acid that can be attributed to a small portion of MA that has hydrolyzed [16, 27]. Upon reaction, the complete disappearance of the anhydride absorption band and appearance of the characteristic peak for cyclic imide (1783 $cm^{-1}$ indicative of symmetrical stretching of carbonyl group of cyclic imide) confirms the reaction was carried out to complete conversion and that aromatic moieties were grafted to the polymer chain backbone.

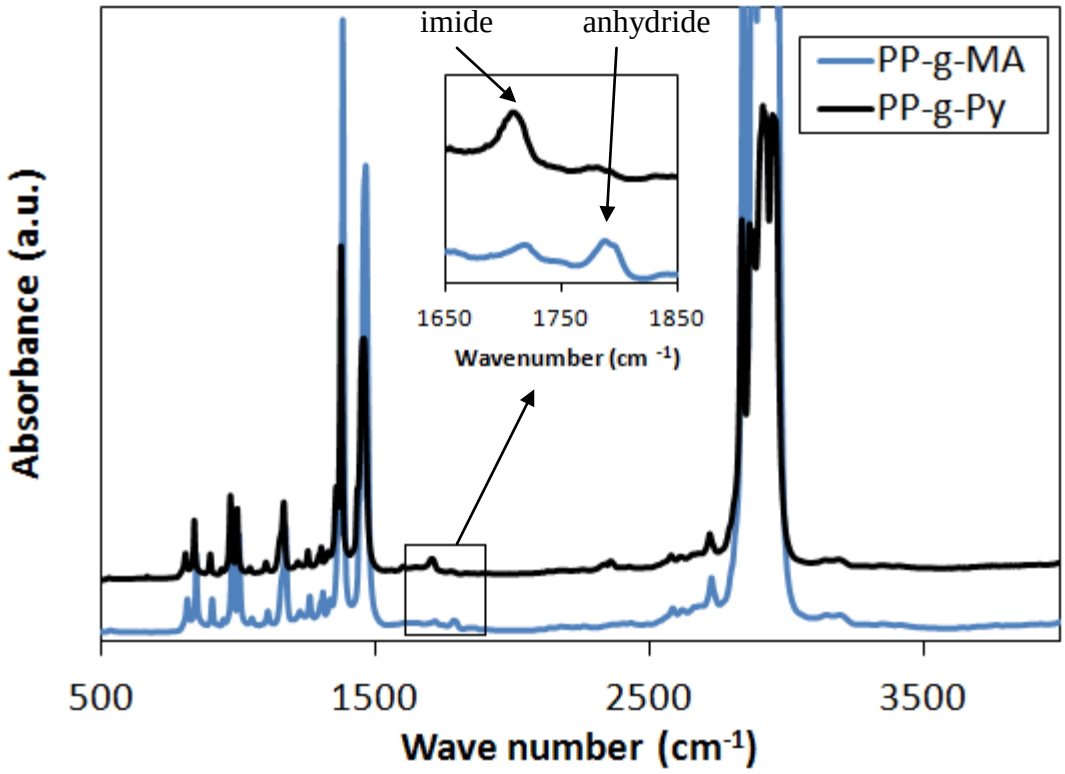


**Figure 4.3: FTIR spectra of PP-g-MA and PP-g-Py. Insert shows close-up of spectra from 1650 to 1850 $cm^{-1}$.**

Given that functionalization reactions may result in changes in molecular weight, and therefore viscosity, it is important to investigate the complex viscosity before and after addition of the pyridine grafts. Figure 4.4 shows that there is no significant difference in matrix viscosity between PP-g-MA and PP-g-Py. The minor decrease in viscosity in PP-g-Py may be attributable to the bulkier side groups with the addition of aminomethylpyridine [11]. The role of polymer matrix viscosity on primary aggregate break-up during melt mixing has been well documented. The higher the viscosity during melt mixing, the more shear force that is generated and thus more energy is put into breaking up aggregates and likely contributes to increased shortening of nanotubes [28, 29]. Differences in matrix viscosities are not expected to be a factor in varied nanotube dispersion and the resulting composite's mechanical and electrical properties.

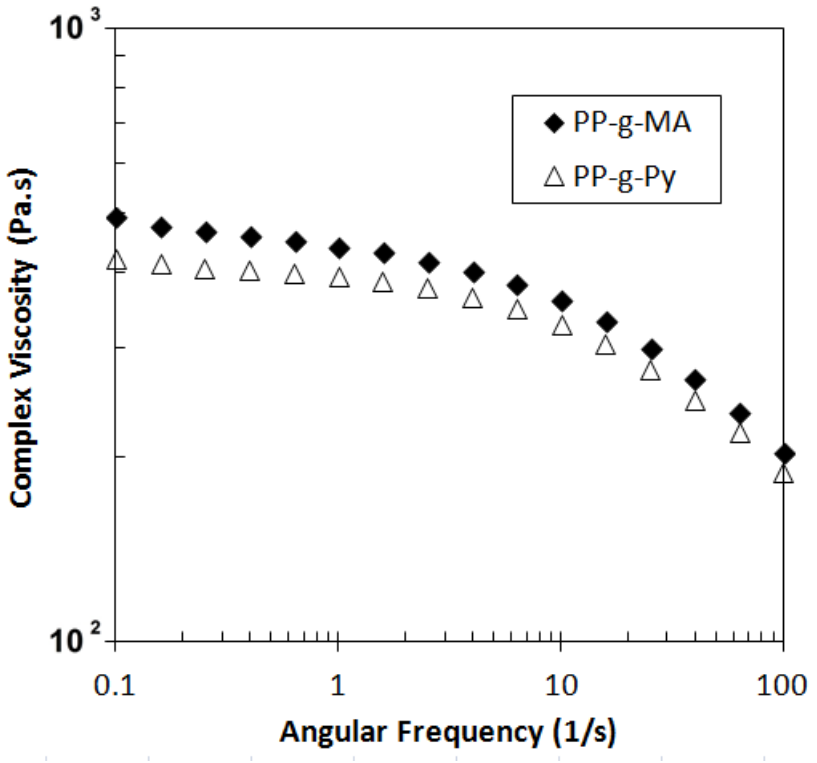


**Figure 4.4: Complex viscosity versus frequency of PP-g-MA and PP-g-Py at 190°C.**

### 4.3.2 MWCNT Dispersion

Comparison of the optical micrographs in Figure 4.5 a) and b) reveals that using PP-g-Py as the matrix results in a drastic reduction in the number and size of aggregates upon melt mixing with 1 wt% of MWCNTs compared to the pure PP homopolymer. This suggests that PP-g-Py is effective in improving nanotube dispersion. Furthermore, the potential of PP-g-Py to act as a compatibilizing agent when added to a neat PP was investigated. As seen in Figure 4.5 c) and d), addition of 50 wt% and 25 wt% of PP-g-Py was sufficient to achieve reduction in the aggregate size, whereas smaller quantities (Figure 4.5 e)) resulted in progressively larger aggregates. Given that in all compatibilization procedures it is advantageous to use the minimum amount of a compatibilizer possible to keep costs low and to avoid altering the mechanical properties, the composition containing 25 wt% PP-g-Py was selected for all the following work done within this chapter.

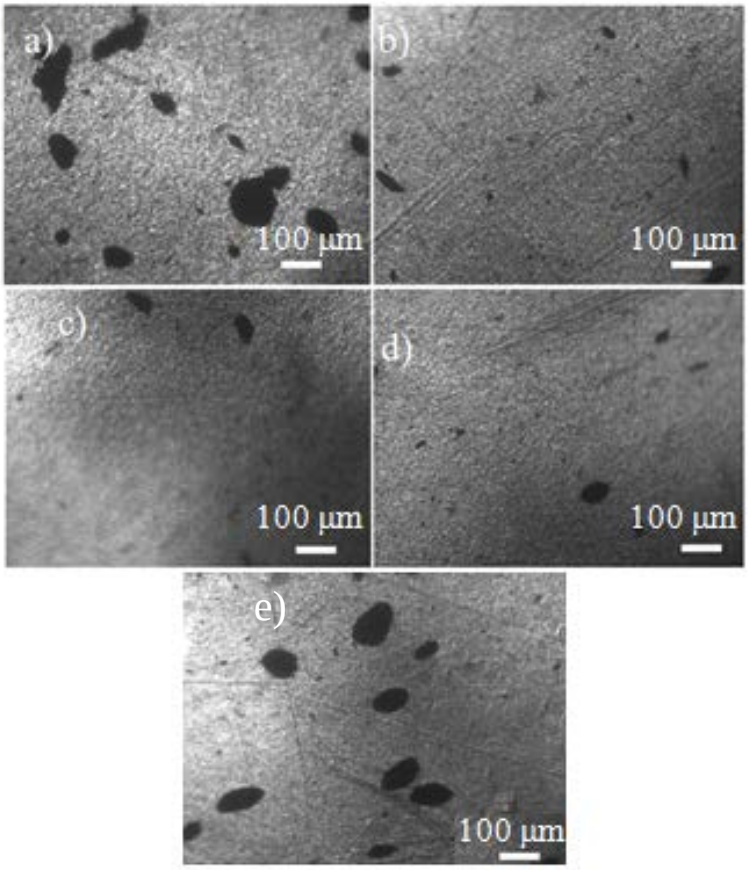


**Figure 4.5: Optical micrographs of a) PP b) PP-g-Py c) PP/PP-g-Py (50/50) d) PP/PP-g-Py (75/25) e) PP/PP-g-Py (90/10) containing 1wt% MWCNTs.**

Figure 4.6 compares optical micrographs of PP/PP-g-Py at a composition of 75/25 containing varying amounts of MWCNTs with composites of PP/PP-g-MA at the same composition. It can be seen that even at 3 wt% MWCNT loading the matrix containing PP-g-Py contains less aggregates. These results suggest that the introduction of the aromatic moieties to the polymer chain provides improved adhesion between the polymer and the nanotubes, thus resulting in better stress transfer between polymer and filler during melt compounding. The reduction in aggregate size with the introduction of pyridine to the polymer chains is further evidenced in SEM images shown in Figure 4.7. Introducing pyridine grafts results in fewer and smaller aggregates, and the nanotubes appear to be more evenly distributed. On the other hand

large aggregates of up to over 20 μm are present in the MA composites (Figure 4.6 and Figure 4.7 top row).

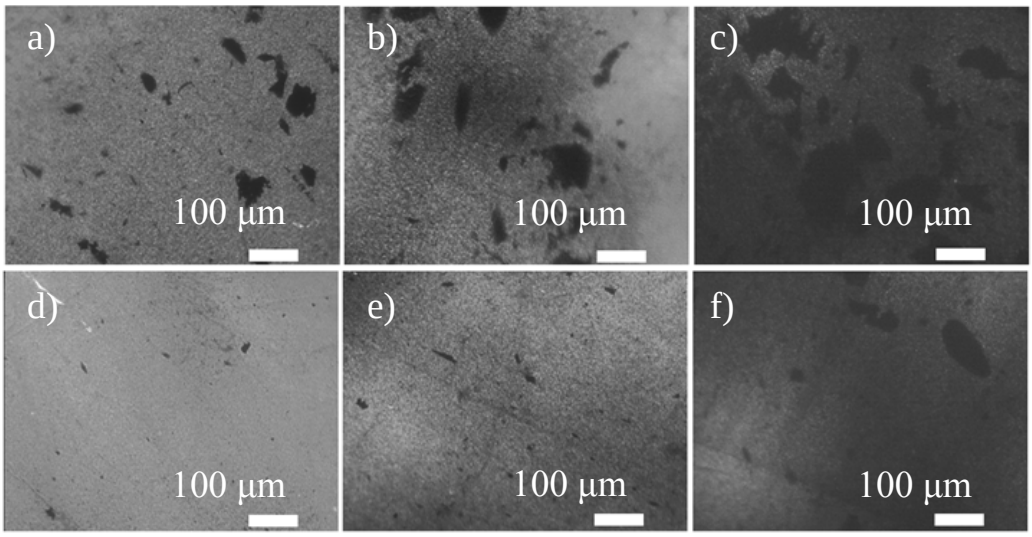


**Figure 4.6: Optical micrographs of PP/PP-g-MA (75/25) (a,b,c) and PP/PP-g-Py(75/25) (d,e,f) with 0.5wt% (a,d), 1.5 wt% (b,e) and 3wt% MWCNTs (c,f).**

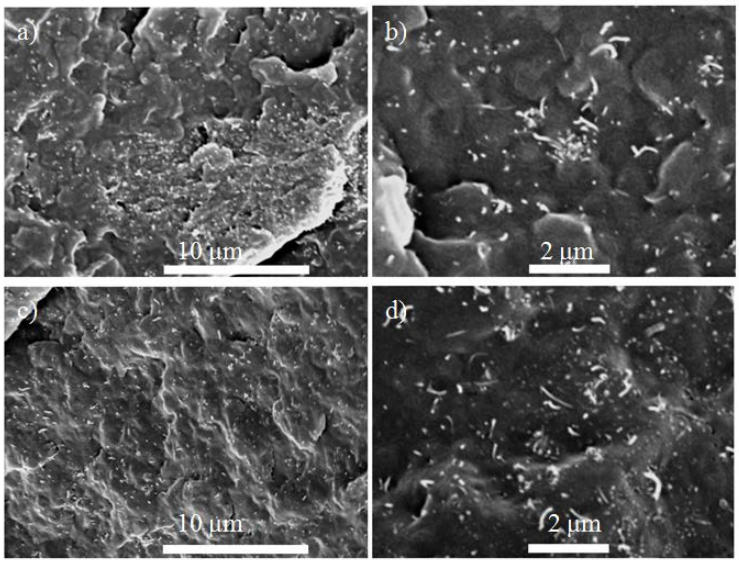


**Figure 4.7: SEM images of PP/PP-g-MA (a,b), PP/PP-g-Py (c,d) with 3wt% MWCNT. Magnification of 4500x (a,c) and 12000x (b,d).**

TEM images shown in Figure 4.8 provide further support for the improvement in MWCNT dispersion with the addition of PP-g-Py. Significantly smaller aggregates and more individually dispersed nanotubes are present. Furthermore, the formation of interconnected

nanotubes at the 3 wt% loading is visible. This is in large contrast to what was seen for the PP grade used in the previous chapter where interconnectivity between nanotubes was not visible and aggregation and poor distribution were a major concern. It must be noted that the PP system used in this chapter has significantly lower viscosity. This may facilitate penetration of the polymer into the MWCNT aggregates, thus favoring break-up.

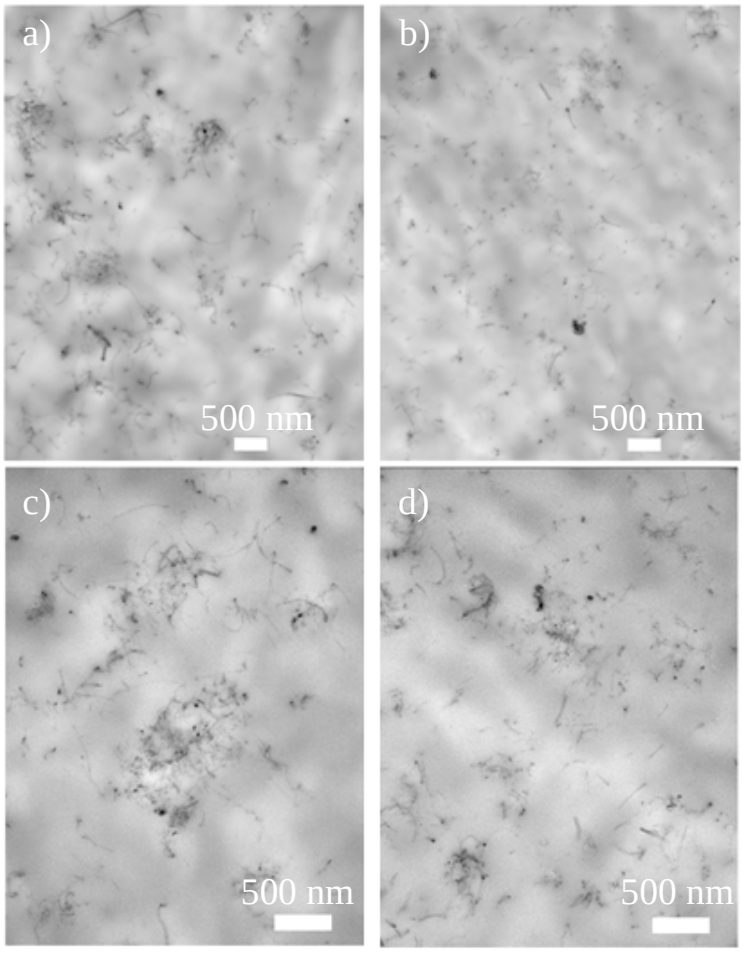


**Figure 4.8: TEM images of PP/PP-g-MA (a,c) and PP/PP-g-Py (b,d) with 3wt% MWCNTs at magnifications of 14500x (a,b) and 25000x (c,d).**

Based on the results from imaging, pyridine functionalization resulted in improved macro and nanostructure of MWCNTs. Raman spectroscopy was also used to provide further evidence of improved interactions between nanotubes and the introduced aromatic functionality. The characteristic peaks of MWCNTs are at approximately 1335 (disorder induced D-band) and 1583

(G-band) $cm^{-1}$. The G-band is assigned to the tangential mode and is associated with the $sp^2$-hybridized carbon network of the MWCNTs. The signature peaks of PP do not exist in this range, therefore shifts to higher values in the G-band and broadening of the peak can be attributed to the penetration of polymer chains into MWCNT bundles causing increased "hydrostatic" compression on the nanotubes [3, 11, 30-33]. Figure 4.9 shows the high frequency Raman spectra associated with the G-band for MWCNTs, as well as for PP composites with and without pyridine functionalization.

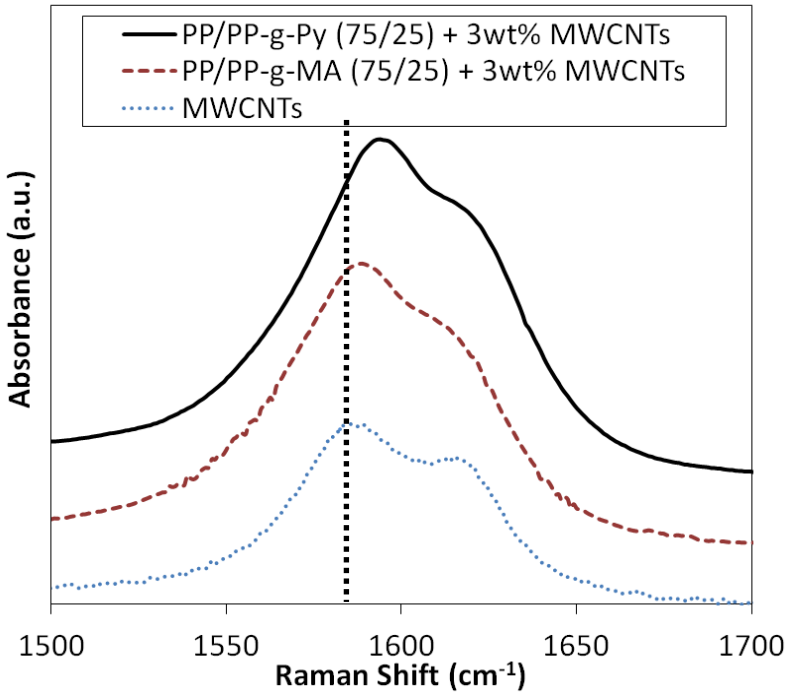


**Figure 4.9: Raman spectra of PP/PP-g-MA, PP/PP-g-Py at 3wt% MWCNT loading and pristine MWCNTs.**

The vertical dotted line has been added to highlight the shift to higher Raman values upon melt compounding in PP. For PP/PP-g-MA and PP/PP-g-Py, a shift in the wave number of 3 $cm^{-1}$ and 8 $cm^{-1}$ is seen respectively, with a broadening of both peaks. This suggests that PP can penetrate the aggregates, thus resulting in aggregate break up. The addition of the aromatic functionality to the PP backbone caused a more pronounced shift, suggesting there is increased

polymer/filler interaction. This is likely attributable to the non-covalent π-π interaction between pyridine groups and nanotube side-walls [3, 30-34].

### 4.3.3 Electrical Properties

Equations 3.1 and 3.2 from Chapter 3 were fit to the experimental data for composite conductivity. Figure 4.10 shows the conductivity values with the power-law models fit above and below percolation. The introduction of MWCNTs at 3wt% loading resulted in an increase in composite conductivity by approximately 13 orders of magnitude. The maximum value of conductivity achieved was similar regardless of the type of PP matrix and was on the order of $10^{-2}$ S/m. Conductivity values are higher compared to what was seen in the previous chapter and better than previous reports using nanotubes from the same manufacturer in other polyolefin matrices [10, 11].

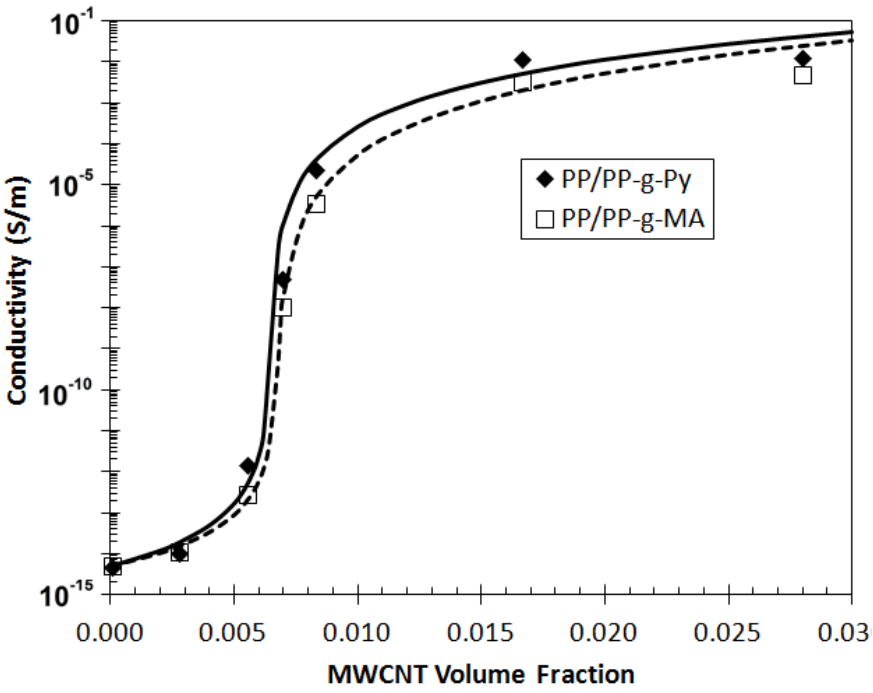


**Figure 4.10: Electrical conductivity measurements for PP/PP-g-MA and PP/PP-g-Py at various volume fractions of MWCNTs. Lines represent power-law model fit above and below percolation (Py: solid, MA: dashed).**

PP/MWCNT composites do not exhibit the super-conductive properties commonly expected based on the theoretical maximum conductivity of nanotubes. Production method and purity of MWCNTs have been shown to impact nanotube conductivity [1, 35]. Achieving a maximum conductivity in these PP composites of around $10^{-2}$ S/m allows for semi-conductive applications and is higher than what is required for dissipation of static charges ($10^{-2}$ to$10^{-9}$ S/m) [36].

Table 4.2 summarizes the model parameters and derived percolation thresholds for the PP/MWCNT composites. The percolation threshold for both matrices was approximately 1.2 wt%. These values are lower than what is regularly reported for PP. Lower matrix viscosity likely results in less nanotube breakage and shortening during compounding, thus maintaining high aspect ratios [2, 29, 37-39].

**Table 4.2: Power-law model parameters for electrical conductivities**

| *Sample* | *s* | *t* | $\varphi_c$ *(vol. %)* | $\varphi_c$ *(wt%)* |
|---|---|---|---|---|
| PP/PP-g-MA | 2.1 | 3.3 | 0.67 | 1.22 |
| PP/PP-g-Py | 2.4 | 2.8 | 0.65 | 1.19 |

MWCNT microstructure within a polymer composite plays an integral part in the electrical conductivity of the materials. For the PP/PP-g-MA samples where large aggregates of nanotubes are present, the percolation is likely due to the formation of interconnected networks of aggregates spanned by few individually dispersed nanotubes. However, the improved dispersion of MWCNTs in the PP/PP-g-Py composites suggests that percolation occurs by the formation of an interconnected conductive network primarily comprised of evenly dispersed and distributed nanotubes. An important aspect of the addition of the aromatic functionalities is that nanotube dispersion is improved without masking or hindering the conductive properties of the composites.

### 4.3.4 Mechanical Properties

It has been shown that MWCNTs can act as reinforcing fillers for polymer composites, increasing their modulus, while greatly reducing ductility [5, 40-42]. Figure 4.11 a) shows a graphical representation of the Young's modulus of the composites at various filler loadings, as determined from tensile testing. A significant increase in composite moduli can be observed regardless of functionalization upon addition of even a small amount of MWCNTs. The matrix containing PP-g-Py resulted in significantly higher moduli at 1.5 and 3 wt% loadings. This may be attributed to improved dispersion of the MWCNTs resulting in better stress transfer from the polymer to the nanotubes. This improvement in composite stiffness with functionalization is more prominent at higher loadings. Aggregation is very pronounced in the PP/PP-g-MA based composites (see Figure 4.6), while the functionalization with PP-g-Py results in a significant improvement in dispersion.

Figure 4.11 b) examines the differences in composite ductility at various filler loadings upon matrix functionalization. In PP composites that do not contain aromatic side groups, addition of even 0.5 wt% MWCNT results in a severe decrease in elongation at break by around 89%. This is indicative of large aggregates acting as defects in the polymer matrix causing poor ductility. Conversely, upon matrix functionalization addition of 0.5 wt% MWCNTs shows a decrease in elongation at break of 40%. Addition of more nanotubes results in further decline in ductility, however showing significant improvement with the addition of aromatic functionality to the PP chains. This improvement can be attributed to enhanced interfacial adhesion between the polymer and the nanotube resulting in the break-up for filler/filler interactions and the formation of fewer aggregates of reduced size.

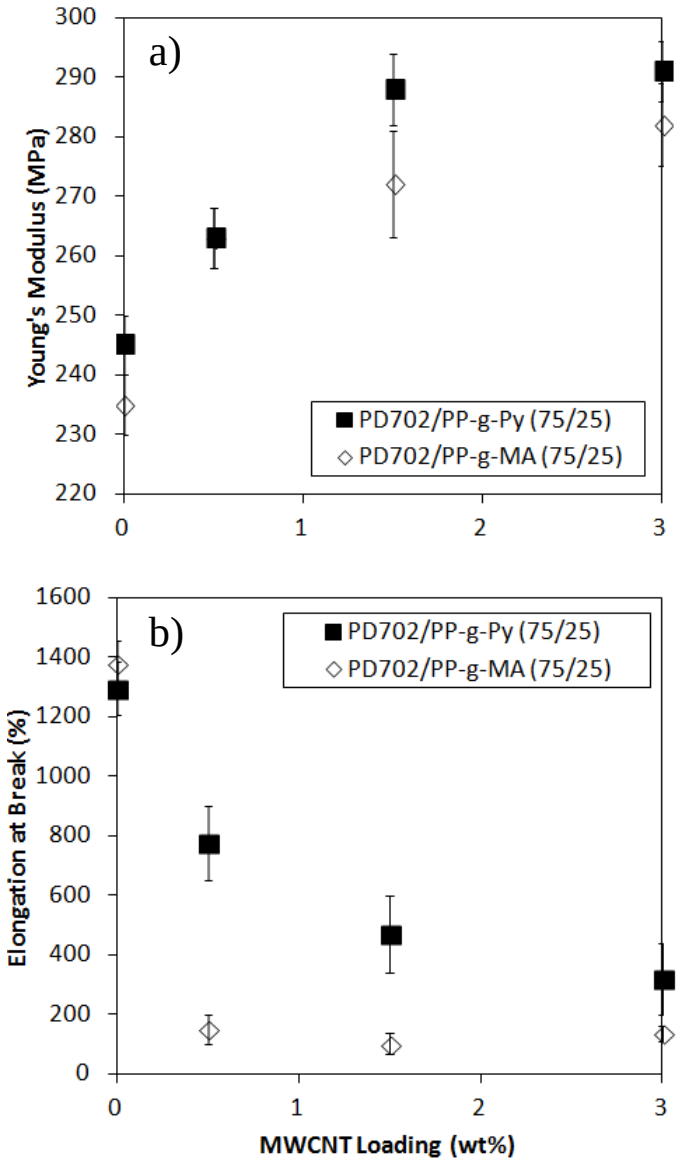


**Figure 4.11: (a) Young's modulus and (b) elongation at break for Py and MA functionalized PP containing various amounts of MWCNTs.**

Increased crystallinity, which occurs through heterogeneous nucleation of PP in composites with MWCNTs may also play a role in increasing composite strength [2, 30, 37, 43]. However, only a slight increase in crystallization with addition of MWCNTs can be seen from the thermal properties exhibited in Table 4.3. The largest increase in crystallization occurs upon addition of a small amount of MWCNTs, with reduced effects at higher loadings. Pyridine

functionalization had no significant impact on crystallization in comparison to similar loadings of MWCNTs.

**Table 4.3: Summary of thermal properties of composites showing melting temperature ($T_m$), crystallization temperature ($T_c$) and Crystallinity ($X_m$).**

| *Sample* | $T_m$ ($^oC$) | $T_c$ ($^oC$) | $X_m$ (%) |
|---|---|---|---|
| PP/PP-g-MA (75/25) | 163 | 115 | 47% |
| + 0.5 wt% MWCNT | 164 | 127 | 51% |
| + 1.5wt% MWCNT | 166 | 126 | 52% |
| + 3.0 wt% MWCNT | 168 | 127 | 53% |
| | | | |
| PP/PP-g-Py (75/25) | 164 | 121 | 48% |
| + 0.5 wt% MWCNT | 164 | 125 | 51% |
| + 1.5wt% MWCNT | 165 | 127 | 53% |
| + 3.0 wt% MWCNT | 168 | 125 | 53% |

### 4.3.5 AC Electric Field Driven MWCNT Alignment

Figure 4.10 above shows that the composites investigated had maximum conductivities of the order of $10^{-2}$ S/m. Higher conductivities are desirable in engineering applications that require lightweight, less expensive alternatives to metals. The ability to achieve electrical percolation at lower MWCNT loadings is also of interest to improve mechanical properties and reduce material cost. As discussed in Chapter 2, alignment of conductive filler in the presence of an external AC electric field offers a promising means to produce composites capable of fulfilling applications as conductors at reduced filler loadings. This section investigates the potential of this approach to impart improvement in the conductive properties of the PP/MWCNT composites developed in this chapter. The impact of matrix functionalization on the composite response is also investigated.

A decrease in the voltage drop across the sample is recorded when composites are subjected to an AC field. This is indicative of a decrease in the resistivity of the sample being tested since the setup used is under constant current. A decrease in resistivity is the result of the formation of a conductive network of MWCNTs by induced polarization forces [17]. Figure 4.12

shows a representative response of electric potential across the electrode cell recorded with time, upon application of 300 $V_{pp}$ for composites containing 0.5 wt% MWCNTs. PP composites with 0.5 wt% MWCNTs show a drastic decrease in resistance which represents an over 50% decrease in the amount of filler required for percolation from unaligned samples (see Table 4.2 above).

Percolation time is defined as the time between the first moment the electric field is applied and the time when the first drop in composite resistivity occurs [17]. Figure 4.12 shows that percolation begins instantaneously upon application of the electric field. This is likely attributable to the high voltage (300 $V_{pp}$) and low viscosity PP matrix that were used in this experiment, which facilitates movement of the filler [19-21]. Samples containing 1 wt% and 3 wt% MWCNTs resulted in an immediate decrease in potential difference across the electrode cell, and are not included in Figure 4.12 for that reason. The nanotube concentrations in these composites were closer to the electrical percolation thresholds in Table 4.2, which is likely the cause of the immediate decrease in potential. It should also be noted that the pyridine functionalized matrix resulted in a longer time for the voltage (or sample resistivity) to reach an equilibrium value. Due to the similarity in composite viscosity, it is possible that the longer time to reach a minimum voltage is the result of improved dispersion of MWCNTs with matrix functionalization. Since the electric field-induced interactions between filler molecules scale with volume, it is predicted that the large aggregates present in the PP-g-MA matrix are able to form conductive bridges at a faster rate than better dispersed nanotubes [17].

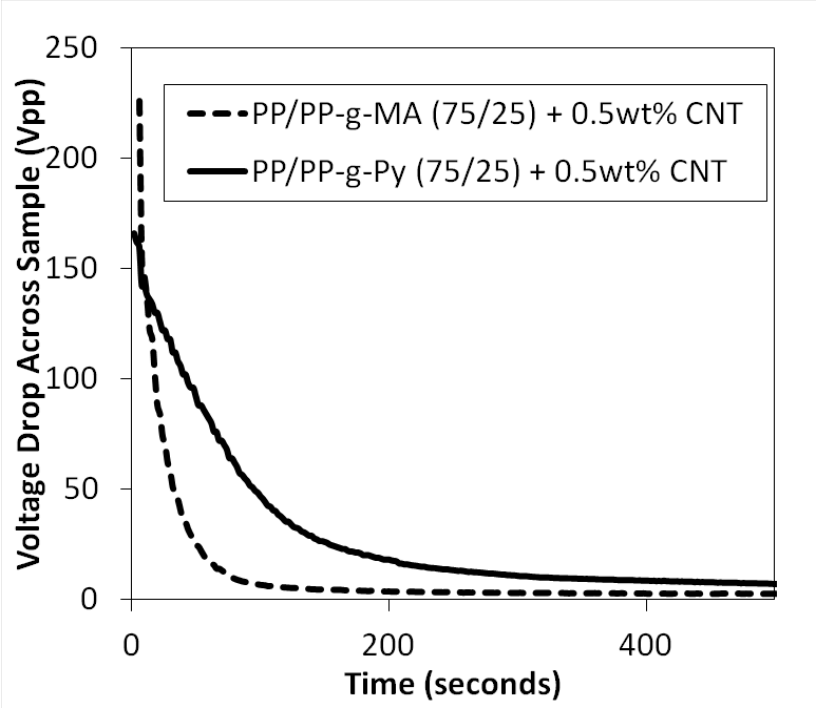


**Figure 4.12: Change in voltage across MWCNT/PP composites in the melt state upon application of an external AC electric field.**

The resistivity values of the aligned composites in the melt state can be measured online using the following relations [17]:

$$|Z| = \frac{E\angle\theta_E}{I\angle\theta_I} = \frac{E}{I}(\angle\theta_E - \angle\theta_I) = Z\angle\theta_Z \qquad (4.2)$$

where $|Z|$ is the magnitude of impedance from the capacitor (sample), E is the voltage across the electrode cell, I is the current through the system and $??_Z$ is the phase angle by which voltage lags current in the capacitance system. Resistance can then be calculated using Equation 4.3 and converted to resistivity using Equation 4.1.

$$R = |Z|\cos\theta_Z \qquad (4.3)$$

Figure 4.13 shows that after 2 hours of electric field application a resistivity on the order of $10^3$ Ωm (conductivity of $10^{-3}$ S/m) is achieved for composites that were initially below the percolation threshold, and therefore non-conductive (Table 4.2). This corresponds to similar

conductivity values as the maximum ones reported in Figure 4.10, however at a much lower filler concentration.

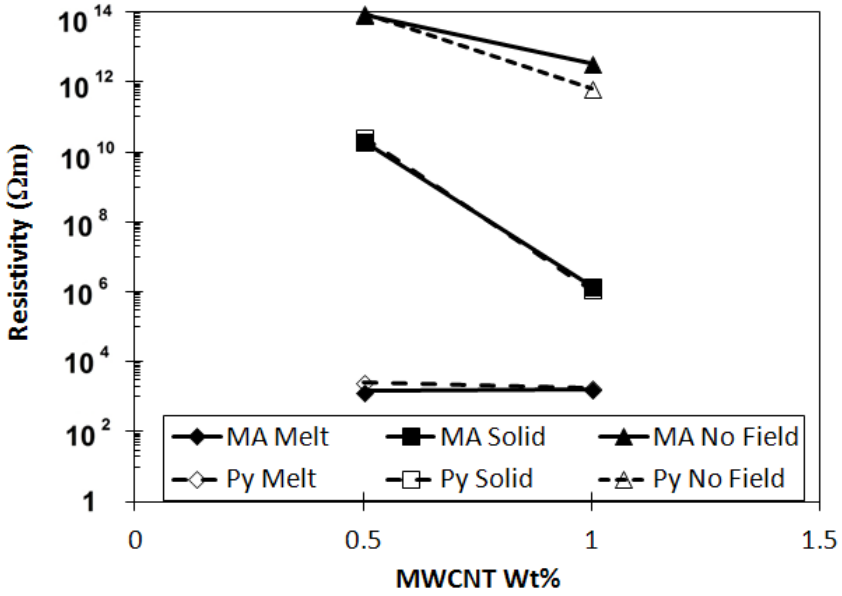


**Figure 4.13: Resistivity of PP/PP-g-MA and PP-g-Py (75/25) measured inline after 2 hours of AC electric field application (melt), upon quenching (solid) and for samples not exposed to AC electric field (no field).**

After removing the electric field and quenching from the melt state, only a fraction of the improvement in conductivity is maintained. Osazuwa et al. have reported similar results [17]. This suggests that upon quenching from the melt state, only a fraction of the electrode spanning nanotube networks remains intact, presumably because of rapid diffusion in a low viscosity matrix. The disruption of the aligned chains because of crystallization and the resulting volume change that occurs during cooling also plays a role. Sample resistivity is better preserved at a higher nanotube loading.

## 4.4 Conclusions

Aromatic moieties have been grafted to PP chains and have shown to improve the interfacial adhesion between melt mixed PP and MWCNTs. This non-covalent interaction resulted in improved MWCNT dispersion without disrupting the electrical properties of the

nanotubes. Percolation was found to occur at 1.2 wt% loading for both matrices and had a maximum conductivity value on the order of $10^{-2}$S/m. MWCNT reinforced composites exhibited improved strength and ductility with Py functionalized PP. It was also shown that application of an external AC electric field can induce lower percolation thresholds, and achieve low resistivity values.

## 4.5 References


[1] M. Moniruzzaman and K. I. Winey, "Polymer nanocomposites containing carbon nanotubes," *Macromolecules 39(16),* pp. 5194-5205. 2006.

[2] D. Bikiaris, "Microstructure and Properties of Polypropylene/Carbon Nanotube Nanocomposites," *Materials 3,* pp. 2884-2946. 2010.

[3] E. Cohen, A. Ophir, S. Kenig, C. Barry and J. Mead, "Pyridine-modified polymer as a non-covalent compatibilizer for multi-walled CNT/Poly[ethylene-co-(methacrylic acid)] composites fabricated by direct melt mixing," *Macromol. Mater. Eng. 298(4),* pp. 419-428. 2013.

[4] C. Dyke and J. Tour, "Covalent functionalization of single-walled carbon nanotubes for materials applications,"*Journal of Physical Chemistry a 108(51),* pp. 11151-11159. 2004.

[5] S. A. Girei, S. P. Thomas, M. A. Atieh, K. Mezghani, S. K. De, S. Bandyopadhyay and A. Al-Juhani, "Effect of -COOH Functionalized Carbon Nanotubes on Mechanical, Dynamic Mechanical and Thermal Properties of Polypropylene Nanocomposites," *J. Thermoplast. Compos. Mater. 25,* pp. 333-350. 2012.

[6] C. Li, H. Deng, K. Wang, Q. Zhang, F. Chen and Q. Fu, "Strengthening and toughening of thermoplastic polyolefin elastomer using polypropylene-grafted multiwalled carbon nanotubes," *J. Appl. Polym. Sci. 121(4),* pp. 2104-2112. 2011.

[7] C. Li, Q. Zhao, H. Deng, C. Chen, K. Wang, Q. Zhang, F. Chen and Q. Fu, "Preparation, structure and properties of thermoplastic olefin nanocomposites containing functionalized carbon nanotubes," *Polym. Int. 60(11),* pp. 1629-1637. 2011.

[8] N. G. Sahoo, S. Rana, J. W. Cho, L. Li and S. H. Chan, "Polymer nanocomposites based on functionalized carbon nanotubes," *Progress in Polymer Science 35(7),* pp. 837-867. 2010.

[9] K. Petrie, A. Docoslis, S. Vasic, M. Kontopoulou, S. Morgan and Z. Ye, "Non-covalent/non-specific functionalization of multi-walled carbon nanotubes with a hyperbranched polyethylene and characterization of their dispersion in a polyolefin matrix," *Carbon 49,* pp. 3378-3382. 2011.

[10] O. Osazuwa, K. Petrie, M. Kontopoulou, P. Xiang, Z. Ye and A. Docoslis, "Characterization of non-covalently, non-specifically functionalized multi-wall carbon nanotubes and their melt compounded composites with an ethylene-octene copolymer," *Composites Sci. Technol. 73,* pp. 27-33. 2012.

[11] A. Vasileiou, A. Docoslis and M. Kontopoulou, "The role of non-covalent functionalization and matrix viscosity on the dispersion and properties of LLDPE/MWCNT nanocomposites," *Polymer (accepted).* 2013.

[12] L. Xu, Z. Ye, Q. Cui and Z. Gu, "Noncovalent nonspecific functionalization and solubilization of multi-walled carbon nanotubes at high concentrations with a hyperbranched polyethylene," *Macromolecular Chemistry and Physics 210(24),* pp. 2194-2202. 2009.

[13] K. Prashantha, J. Soulestin, M. F. Lacrampe, M. Claes, G. Dupin and P. Krawczak, "Multi-walled carbon nanotube filled polypropylene nanocomposites based on masterbatch route: Improvement of dispersion and mechanical properties through PP-g-MA addition," *Express Polym. Lett. 2(10),* pp. 735-745. 2008.

[14] S. H. Lee, E. Cho, S. H. Jeon and J. R. Youn, "Rheological and electrical properties of polypropylene composites containing functionalized multi-walled carbon nanotubes and compatibilizers," *Carbon 45(14),* pp. 2810-2822. 2007.

[15] G. S. Ezat, A. L. Kelly, S. C. Mitchell, M. Youseffi and P. D. Coates, "Effect of maleic anhydride grafted polypropylene compatibilizer on the morphology and properties of polypropylene/multiwalled carbon nanotube composite," *Polym. Compos. 33,* pp. 1376-1386. 2012.

[16] J. Thomassin, I. Huynen, R. Jerome and C. Detrembleur, "Functionalized polypropylenes as efficient dispersing agents for carbon nanotubes in a polypropylene matrix; application to electromagnetic interference (EMI) absorber materials," *Polymer 51(1),* pp. 115-121. 2010.

[17] O. Osazuwa, M. Kontopoulou, P. Xian, Z. Ye and A. Docoslis, "Polymer composites containing non-covalently functionalized carbon nanotubes: A study of their dispersion characteristics and response to AC electric field," in *20th International Congress of Chemical and Process Engineering CHISA 2012,* 25-29 August 2012, Prague, Czech Republic. 2012.

[18] L. J. Lanticse, Y. Tanabe, K. Matsui, Y. Kaburagi, K. Suda, M. Hoteida, M. Endo and E. Yasuda, "Shear-induced preferential alignment of carbon nanotubes resulted in anisotropic electrical conductivity of polymer composites," *Carbon 44(14),* pp. 3078-3086. 2006.

[19] K. Iakoubovskii, "Techniques of aligning carbon nanotubes," *Central European Journal of Physics 7(4),* pp. 645-653. 2009.

[20] L. Tang, X. Yan, M. Kontopoulou and A. Docoslis, "The effect of electric field parameters on the resistivity and induced percolation time of carbon black-filled polystyrene composites," *Polymer Composites 32(7),* pp. 1106-1114. 2011.

[21] T. Prasse, L. Flandin, K. Schulte and W. Bauhofer, "In situ observation of electric field induced agglomeration of carbon black in epoxy resin," *Appl. Phys. Lett. 72(22),* pp. 2903-2905. 1998.

[22] M. Schwarz, W. Bauhofer and K. Schulte, "Alternating electric field induced agglomeration of carbon black filled resins," *Polymer 43(10),* pp. 3079-3082. 2002.

[23] M. Kontopoulou, M. Kaufman and A. Docoslis, "Electrorheological properties of PDMS/carbon black suspensions under shear flow," *Rheologica Acta 48(4),* pp. 409-421. 2009.

[24] J. Li, W. Cheung and D. Jia, "A study on the heat of fusion of beta-polypropylene," *Polymer 40(5),* pp. 1219-1222. 1999.

[25] C. Orr, J. Cernohous, P. Guegan, A. Hirao, H. Jeon and C. Macosko, "Homogeneous reactive coupling of terminally functional polymers," *Polymer 42(19),* pp. 8171-8178. 2001.

[26] M. R. Vakili, S. Zahmatkesh, H. K. Saadi and F. Razaghzadeh, "Synthesis and characterization of novel polyhydrazides containing pendant amide-imide-pyridine moiety," *Polym. Bull. 69(2),* pp. 163-174. 2012.

[27] Q. Lu, C. Macosko and J. Horrion, "Melt amination of polypropylenes," *Journal of Polymer Science Part A-Polymer Chemistry 43(18),* pp. 4217-4232. 2005.

[28] T. Skipa, D. Lellinger, W. Boehm, M. Saphiannikova and I. Alig, "Influence of shear deformation on carbon nanotube networks in polycarbonate melts: Interplay between build-up and destruction of agglomerates," *Polymer 51(1),* pp. 201-210. 2010.

[29] R. Socher, B. Krause, M. T. Mueller, R. Boldt and P. Poetschke, "The influence of matrix viscosity on MWCNT dispersion and electrical properties in different thermoplastic nanocomposites," *Polymer 53,* pp. 495-504. 2012.

[30] L. Valentini, J. Biagiotti, J. Kenny and S. Santucci, "Morphological characterization of single-walled carbon nanotubes-PP composites," *Composites Sci. Technol. 63(8),* pp. 1149-1153. 2003.

[31] T. McNally, P. Potschke, P. Halley, M. Murphy, D. Martin, S. Bell, G. Brennan, D. Bein, P. Lemoine and J. Quinn, "Polyethylene multiwalled carbon nanotube composites," *Polymer 46(19),* pp. 8222-8232. 2005.

[32] P. V. Kodgire, A. R. Bhattacharyya, S. Bose, N. Gupta, A. R. Kulkarni and A. Misra, "Control of multiwall carbon nanotubes dispersion in polyamide6 matrix: An assessment through electrical conductivity," *Chemical Physics Letters 432(4-6),* pp. 480-485. 2006.

[33] J. Rouse, "Polymer-assisted dispersion of single-walled carbon nanotubes in alcohols and applicability toward carbon Nanotube/Sol-gel composite formation," *Langmuir 21(3),* pp. 1055-1061. 2005.

[34] E. Cohen, H. Dodiuk, A. Ophir, S. Kenig, C. Barry and J. Mead, "Evidences for pi-interactions between pyridine modified copolymer and carbon nanotubes and its role as a compatibilizer in poly(methyl methacrylate) composites," *Composites Sci. Technol. 79,* pp. 133-139. 2013.

[35] E. Thostenson, Z. Ren and T. Chou, "Advances in the science and technology of carbon nanotubes and their composites: A review," *Composites Sci. Technol. 61(13),* pp. 1899-1912. 2001.

[36] R. Baughman, A. Zakhidov and W. de Heer, "Carbon nanotubes - the route toward applications," *Science 297(5582),* pp. 787-792. 2002.

[37] D. Bikiaris, A. Vassiliou, K. Chrissafis, K. M. Paraskevopoulos, A. Jannakoudakis and A. Docoslis, "Effect of acid treated multi-walled carbon nanotubes on the mechanical, permeability, thermal properties and thermo-oxidative stability of isotactic polypropylene," *Polym. Degrad. Stab. 93(5),* pp. 952-967. 2008.

[38] Y. Pan and L. Li, "Percolation and gel-like behavior of multiwalled carbon nanotube/polypropylene composites influenced by nanotube aspect ratio," *Polymer 54(3),* pp. 1218-1226. 2013.

[39] I. Alig, P. Poetschke, D. Lellinger, T. Skipa, S. Pegel, G. R. Kasaliwal and T. Villmow, "Establishment, morphology and properties of carbon nanotube networks in polymer melts," *Polymer 53,* pp. 4-28. 2012.

[40] M. A. Haque, M. F. Mina, A. K. M. M. Alam, M. J. Rahman, M. A. H. Bhuiyan and T. Asano, "Multiwalled carbon nanotubes-reinforced isotactic polypropylene nanocomposites: Enhancement of crystallization and mechanical, thermal, and electrical properties," *Polym. Compos.33,* pp. 1094-1104. 2012.

[41] K. Prashantha, J. Soulestin, M. F. Lacrampe, P. Krawczak, G. Dupin and M. Claes, "Masterbatch-based multi-walled carbon nanotube filled polypropylene nanocomposites: Assessment of rheological and mechanical properties," *Composites Sci. Technol. 69(11-12),* pp. 1756-1763. 2009.

[42] S. C. Tjong, "Structural and mechanical properties of polymer nanocomposites," *Mater. Sci. Eng. R-Rep. 53,* pp. 73-197. 2006.

[43] E. Assouline, A. Lustiger, A. Barber, C. Cooper, E. Klein, E. Wachtel and H. Wagner, "Nucleation ability of multiwall carbon nanotubes in polypropylene composites," *Journal of Polymer Science Part B-Polymer Physics 41(5),* pp. 520-527. 2003.

# Chapter 5

# Composites of Polypropylene and Ethylene-Octene Copolymer blends with MWCNTs Prepared by Melt Compounding

## 5.1 Introduction

Polypropylene (PP) is commonly utilized for a variety of important industrial and everyday applications because of its low density, high stiffness and low cost. However, PP shows brittle performance at reduced temperatures. Impact modifiers such as ethylene/propylene rubber (EPR), ethylene/propylene diene terpolymer (EPDM) and metallocene-catalyzed ethylene/α-olefin copolymers (ECs) are commonly employed to improve the low temperature impact resistance of PP in Thermoplastic Olefin (TPO) blends [1-5]. ECs are preferred because they are easily processed and form a finely dispersed phase when melt mixed with a PP matrix [2]. The mechanical properties of these immiscible polymer blends are directly related to their morphology [6-8]. Blend morphology is dictated by the counter-acting mechanisms of droplet break-up and coalescence. These mechanisms are influenced upon melt compounding by blend composition, viscosity ratio, mixing time, shear rate and thermodynamic considerations [9]. Finely dispersed and distributed droplets of EC in a PP matrix result in improved impact properties while maintaining composite strength in comparison to co-continuous matrix morphology [2, 3, 6].

Rigid fillers, such as talc, glass fibers, silica, and more recently nanofillers such as nanosilica, organoclay, carbon black and multi-walled carbon nanotubes (MWCNTs) have been studied as a means to reinforce polymer blends [6, 10-16]. The degree of improvement in stiffness with the addition of nanofillers depends on filler dispersion and has been shown to frequently come at the expense of ductility [6, 10, 12, 17]. Nanofiller localization to the matrix phase is integral for the effective reinforcement of TPO blends [10]. Matrix and filler

functionalization approaches have been employed to achieve selective localization of a filler within a particular blend phase [6, 10, 16, 18, 19].

The introduction of electrically conductive nanofillers (carbon black and MWCNTs) into polymer blends not only offers potential reinforcement, but has been shown to reduce the electrical percolation threshold in many systems if the filler is localized in the matrix phase or at the interface of the blends [20, 21]. This decrease in electrical percolation is governed by the concentration in the filler rich phase and the continuity of that phase, which is commonly referred to as "double percolation" [20].

Blends with MWCNTs containing polymers with polar components have been previously studied [15, 21-24], while studies of commercially relevant TPOs remains scarce due to the difficulty to disperse nanotubes in non-polar matrices and controlling filler localization[16, 25-27]. In the present chapter a ternary TPO blend system, comprising of the PP matrix characterized in detail in the previous chapter, and an EC, filled with MWCNTs is studied. The effect of grafting of aromatic moieties to the PP chains on blend morphology and MWCNT localization is investigated. The electrical performance of these blends is reported as a function of compounding time and composition.

## 5.2 Experimental

### 5.2.1 Materials

MWCNTs were used as supplied from Nanolab Inc. (purity: >95%, diameter: 30±15nm and length: 1-5 μm). The specific surface area (SSA) of the MWCNTs was 300 $m^2/g$ based on Brunauer-Emmett-Teller characterization. The average pore size of the MWCNTs as determined by $N_2$ sorption experiments is about 2.3 nm [28].

A PP homopolymer, Pro-fax® PD 702 by LyondellBasell was used in this work. Fusabond® PMD 511D is a polypropylene-grafted-maleic anhydride (PP-g-MA) that was used for the grafting reaction with 4-aminomethylpryridine (AMP) (98% purity, supplied by Aldrich). The

procedure to make PP-grafted-aminopyridine (PP-g-Py) is outlined in the previous chapter. A high melt flow index, injection molding grade ethylene-octene copolymer Engage® 8407 (EOC) was used as the elastomeric phase for the blended composites. The properties of all polymers can be seen in Table 5.1. Irganox B225 is a hindered phenol antioxidant that was added to each composite at 0.2 wt% for improved thermal stability.

**Table 5.1: Properties of polymer materials.**

| *Material* | *PP* | *PP-g-MA* | *EOC* |
|---|---|---|---|
| Trade Name | Pro-fax® PD702 | Fusabond® P MD 511D | Engage® 8407 |
| MFR (g/10min.) | 35 @ 230°C | 25 @ 190°C | 30 @ 190°C |
| Density (kg/m$^3$) | 900 | 900 | 870 |
| Melting Point (°C) | 165 | 159 | 65 |
| Co-monomer Content (wt%) | - | - | 40 |
| Graft Content (wt%) | - | 0.25-0.5 | - |

### 5.2.2 Melt Blending Procedure

The polypropylene phase used in the TPO blends, containing weight ratios of PP/PP-g-MA or PP/PP-g-Py (75/25) was prepared as described in the previous chapter. For convenience in the rest of the chapter, the abbreviation PP corresponds to the mixture of PD702 and PP-g-MA or PP-g-Py. Two mixing procedures were used: The first involved the addition of MWCNTs in the mixer after the PP and EOC were pre-blended. In the second procedure MWCNTs were pre-mixed with the PP in a Carver hot press at 200°C for 1 minute, by folding and hot-pressing 3 times. MWCNTs were then melt mixed with the PP matrix in a DSM Research 5ml co-rotating twin-screw micro-compounder at 180°C, 120 RPM and a mixing time of 8 minutes under nitrogen purge. Corresponding amounts of EOC were then added to the compounder to produce blends containing 0.5 to 3 wt% (0.3 to 1.7 vol.% converted using densities of 0.9, 0.87 and 1.65

g/cm$^3$ for PP, EOC and MWCNTs, respectively) and were blended for the designated time (1, 2, 4, 8 minutes). Neat PP/EOC blends were subjected to a similar processing history, to provide a basis for comparison.

### 5.2.3 Composite Characterization

#### 5.2.3.1 Rheology

Measurements of the linear viscoelastic properties (LVE) were carried out using an oscillatory rheometer (Anton Paar MCR 301 with a convection CTD 450 oven attached) using a parallel plate measuring system (PP25). The complex viscosity, storage and loss modulus were measured versus frequency in the linear viscoelastic region at a strain of 2% and 190$^o$C.

#### 5.2.3.2 Morphology

The dispersion of MWCNTs in the melt blended composites was investigated using an Olympus BX 51 optical microscope. Composite films were loaded on a Linkam SCC 450 Hot Stage at 180$^o$C and pressed to a thickness of 50 μm. Images were recorded using transmitted light. Blend morphology was investigated using scanning electron microscopy (SEM). Images were taken using a JEOL JMS-840A scanning microscope. Samples were first cold fractured in liquid nitrogen after 1 minute of cooling. The elastomer phase was then selectively etched using toluene at 70$^o$C for 2 hours. The fracture surface was gold coated prior to imaging. SigmaScan Pro image analysis software was used to estimate the average diameter of the etched elastomer phase. Contrast and brightness were varied to isolate etched elastomer phases, with residual removal and dilation filters applied. Transmission electron microscopy (TEM) images were taken using a FEI Tecnai 20 instrument to investigate blend morphology and filler localization. Ultra-thin films of the composites were prepared by cryosectioning, using a Leica ultra-microtome. Samples were first stained with ruthenium tetroxide ($RuO_4$) prior to imaging to increase the contrast between the phases [29].

5.2.3.3 Electrical Conductivity

A Keithley 8009 Resistivity Test Fixture connected to a Keithley 6517B Electrometer/High Resistance Meter was used under DC current at room temperature for samples having a volume resistivity above $10^6$ Ωcm and an Agilent 34401A 6 Digit Multimeter was used for samples exhibiting resistivity below this, as outlined in detail in Chapter 4.

## 5.3 Results and Discussion

### 5.3.1 Blend Morphology

An EOC, with similar MFI as the PP phase was selected for the TPO blends in this Chapter. As shown in Figure 5.1, EOC has lower viscosity than PP in the entire shear rate range relevant to compounding. This should facilitate droplet break up during melt mixing.

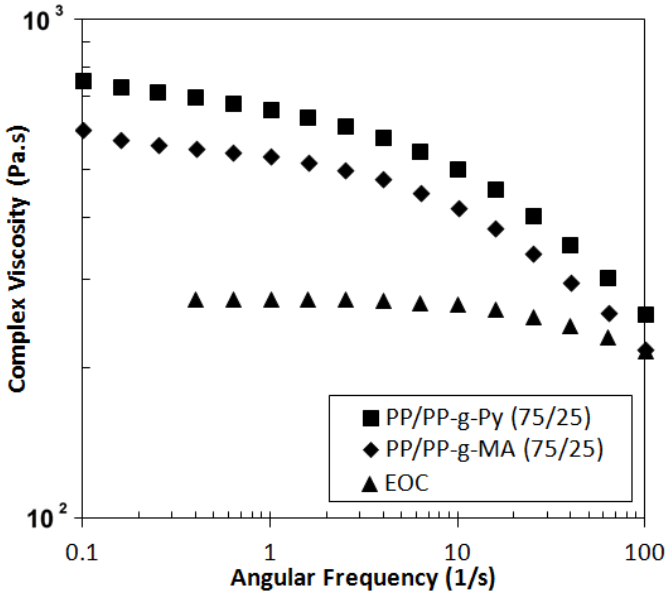


**Figure 5.1: Complex viscosity versus frequency for blend components at 190°C.**

Representative SEM images in Figure 5.2 show matrix/droplet morphology for (PP/PP-g-Py)/EOC blend compositions of 80/20 and 70/30, while a co-continuous morphology is obtained at a 50/50 composition. The EOC phase becomes the continuous phase with PP droplets at a composition of 30/70 PP/EOC. The complex viscosity values at shear rates of 80-100 $s^{-1}$ from

Figure 5.1 were used to estimate the type of morphology obtained at the various blend compositions (droplet/matrix or co-continuous) using Equation 5.1 below:

$$\frac{\eta_1}{\eta_2} \cdot \frac{\phi_2}{\phi_1} \cong 1 \qquad (5.1)$$

where η is viscosity and φ is the volume fraction of polymer phases 1 and 2 respectively. If the quantity on the left is greater than unity or less than unity, phase 2 or 1 is likely to be continuous, respectively. If the left side is approaching unity, it is likely that both phases are continuous [30]. The model in Equation 5.1 predicts a continuous PP phase exists until approximately 60/40 (PP/EOC) at the investigated shear rates. A co-continuous morphology should be present at a blend composition of 50/50, and a continuous EOC phase at 30/70.

The (PP/PP-g-Py)/EOC 80/20 blend contains well-dispersed, fine EOC droplets, which are ideal for improved mechanical properties [2] and was therefore chosen for the investigation of the effect of blend time on filler localization.

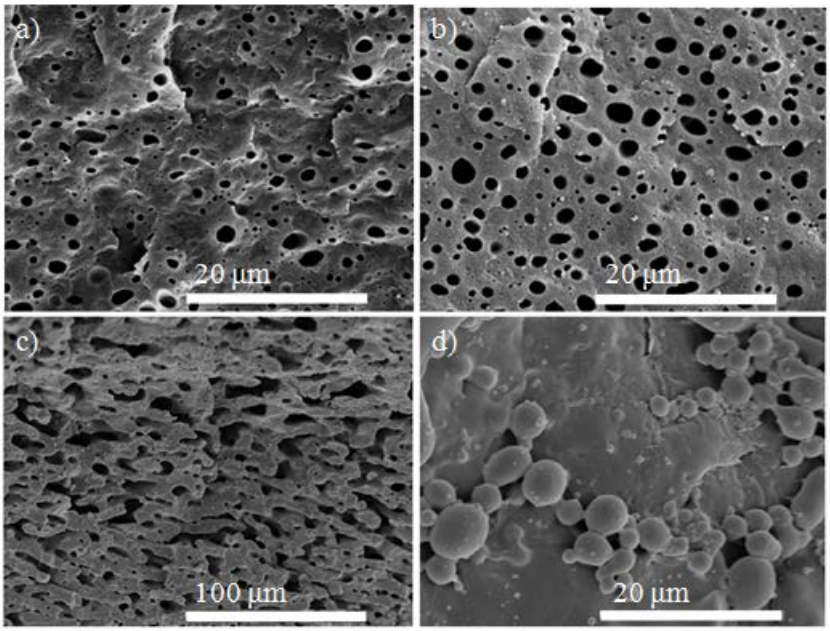


**Figure 5.2: SEM images of a) 80/20 b) 70/30 c) 50/50 and d) 30/70 (PP/PP-g-Py)/EOC blends at 4 minutes of blending time.**

### 5.3.2 Partitioning of MWCNTs

Droplet phase morphology and localization of fillers impacts the resulting properties of ternary nanocomposites. It has been shown that it is desirable in PP rich blends with EOC that the filler reside exclusively in the matrix phase for composite reinforcement and at the interface for decreased electrical percolation thresholds [10, 14, 15, 27, 31]. TEMs images (Figure 5.3) revealed that when MWCNTs are added to premixed blends of PP/EOC (70/30), the filler tends to localize in the EOC phase. Research from other groups has also shown that MWCNTs preferentially locate in the EOC phase for TPO blends [16, 27].

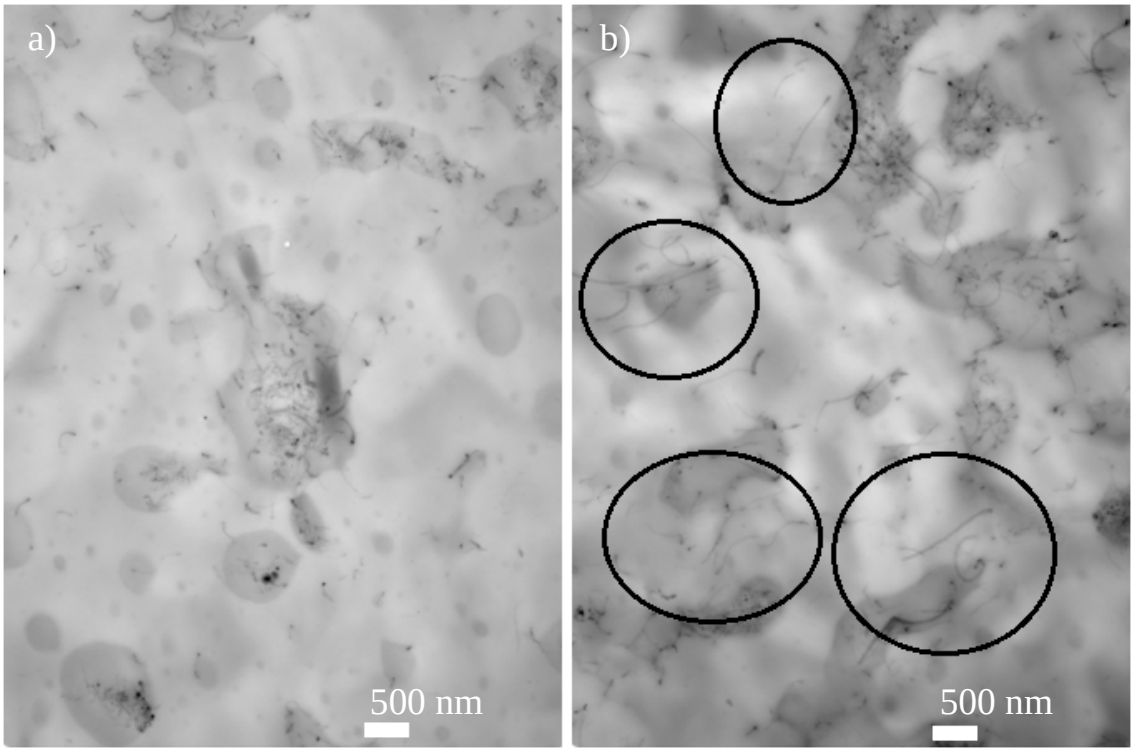


**Figure 5.3: TEM images of PP/EOC (70/30) with 3wt% MWCNTs a) PP/PP-g-MA and b) PP/PP-g-Py. Darker droplets are EOC dispersed in PP.**

The grafting of aminomethylpyridine to the PP backbone appears to have only a slight effect in MWCNT localization, as more nanotubes can be seen outside of the elastomer droplets and along the interface (circled). Filler localization in the elastomer phase will not result in bulk composite reinforcement [10, 12, 14, 16, 25].

As mentioned in section 2.3.2, preferential filler localization may be attributed to thermodynamic or kinetic effects. Viscosity mismatch and melting point differences may influence the localization of the filler. Lower viscosities and lower melting points of one phase are generally considered favorable for filler partitioning in that particular phase. In the present case the blend was already pre-melted inside the compounder. Therefore the differences in the melting point are likely not the reason. EOC has lower viscosity at the compounding temperature (see Figure 5.3). However the viscosity differences are not significant at shear rates relevant to compounding (between 50 and 100 $s^{-1}$).

The migration of MWCNTs to the EOC phase can be explained by the tendency of the system to minimize interfacial energy by the filler arranging into a particular blend phase. A wetting coefficient ($\omega_a$) can be estimated using Equation 5.2 based on interfacial tensions between the various ternary blend components ($\sigma_{i/j}$) from surface tension values ($\sigma_i$) of the individual components involved.

$$\omega_a = \frac{\sigma_{MWCNT/EOC} - \sigma_{MWCNT/PP}}{\sigma_{PP/EOC}} \qquad (5.2)$$

Filler partitioning criteria are as follows [20]:

If $\omega_a$ > 1, MWCNTs distribute within PP phase

If -1 < $\omega_a$ < 1, MWCNTs reside at interface between phases

If $\omega_a$ < -1, MWCNTs distribute within EOC phase

Table 5.2 exhibits interfacial tension values used in this work, where the total surface tension value is the sum of the dispersive (d) and polar (p) component. All values are from the specified reference in Table 5.2, extrapolated to 180$^{o}$C with the assumption that the percent polarity is independent of temperature.

**Table 5.2: Surface tension values**

| *Component* | $\sigma_d$ *(mJ/m$^2$)* | $\sigma_p$ *(mJ/m$^2$)* |
|---|---|---|
| MWCNT[1] | 18.6 | 26.7 |
| PP[2] | 20.5 | 0.9 |
| EOC[3] | 15.6 | 1.9 |

The interfacial tension between the components can be estimated using the harmonic and geometric mean equations. Equation 5.3 is the harmonic mean equation which can be used to estimate interfacial energy between low energy materials and Equation 5.4 is the geometric mean equation which can be used to estimate interfacial energy between high and low energy materials. In this work, both will be used to predict wetting coefficients [32].

Harmonic Mean

$$\sigma_{1/2} = \sigma_1 + \sigma_2 - 4\left(\frac{\sigma_1^{\mathrm{d}}\sigma_2^{\mathrm{d}}}{\sigma_1^{\mathrm{d}}+\sigma_2^{\mathrm{d}}} + \frac{\sigma_1^{\mathrm{p}}\sigma_2^{\mathrm{p}}}{\sigma_1^{\mathrm{p}}+\sigma_2^{\mathrm{p}}}\right) \quad (5.3)$$

Geometric Mean

$$\sigma_{1/2} = \sigma_1 + \sigma_2 - 2\left(\sqrt{\sigma_1^d \sigma_2^d} + \sqrt{\sigma_1^p \sigma_2^p}\right) \quad (5.4)$$

Table 5.3 shows the estimated values of interfacial tension and wetting coefficients. It can be seen that for both methods of interfacial tension estimation, the wetting coefficient is less than -1. Due to the lack of data, it is impossible to estimate the interfacial tension values and wetting coefficients for the blends that contain PP-g-Py, but based on the imaging results functionalization with pyridine did not affect significantly the wetting coefficient.

[1] Value from ref. [37] extrapolated to 180$^o$C with assuming percent polarity is independent of temperature.
[2] Weighted average value for PP and PP-g-MA from ref. [20] and [38] extrapolated to 180$^o$C with assuming percent polarity is independent of temperature.
[3] Value from ref. [39] extrapolated to 180$^o$C with assuming percent polarity is independent of temperature.

**Table 5.3: Interfacial tension values and corresponding wetting coefficients**

| | *Harmonic Mean* ($mJ/m^2$) | *Geometric Mean* ($mJ/m^2$) |
|---|---|---|
| $\sigma_{MWCNT/EOC}$ | 21.8 | 14.5 |
| $\sigma_{MWCNT/PP}$ | 24.3 | 18.8 |
| $\sigma_{PP/EOC}$ | 1.3 | 0.7 |
| $\omega_a$ | -1.9 | -5.9 |

These results confirm that MWCNTs are thermodynamically driven to partition within the EOC phase. It was decided therefore to attempt a kinetic approach in an effort to achieve localization of the filler within the PP matrix. This involves pre-blending the MWNCTs with the PP, and subsequent addition of the EOC component. The morphological evolution of the blends was subsequently monitored as a function of time.

### 5.3.3 Kinetic Approach to MWCNT Partitioning

The effect of various blending times on the morphology of 80/20 blends of PP/EOC with both MA and Py functionalities, with and without 3 wt% MWCNTs can be seen in Figure 5.4. When comparing Figure 5.4 rows a) and c) it can be concluded that the Py functionalization has an insignificant effect on the size of the dispersed phase. This is expected since there is an insignificant change in viscosity with Py functionalization as shown in Figure 5.1. Detailed image analysis (Figure 5.5) confirms that the average diameter of the dispersed phase at various blending times does not change with Py matrix functionalization. A slight increase in droplet diameter and polydispersity is also detected above 4 minutes of blending time for both unfilled MA and Py functionalized matrices. This can be attributed to droplet instability and increased coalescence at the highest blend time. On the contrary, in the presence of the nanofiller the morphology appears more stable and with a slight decrease in average dispersed droplet size. This

has been seen in other ternary blends upon addition of nanofillers [10-12, 16, 27]. A possible explanation for the observed decrease involves the modification of interfacial tension between the blend components in the presence of the nanofiller [10, 12, 16, 33, 34]. The composites based on PP-g-Py had overall the smallest droplet size. This may be associated to the presence of a few MWCNTs that span EOC droplets and reside at the interface, thus potentially altering the interfacial tension between the blend phases.

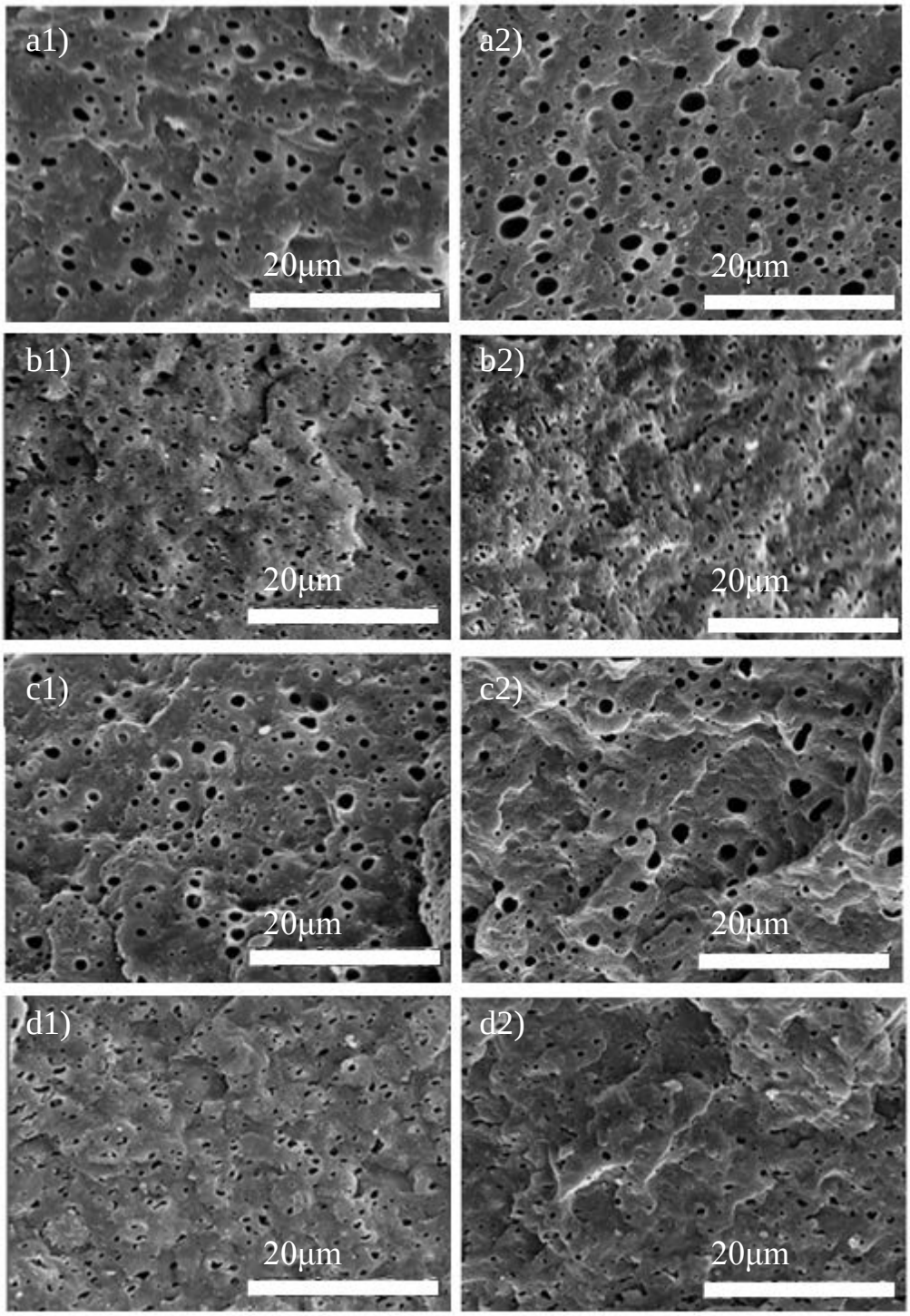


**Figure 5.4: SEM images of 80/20 blends of PP/EOC (a,b) (PP/PP-g-MA) and (c,d) (PP/PP-g-Py) at blend times of 2 minutes (1) and 8 minutes (2). Rows b) and d) contain 3 wt% MWCNTs. Dark holes correspond to etched EOC phase.**

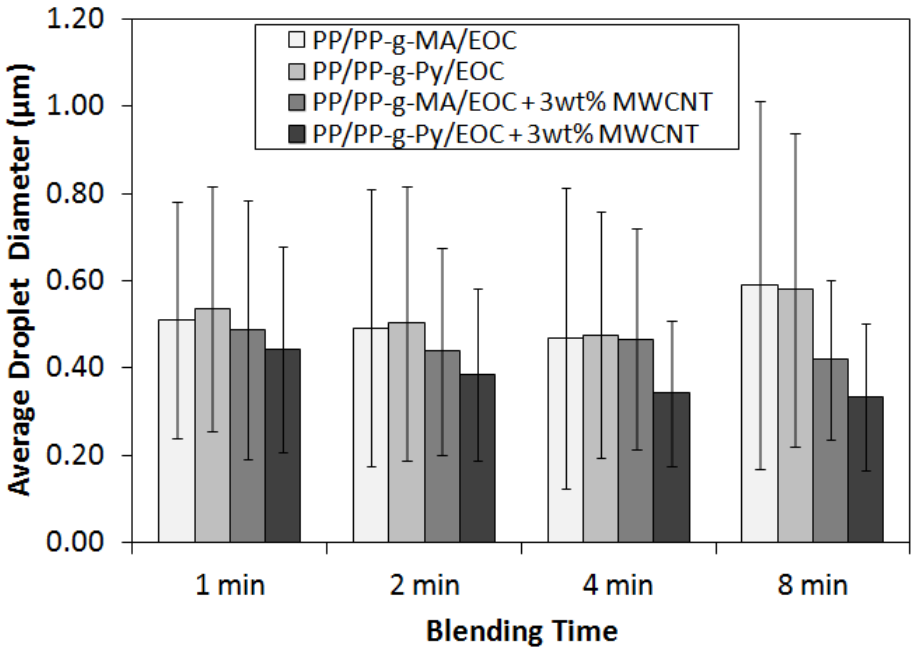


**Figure 5.5: Detailed image analysis of 80/20 blends of PP/EOC after various blending times.**

Migration to the EOC phase after various blending times can be seen in Figure 5.6. It appears that after 2 minutes for both the MA and Py functionalized matrices, MWCNTs have already begun to migrate. The majority of MWCNTs have migrated to the dispersed EOC phase after 4 minutes of blending. The PP/PP-g-MA matrix shows almost all MWCNTs in the EOC phase after 8 minutes, while the PP/PP-g-Py matrix still contains some MWCNTs spanning dispersed droplets in the PP phase.

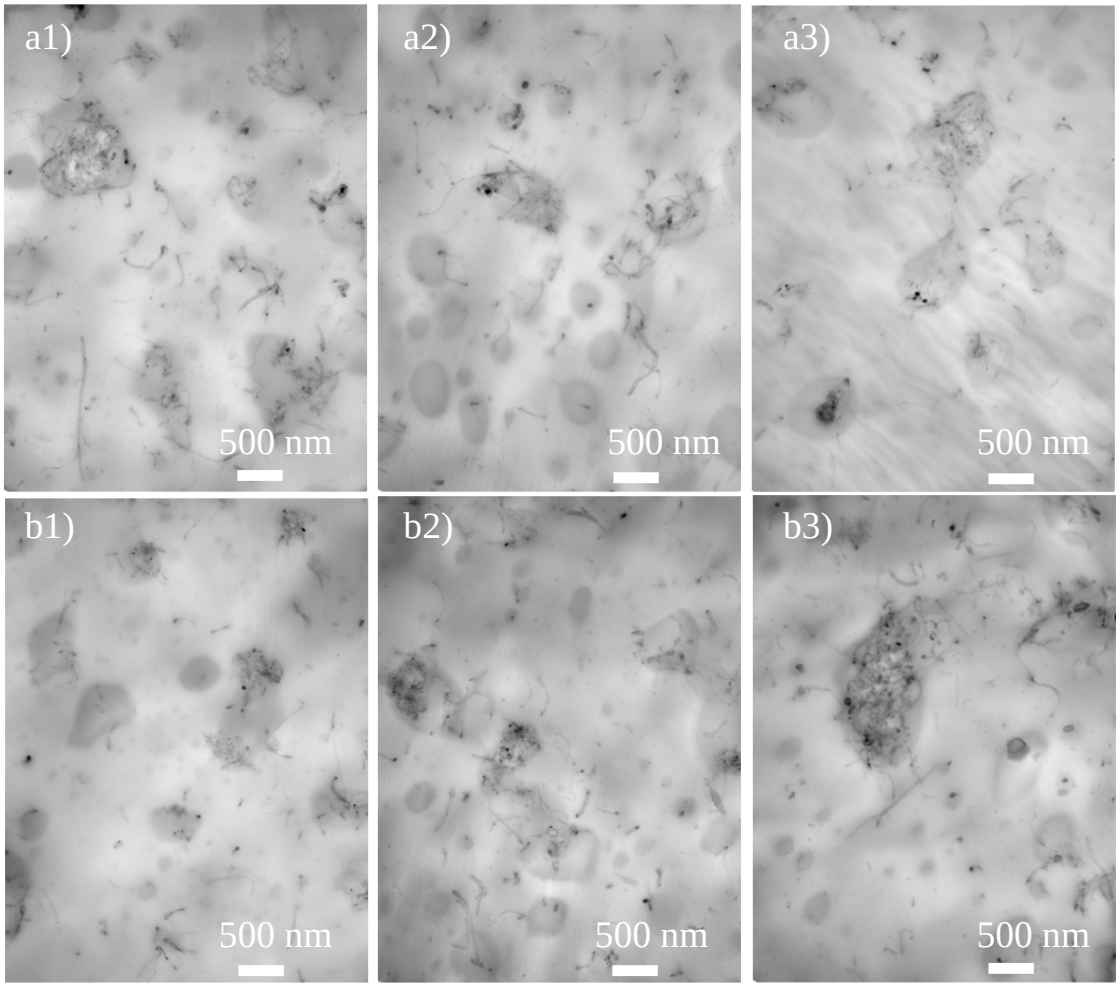


**Figure 5.6: TEM images of PP/EOC (80/20) with (a) PP/PP-g-MA and (b) PP/PP-g-Py containing 3 wt% MWCNTs at blend times of (1) 2 minutes, (2) 4 minutes and (3) 8 minutes**

These results confirm that the MWCNTs are thermodynamically driven to locate within the EOC phase, and a kinetic approach for localizing nanotubes in the PP matrix phase is not effective.

In the system under study, there exists only a small amount of aromatic functionality grafted to PP chains. This functionalization approach appears to be marginally effective in maintaining MWCNTs in the PP phase in comparison to PP-g-MA. Similar amounts of PP-g-MA

have been shown to be significantly more effective in localizing siliceous fillers, such as nanosilica in a PP matrix phase [6, 10]. The increased filler-matrix interaction between the MA functionality and the surface silanol groups of the nanosilica is likely more effective in selectively partitioning the filler in the matrix phase in comparison to the current system with MWCNTs. Additionally nanosilica comprises of spherical primary particles. On the contrary CNTs have high aspect ratios, which may also play a role in the ability for nanotubes to be distributed exclusively in either phase [27, 35]. Goeldel et al. [35] have proposed a Slim-Fast Mechanism where high aspect ratio nanofillers rapidly localize in the thermodynamically desirable phase due to low interfacial stabilities, and are unlikely to reside at the interface of the immiscible phases.

The use of an exclusively PP-g-Py matrix phase, which would provide improved interactions with the MWCNT should be tested in the future. Coupling the Py matrix functionalization with a partial surface modification of the MWCNTs to achieve exclusive PP matrix partitioning of the nanotubes should also be investigated.

### 5.3.4 Electrical Properties

An important consideration is the ability to produce electrically conductive thin films at reduced percolation thresholds for thin-film applications. In this section the effect of blending time (blend morphology and nanotube location) and blend composition on electrical conductivity are investigated with both MA and Py grafted PP matrices.

#### 5.3.4.1 Effect of Blend Time

Figure 5.7 shows the measured conductivity of 80/20 blends of PP/EOC and 3 wt% MWCNTs with MA and Py functionalized matrices. It can be seen that the conductivity values are very high, approaching $10^{-1}$ S/m after 1 and 2 minutes of blending time with EOC. These values are within the range of conductive materials. After 4 minutes of blending, there is a 2

orders of magnitude drop in conductivity. It is likely that the migration of the MWCNTs from the PP phase to the EOC phase occurs primarily between 2 to 4 minutes of blending time. As this happens, the MWCNTs are confined within the droplets and are less likely to span the entire sample and form conductive networks. Another possible consideration is nanotube shortening at higher blend times limiting potential network formation [36].

It is also important to note that there is a pronounced increase in conductivity for the Py functionalized matrix. The presence of Py functionality by itself is not responsible for this increase, as discussed in the previous chapter. Therefore, the observed increase in conductivity is likely attributable to a higher number of nanotubes residing in the PP matrix phase as filler/matrix interactions are stronger, resisting partitioning in the EOC phase. These nanotubes would be capable of spanning droplets, creating a more conductive network.

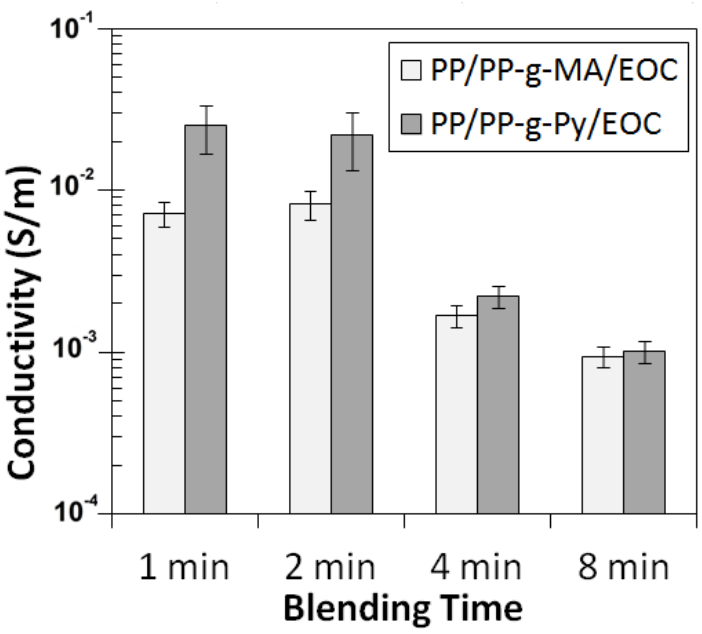


**Figure 5.7: Conductivity measurements for 80/20 PP/EOC blends with 3wt% MWCNTs at various blending times.**

5.3.4.2 Effect of Composition

Blend morphology and composition within nanocomposites with conductive fillers plays an integral part in the electrical performance of the materials [20]. The formation of an interconnected percolating network results in a transition from an insulating to conductive material as conductive pathways through the material are created with the addition of more MWCNTs [36]. The electrical percolation threshold can be estimated by fitting the power-law models from Equation 3.1 and 3.2 in Chapter 3.

Figure 5.8 shows the experimental and subsequent power-law model fit of different PP/EOC blend compositions at various MWCNT loadings.

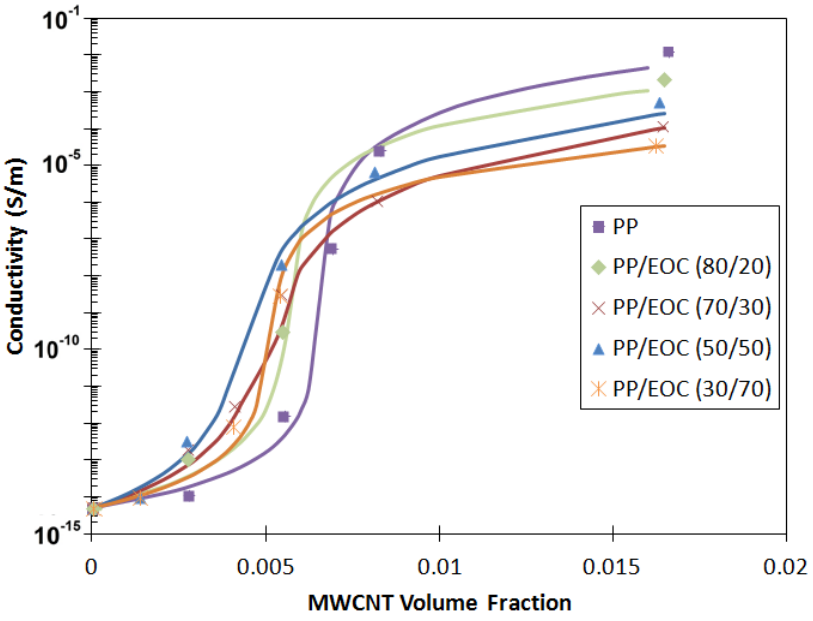


**Figure 5.8: Electrical conductivity versus MWCNT loading at various PP/PP-g-Py/EOC blend compositions with lines representing model fit according to power law model.**

From Table 5.4, the maximum values of conductivity at 3 wt% MWCNT loading decrease with larger fractions of EOC in the system. This is in agreement with previous

observations in the literature [27], possibly because of the migration of the MWCNTs to the EOC phase.

**Table 5.4: Percolation threshold and maximum electrical conductivity values at various blend compositions of PP/PP-g-Py/EOC.**

| *Sample* | $\varphi_c$ *(wt%)* | *Maximum* $\sigma$ *(S/m)* |
|---|---|---|
| PP | 1.19 | $1.3x10^{-2}$ |
| 80/20 | 1.05 | $4.5x10^{-3}$ |
| 70/30 | 0.92 | $1.2x10^{-4}$ |
| 50/50 | 0.81 | $5.3x10^{-4}$ |
| 30/70 | 0.95 | $3.7x10^{-5}$ |

Previous work [28] has shown that EOC/MWCNT composites have generally lower conductivities, in the range of $10^{-4}$ S/m. Further increase of the amount of EOC in the blend results in a dilution effect with a smaller effective concentration of MWCNTs in the EOC, therefore reducing conductivity even further.

It can also be seen in Table 5.4 and Figure 5.8 that the percolation threshold decreases as the blend morphology transitions from droplet/matrix to co-continuous morphology (80/20 to 70/30 to 50/50). This is an interesting result because it suggests that percolation can be achieved in TPO blends with MWCNTs at reduced loadings; as the MWCNTs preferentially locate in one of the blend phases, smaller amounts are required to achieve percolation, consistent with the concept of "double percolation"[20, 21].

## 5.4 Conclusion

Ternary TPO blends with MWCNTs were melt compounded in this study. The addition of MWCNTs resulted in a decrease in average droplet diameter for TPO blends with

droplet/matrix morphology. It was found that the MWCNTs were thermodynamically driven to the EOC phase and a kinetic approach to partitioning the filler in the matrix phase for mechanical reinforcement was ineffective. The grafting of aromatic moieties to PP chains resulted in minimal improvement in partitioning MWCNTs in the matrix phase as evidenced by TEM and improved electrical conductivity at lower blending times. Electrical percolation thresholds were reduced with the addition of EOC to co-continuous matrix morphology.

## 5.5 References


[1] A. L. N. Da Silva, M. C. G. Rocha, F. M. B. Coutinho, R. Bretas and C. Scuracchio, "Rheological, mechanical, thermal, and morphological properties of polypropylene/ethylene-octene copolymer blends," *J. Appl. Polym. Sci. 75(5),* pp. 692-704. 2000.

[2] M. Kontopoulou, W. Wang, T. G. Gopakumar and C. Cheung, "Effect of composition and comonomer type on the rheology, morphology and properties of ethylene-alpha-olefin copolymer/polypropylene blends," *Polymer 44(24),* pp. 7495-7504. 2003.

[3] T. McNally, P. McShane, G. M. Nally, W. R. Murphy, M. Cook and A. Miller, "Rheology, phase morphology, mechanical, impact and thermal properties of polypropylene/metallocene catalysed ethylene 1-octene copolymer blends," *Polymer 43(13),* pp. 3785-3793. 2002.

[4] L. Dorazio, C. Mancarella, E. Martuscelli, G. Sticotti and P. Massari, "Melt rheology, phase-structure and impact properties of injection-molded samples of isotactic polypropylene ethylene-propylene copolymer (ipp epr) blends - influence of molecular-structure of epr copolymers," *Polymer 34(17),* pp. 3671-3681. 1993.

[5] V. Choudhary, H. S. Varma and I. K. Varma, "Polyolefin blends - effect of epdm rubber on crystallization, morphology and mechanical-properties of polypropylene epdm blends," *Polymer 32(14),* pp. 2534-2540. 1991.

[6] S. H. Lee, M. Bailly and M. Kontopoulou, "Morphology and properties of poly(propylene)/Ethylene-octene copolymer blends containing nanosilica," *Macromolecular Materials and Engineering 297(1),* pp. 95-103. 2012.

[7] S. Wu, "A generalized criterion for rubber toughening - the critical matrix ligament thickness," *J. Appl. Polym. Sci. 35(2),* pp. 549-561. 1988.

[8] S. Wu, "Phase-structure and adhesion in polymer blends - a criterion for rubber toughening," *Polymer 26(12),* pp. 1855-1863. 1985.

[9] L. Utracki and Z. Shi, "Development of polymer blend morphology during compounding in a twin-screw extruder .1. droplet dispersion and coalescence - a review," *Polym. Eng. Sci. 32(24),* pp. 1824-1833. 1992.

[10] Y. Liu and M. Kontopoulou, "The structure and physical properties of polypropylene and thermoplastic olefin nanocomposites containing nanosilica," *Polymer 47(22),* pp. 7731-7739. 2006.

[11] J. R. Austin and M. Kontopoulou, "Effect of organoclay content on the rheology, morphology, and physical properties of polyolefin elastomers and their blends with polypropylene," *Polym. Eng. Sci. 46(11),* pp. 1491-1501. 2006.

[12] M. Bailly and M. Kontopoulou, "Preparation and characterization of thermoplastic olefin/nanosilica composites using a silane-grafted polypropylene matrix," *Polymer 50(11),* pp. 2472-2480. 2009.

[13] M. Kontopoulou, Y. Liu, J. R. Austin and J. S. Parent, "The dynamics of montmorillonite clay dispersion and morphology development in immiscible ethylene-propylene rubber/polypropylene blends," *Polymer 48(15),* pp. 4520-4528. 2007.

[14] Y. Liu and M. Kontopoulou, "Effect of filler partitioning on the mechanical properties of TPO/nanosilica composites," *Journal of Vinyl & Additive Technology 13(3),* pp. 147-150. 2007.

[15] A. Goeldel, G. Kasaliwal and P. Poetschke, "Selective localization and migration of multiwalled carbon nanotubes in blends of polycarbonate and poly(styrene-acrylonitrile)," *Macromolecular Rapid Communications 30(6),* pp. 423-429. 2009.

[16] C. Li, Q. Zhao, H. Deng, C. Chen, K. Wang, Q. Zhang, F. Chen and Q. Fu, "Preparation, structure and properties of thermoplastic olefin nanocomposites containing functionalized carbon nanotubes," *Polym. Int. 60(11),* pp. 1629-1637. 2011.

[17] F. Fenouillot, P. Cassagnau and J. Majeste, "Uneven distribution of nanoparticles in immiscible fluids: Morphology development in polymer blends," *Polymer 50(6),* pp. 1333-1350. 2009.

[18] A. Goeldel, G. R. Kasaliwal, P. Poetschke and G. Heinrich, "The kinetics of CNT transfer between immiscible blend phases during melt mixing," *Polymer 53,* pp. 411-421. 2012.

[19] C. Li, H. Deng, K. Wang, Q. Zhang, F. Chen and Q. Fu, "Strengthening and toughening of thermoplastic polyolefin elastomer using polypropylene-grafted multiwalled carbon nanotubes," *J. Appl. Polym. Sci. 121(4),* pp. 2104-2112. 2011.

[20] M. Sumita, K. Sakata, S. Asai, K. Miyasaka and H. Nakagawa, "Dispersion of fillers and the electrical-conductivity of polymer blends filled with carbon-black," *Polymer Bulletin 25(2),* pp. 265-271. 1991.

[21] P. Potschke, A. Bhattacharyya and A. Janke, "Carbon nanotube-filled polycarbonate composites produced by melt mixing and their use in blends with polyethylene," *Carbon 42(5-6),* pp. 965-969. 2004.

[22] L. Liu, Y. Wang, Y. Li, J. Wu, Z. Zhou and C. Jiang, "Improved fracture toughness of immiscible polypropylene/ethylene-co-vinyl acetate blends with multiwalled carbon nanotubes," *Polymer 50(14),* pp. 3072-3078. 2009.

[23] A. Baudouin, J. Devaux and C. Bailly, "Localization of carbon nanotubes at the interface in blends of polyamide and ethylene-acrylate copolymer," *Polymer 51(6),* pp. 1341-1354. 2010.

[24] F. Tao, B. Nysten, A. Baudouin, J. Thomassin, D. Vuluga, C. Detrembleur and C. Bailly, "Influence of nanoparticle-polymer interactions on the apparent migration behaviour of carbon nanotubes in an immiscible polymer blend," *Polymer 52(21),* pp. 4798-4805. 2011.

[25] F. Ciardelli, S. Coiai, E. Passaglia, A. Pucci and G. Ruggeri, "Nanocomposites based on polyolefins and functional thermoplastic materials,"*Polym. Int. 57(6),* pp. 805-836. 2008.

[26] L. Valentini, J. Biagiotti, J. Kenny and M. Manchado, "Physical and mechanical behavior of single-walled carbon nanotube/polypropylene/ethylene-propylene-diene rubber nanocomposites," *J. Appl. Polym. Sci. 89(10),* pp. 2657-2663. 2003.

[27] S. Hom, A. R. Bhattacharyya, R. A. Khare, A. R. Kulkarni, M. Saroop and A. Biswas, "Blends of polypropylene and ethylene octene comonomer with conducting fillers: Influence of state of dispersion of conducting fillers on electrical conductivity," *Polym. Eng. Sci. 49(8),* pp. 1502-1510. 2009.

[28] O. Osazuwa, K. Petrie, M. Kontopoulou, P. Xiang, Z. Ye and A. Docoslis, "Characterization of non-covalently, non-specifically functionalized multi-wall carbon nanotubes and their melt compounded composites with an ethylene-octene copolymer," *Composites Sci. Technol. 73*pp. 27-33. 2012.

[29] J. Trent, J. Scheinbeim and P. Couchman, "Ruthenium tetraoxide staining of polymers for electron-microscopy," *Macromolecules 16(4),* pp. 589-598. 1983.

[30] G. Jordhamo, J. Manson and L. Sperling, "Phase continuity and inversion in polymer blends and simultaneous interpenetrating networks," *Polym. Eng. Sci. 26(8),* pp. 517-524. 1986.

[31] P. Poetschke, S. Pegel, M. Claes and D. Bonduel, "A novel strategy to incorporate carbon nanotubes into thermoplastic matrices," *Macromol. Rapid Commun. 29(3),* pp. 244-251. 2008.

[32] S. Wu, *Polymer Interface and Adhesion.* New York: Macel Dekker, 1982.

[33] S. Ray, S. Pouliot, M. Bousmina and L. Utracki, "Role of organically modified layered silicate as an active interfacial modifier in immiscible polystyrene/polypropylene blends," *Polymer 45(25),* pp. 8403-8413. 2004.

[34] B. Khatua, D. Lee, H. Kim and J. Kim, "Effect of organoclay platelets on morphology of nylon-6 and poly(ethylene-ran-propylene) rubber blends," *Macromolecules 37(7),* pp. 2454-2459. 2004.

[35] A. Goeldel, A. Marmur, G. R. Kasaliwal, P. Poetschke and G. Heinrich, "Shape-dependent localization of carbon nanotubes and carbon black in an immiscible polymer blend during melt mixing," *Macromolecules 44(15),* pp. 6094-6102. 2011.

[36] I. Alig, P. Poetschke, D. Lellinger, T. Skipa, S. Pegel, G. R. Kasaliwal and T. Villmow, "Establishment, morphology and properties of carbon nanotube networks in polymer melts," *Polymer 53,* pp. 4-28. 2012.

[37] S. Nuriel, L. Liu, A. Barber and H. Wagner, "Direct measurement of multiwall nanotube surface tension," *Chemical Physics Letters 404(4-6),* pp. 263-266. 2005.

[38] I. Novak, E. Borsig, L. Hrckova, A. Fiedlerova, A. Kleinova and V. Pollak, "Study of surface and adhesive properties of polypropylene grafted by maleic anhydride," *Polym. Eng. Sci. 47(8),* pp. 1207-1212. 2007.

[39] C. G. Ma, M. Q. Zhang and M. Z. Rong, "Morphology prediction of ternary polypropylene composites containing elastomer and calcium carbonate nanoparticles filler," *J. Appl. Polym. Sci. 103(3),* pp. 1578-1584. 2007.

# Chapter 6

# Conclusions and Future Work

## 6.1 Conclusions

Multi-walled carbon nanotubes (MWCNTs) were non-covalently functionalized with hyperbranched polyethylene (HBPE). Approximately 35% of the surface of the nanotubes was covered upon functionalization with HBPE as determined through adsorption experiments. The HBPE functionalization of the MWCNTs resulted in a reduction in aggregate size when melt compounded with a polypropylene (PP) homopolymer. The reduction in aggregate size with nanotube functionalization resulted in a shift to higher electrical percolation thresholds and more highly conductive composites. The maximum conductivity values of the composites remained unchanged with HBPE functionalization, confirming that the non-covalent approach does not disrupt the conductivity of nanotubes. MWCNTs resulted in increased Young's modulus in comparison to unfilled composites at compositions up to 3 wt% MWCNTs. Addition of HBPE onto MWCNTs resulted in composites with improved ductility when compared to pristine MWCNT/PP composites. This can be attributed to aggregate break-up and improved interfacial adhesion with HBPE functionalization.

The addition of aromatic moieties to PP chains was also investigated as a compatibilizing method to facilitate the dispersion of MWCNTs in melt compounded composites of PP. Amino-pyridine (Py) functional groups were grafted to PP in a melt-state reaction between PP-g-maleic anhydride (MA) and 4-aminomethylpyridine (AMP). Conversion was confirmed by FTIR. Matrix viscosity was not affected upon Py grafting. The non-covalent interaction between Py side groups and nanotubes for the matrix functionalization was more efficient in achieving improved

dispersion and breaking up aggregates than the previously explored HBPE functionalization. Improved nanotube dispersion with Py matrix functionalization was confirmed via various microscopy techniques and Raman spectroscopy. Electrical percolation was achieved at MWCNT loadings of approximately 1.2 wt%. There was no change in the electrical percolation threshold between the Py functionalized matrix and its MA counterpart, despite their different morphologies. This suggests that percolation can be achieved through contacts between individually dispersed MWCNTs, or between aggregates that are interconnected with nanotubes. Composites with conductivity on the order of $10^{-2}$ S/m were achieved with Py matrix functionalization, increasing the potential conductive applications for these materials. The strength of the composites was improved with addition of the nanotubes while ductility was better maintained with the Py functionalized matrix.

TPO blends containing PP/EOC/MWCNTs were investigated. All PP compositions contained either 25 wt% PP-g-MA or PP-g-Py as a compatibilizer. The addition of MWCNTs resulted in a slight decrease in average droplet diameter for TPO blends, which had droplet/matrix morphology. MWCNTs were first dispersed in PP and a kinetic approach was employed using 80/20 PP/EOC blends to monitor the MWCNT migration to the EOC phase. After 2 minutes of blending time MWCNTs had begun to preferentially locate in the EOC phase. Values of wetting coefficients were estimated from the interfacial tensions of the blend components. These predictions confirmed that the MWCNTs partition in the EOC phase to minimize interfacial energy. The blends containing PP-g-Py showed a slightly higher amount of MWCNTs in the PP phase, connecting dispersed EOC droplets. This likely contributed to the increased conductivity experienced for Py functionalized blends. Decreases in the electrical

percolation threshold were achieved by varying blend composition. A co-continuous blend morphology resulted in the lowest percolation threshold.

## 6.2 Recommendations for Future Work

1. Systematic study to investigate the impact of sample thickness on electrical conductivity of polymer/MWCNT composites is required. This would be important to supplement the commonly used but misguided assumption that electrical percolation is exclusively achieved by the formation of a three-dimensional network of dispersed nanotubes. It is believed that nanotube aggregation produces artificially high levels of conductivity, due to measurement methods involving thin films.
2. The use of PP-g-Py for improved dispersion of other nanofillers capable of similar non-covalent interaction, such as graphene, in PP would be of interest.
3. The influence of matrix viscosity and electric field strength on percolation time upon application of an external AC electric field for PP/MWCNT composites should be investigated. Novel approaches to maintain aligned MWCNT networks should be explored. Also, testing methods need to be developed to determine the mechanical properties in the direction of alignment. A review article summarizing the mechanism behind electric field alignment of MWCNTs in polymer composites and the current state of research would benefit future contributions in this field.
4. Investigate alternative approaches for partitioning MWCNTs exclusively in PP phase for TPO blends. Producing blends with the PP phase entirely composed of PP-g-Py may reduce interfacial energy to allow MWCNT to localize in that phase. Using HBPE functionalized nanotubes may also be a possible solution. If this can be achieved, the effect of MWCNT addition on mechanical and impact properties of TPO blends should

be reported. The impact of nanotube length on partitioning in immiscible polymer blends could be of interest.